



저작자표시-비영리-변경금지 2.0 대한민국

이용자는 아래의 조건을 따르는 경우에 한하여 자유롭게

- 이 저작물을 복제, 배포, 전송, 전시, 공연 및 방송할 수 있습니다.

다음과 같은 조건을 따라야 합니다:



저작자표시. 귀하는 원저작자를 표시하여야 합니다.



비영리. 귀하는 이 저작물을 영리 목적으로 이용할 수 없습니다.



변경금지. 귀하는 이 저작물을 개작, 변형 또는 가공할 수 없습니다.

- 귀하는, 이 저작물의 재이용이나 배포의 경우, 이 저작물에 적용된 이용허락조건을 명확하게 나타내어야 합니다.
- 저작권자로부터 별도의 허가를 받으면 이러한 조건들은 적용되지 않습니다.

저작권법에 따른 이용자의 권리는 위의 내용에 의하여 영향을 받지 않습니다.

이것은 [이용허락규약\(Legal Code\)](#)을 이해하기 쉽게 요약한 것입니다.

[Disclaimer](#)

공학박사 학위논문

Simulation-Based Prediction for
Speed Excursion of PIG in Natural
Gas Pipeline: Modeling,
Simulation, and Experiment

시뮬레이션 기반 천연가스 파이프라인에서의
배관검사робот 속도 이탈 예측: 모델링, 시뮬레이션,
실험

2022년 8월

서울대학교 대학원

조선해양공학과

김 승 만

Simulation-Based Prediction for Speed Excursion of PIG in Natural Gas Pipeline: Modeling, Simulation, and Experiment

지도 교수 서 유 택

이 논문을 공학박사 학위논문으로 제출함
2022년 6월

서울대학교 대학원
조선해양공학과
김 승 만

김승만의 공학박사 학위논문을 인준함
2022년 6월

위 원 장 _____ 임 영 섭 _____ (인)

부위원장 _____ 서 유 택 _____ (인)

위 원 _____ 김 도 균 _____ (인)

위 원 _____ 남 보 우 _____ (인)

위 원 _____ 안 윤 호 _____ (인)

Abstract

Seungman Kim

Department of Naval Architecture and Ocean Engineering

The Graduate School

Seoul National University

Natural gas pipeline pigging with speed excursions may lead to potential loss of inspection data and possible dangers due to high acceleration; however, the operation relies heavily on a rule of thumb. Most pigging operations in gas pipelines are performed at normal operating pressures with regular flow rates, and the PIG velocity is generally in the range of 2–5 m/s. However, pigging in low-pressure and low-flowrate gas pipelines is very difficult due to speed excursion, which rapidly increases the PIG velocity. Mitigating speed excursions is an important challenge during the gas pipeline pigging process, but fundamental studies on this phenomenon have not been conducted.

This study presents various models, solvers, and methodologies that can predict unstable behavior of PIG such as speed excursion through modeling, simulation, and experiment.

In the first part, two novel friction models to simulate speed excursion due to friction variation were proposed. The first friction model, Tuned friction model, adopts a dynamic friction table coupled with an exponential friction model to simulate the speed excursion due to friction variation. The second friction model utilizes a linear equation for friction variation caused by changes in wall thickness and pipe bends, then weight parameters are applied to determine the influence of each factor. These two friction models are tuning models based on field data to simulate speed excursions caused by frictional variation, which can be strategically selected according to the purpose of the simulation. In the numerical model, the

transient gas flow equations are solved by the method of characteristics (MOC), and then the Runge–Kuta method is used to solve the dynamic equation of the PIGs. Simulation results applying the proposed friction models are compared to the field pigging data for three different routes operated by the Korea Gas Corporation (KOGAS), and the obtained simulation results are in good agreement with the field pigging data. The first model, tuned friction model, was able to simulate the average pigging velocity and speed excursions of the total distance ratio with high accuracy. The second proposed model, weighted friction model, was slightly less accurate than the first friction model, however it was able to predict the average pigging velocity and speed excursions under different operating conditions.

In the second part, this study is the first to conduct a lab-scale experiment on speed excursion due to friction variation during gas pipeline pigging to investigate the mechanism of speed excursion and the relationship between the main variables and speed excursion. Based on the differential pressure results, mechanism of speed excursion was derived as 5 phases of speed excursion process: Stable behavior, build-up phase, pre-speed excursion phase, speed excursion phase, recovery phase. In the results of relationship between main variables and speed excursion, it was found that the flow velocity has a linear relationship with the speed excursion, but the excursion ratio has an exponential fit curve that rapidly increased at low flow velocity. These result means that low-flow pigging produces relatively low-speed excursions, but can be a very risky operation due to the rapid increase in excursion ratio. Both build-up time and recovery time also showed an exponential fit curve that increased rapidly at low flow velocity. These results indicate that pigging behavior is significantly unstable due to the long build up time and recovery time during low-flow pigging. When the linepack length changed, higher speed excursions occurred as the linepack length increases even at same friction conditions. The results indicated that the linepack length is the main factor in pigging behavior. In particular, linepack should also be considered as an important variable that affects speed excursion, and behavior in long-distance pipeline pigging.

In the third part, this study evaluates four pigging solvers, based on combinations of two proposed flow models and two friction models, for predicting the speed excursions in natural gas pipeline pigging. The simulation and prediction performances of solvers are evaluated by comparing the results of each solver with field pigging data from the Korea gas corporation. A dynamic model of the pipeline inspection gauge is developed by adopting the Stoner-based method of characteristics (MOC) and MOC-finite volume method (FVM) hybrid models for the fluid part and the tuned friction and weighted friction models for the friction part. Although the overall results of the proposed pigging solvers are in good agreement with the field pigging data, the performance differences between the solvers are clearly identified through error evaluations. Among the flow models, the MOC-FVM hybrid model exhibits higher accuracy than the Stoner-based MOC in both simulation and prediction performances. Among the friction models, the tuned friction model exhibits higher accuracy in simulation performance, whereas the weighted model exhibits higher prediction performance. Therefore, among the four solvers, the solver based on the hybrid-tuned friction model exhibits the best simulation performance, and the solver based on the hybrid-weighted friction model exhibits the best prediction performance. These results indicate that the flow model and friction models can be strategically combined to develop a pigging solver depending on the usage requirements.

Keyword: Pipeline inspection gauge (PIG), Natural gas pipeline, Speed excursion, Dynamic model, Flow model, Friction model, Numerical simulation

Student Number: 2018-32032

Table of Contents

Abstract	i
Contents	iv
List of Tables	vii
List of Fables	ix
Nomeclature	xii
Chapter 1. Introduction	1
1.1. Research Background.....	1
Chapter 2. Modelling and simulation of speed excursion of PIG in natural gas pipeline	7
2.1. Introduction	7
2.2. Model description.....	10
2.2.1 PIG dynamic model.....	10
2.2.2 Gas flow model	11
2.3. Novel friction models.....	16
2.3.1 Tuned friction model	17
2.3.2 Weighted friction model	20
2.4. Validation	23
2.5. Results and discussion.....	26
2.5.1 Simulation of Route-A and Route-B	26
2.5.2 Simulation and prediction of Route-C.....	31
2.5.3 Comparison of the proposed models	37
2.5.4 Linepack effect on simulation results.....	40
2.6. Summary	41
2.7. Acknowledgement.....	42
Chapter 3. Experiment investigation on speed excursion of PIG due to friction variation in natural gas pipeline	43

3.1. Introduction	43
3.2. Experimental system	45
3.2.1 Speed excursion experimental system.....	45
3.2.2 Wall thickness change section	49
3.2.3 Design of experimental PIG	50
3.3. Results and discussion.....	51
3.3.1 Mechanism of speed excursion	52
3.3.2 Effect of flowrate.....	54
3.3.3 Effect of wall thickenss change	58
3.3.4 Effect of Linepack	61
3.3.5 Numerical simulation	65
3.4. Summary	69
3.5. Acknowledgement.....	70
Chapter 4. Speed excursion predictions of PIG in natura gas pipeline using pigging solvers based on flow and friction model combinations.....	71
4.1. Introduction	71
4.2. Dynamic model and solver.....	75
4.2.1 Stoner-MOC	77
4.2.2 MOC-FVM Hybrid	80
4.2.3 Tuned friction model	89
4.2.4 Weighted friction model.....	90
4.3. Solver evaluation method.....	93
4.4. Results and discussion.....	94
4.4.1 Simulation performance of the solvers.....	96
4.4.2 Prediction performance of the solvers.....	99
4.4.3 Difference between flow models.....	102
4.4.4 Difference between friction models	104
4.5. Summary	106

4.6. Acknowledgement.....	106
Chapter 5. Industrial application for CO₂ and H₂ pipeline pigging	107
5.1. Introduction.....	107
5.2. Methodology	109
5.3. Phase behaviour analysis for speed excursion zone.....	110
5.4. Simulation	113
5.4.1 Simulation case	113
5.4.2 Case study – H ₂ pipeline pigging.....	115
5.4.3 Case study – CO ₂ pipeline pigging.....	117
5.5. Summary	119
Chapter 6. Concluding remarks.....	120
6.1. Conclusions.....	120
6.2. Future works.....	122
Bibliography	123
Abstract in Korean.....	130
Acknowledgement in Korean	133

List of Table

Table 2-1. Dynamic friction table of the tuned friction model for each route.....	26
Table 2-2. Error evaluation in total distance ratio of pipeline – Route-A	28
Table 2-3. Speed excursion error using the tuned friction model – Route-A.....	28
Table 2-4. Error evaluation in total distance ratio of pipeline – Route-B	29
Table 2-5. Speed excursion error using the tuned friction model – Route-B	30
Table 2-6. Friction increase by weight parameter for each variable	32
Table 2-7. Error evaluation in total distance ratio of pipeline – Route-C (1st and 2nd pigging)	34
Table 2-8. Speed excursion error of 1st pigging using weighted friction model – Route-C	35
Table 2-9. Speed excursion error of 2nd pigging using weighted friction model – Route-C	36
Table 2-10. Comparison of speed excursion error between tuned friction model and weighted friction model	39
Table 3-1. Properties of speed excursion experimental system.....	47
Table 3-2. Materials used in speed excursion experimental system.....	48
Table 3-3. Structural parameters of experimental PIG.....	50
Table 3-4. Controllable variables for speed excursion experiment	51
Table 3-5. Fitting formula, R-squared, and covariance of the average PIG velocity according to the flow velocity	55
Table 3-6. Fitting formula of experimental results and flowrate.....	64
Table 3-7. Fitting formula of friction increase ratio and wall thickness change ratio	66
Table 3-8. Numerical parameters for simulation using Kim’s solver	67
Table 3-9. Speed excursion error between experiment and Kim’s solver	69
Table 4-1. Pigging solver list based on flow and friction model combinations ...	76

Table 4-2. Friction values for weighted friction model.....	95
Table 4-3. Simulation performance of solvers through error evaluation.....	98
Table 4-4. Prediction performance of solvers through error evaluation.....	101
Table 5-1. Critical point according to fluid mixture.....	111
Table 5-2. Numerical parameters for CO ₂ , H ₂ , CH ₄ pipeline pigging simulation using Kim's solver	113
Table 5-3. Simulation case CO ₂ and H ₂ pipeline pigging simulation	114

List of Figures

Figure 1-1. Scope of the Phd thesis.....	6
Figure 2-1. Schematic of conventional PIG	10
Figure 2-2. Backward and forward characteristic lines using method of characteristics (MOC).	11
Figure 2-3. Characteristic lines used in MOC.....	14
Figure 2-4. Friction force of basic friction model when PIG starts to move.....	16
Figure 2-5. Range of dynamic friction table and exponential friction model	17
Figure 2-6. Calculation method of friction variation caused by bends and wall thickness changes in tuned friction model	18
Figure 2-7. Flowchart of simulation algorithms for tuned friction model	19
Figure 2-8. Schematic network for weighted friction model	20
Figure 2-9. Flowchart of simulation algorithms for weighted friction model.....	22
Figure 2-10. Field pigging data of Route-A.....	24
Figure 2-11. Simulated PIG velocity using the tuned friction model - Route-A..	27
Figure 2-12. Simulated PIG velocity using the tuned friction model - Route-B..	29
Figure 2-13. Prediction of PIG velocity for future pigging using the weighted friction model - (a) simulated PIG velocity at the 1st pigging (b) predicted PIG velocity at the 2nd pigging.....	33
Figure 2-14. Comparison of tuned friction model and weighted friction model. (a) Simulated PIG velocity with tuned friction model. (b) Simulated PIG velocity with weighted friction model	38
Figure 2-15. Simulation accuracy according to linepack (a) Low accuracy (b) High accuracy.....	40
Figure 3-1. Schematic of speed excursion experimental system.....	46
Figure 3-2. Experimental apparatus (a) Horizontal pipeline system (b) Wall thickness change section (c) Experimental PIG	46

Figure 3-3. Schematic of wall thickness change section.....	49
Figure 3-4. Experimental PIG with all design dimensions	50
Figure 3-5. (a) Mechanism of speed excursion. (b) Speed excursion process based on the differential pressure is displayed through: (i) Stable behavior, (ii) Build-up phase, (iii) Pre-speed excursion phase, (iv) Speed excursion phase, and (v) Recovery phase.	53
Figure 3-6. Measured average PIG velocity as function of flow velocity.....	70
Figure 3-7. Speed excursion versus flow velocity with $\gamma_{wt}=1.97\%$, and $L_{wt}=4.5$ m are shown for: (a) Speed excursion, (b) Excursion ratio, (c) Build up time, (d) Recovery time, (e) Speed excursion phase at low flowrate, $v_{air}=0.392$ m/s, and (f) Speed excursion phase at high flowrate, $v_{air}=3.136$ m/s.	57
Figure 3-8. Comparison of speed excursion of $\gamma_{wt}=1.97\%$, and $\gamma_{wt}=3.94\%$ is shown for: (a) Speed excursion, (b) Excursion ratio, (c) Build-up time, (d) Recovery time, (e) Speed excursion phase at low friction, $\gamma_{wt}=1.97\%$, and (f) Speed excursion phase at high friction, $\gamma_{wt}=3.94\%$,	60
Figure 3-9. Comparison of speed excursion of $L_{wt}=4.5$ m, and $L_{wt}=9$ m is shown for: (a) Speed excursion, (b) Excursion ratio, (c) Build-up time, and (d) Recovery time. Speed excursion phase at short linepack length, $L_{wt}=4.5$ m and long linepack length, $L_{wt}=9$ m is shown in (e) and (f), respectively	63
Figure 3-10. Friction increase ratio according to wall thickness change ratio	65
Figure 3-11. Results using Kim's solver by applying the proposed equation of wall thickness change (a) Differential pressure (b) Speed excursion	68
Figure 4-1. Field pigging data of Route-A (1st & 2nd pigging).....	72
Figure 4-2. PIG moving in an inclined pipeline	75
Figure 4-3. Schematic of characteristic lines of MOC and space-time grid configuration	78
Figure 4-4. General solver configuration	80
Figure 4-5. Comparison of pressure distribution along the x-axis	87

Figure 4-6. Interface between FVM and MOC computation regions	88
Figure 4-7. Schematic of the tuned friction model.....	89
Figure 4-8. Calculation scheme of weighted friction model	90
Figure 4-9. Simulation algorithms for: (a) Tuned friction model; (b) Weighted friction model.....	92
Figure 4-10. Numerical inputs for simulation: (a) Tuned friction in the dynamic friction table	95
Figure 4-11. Simulated velocity obtained from four solvers for first pigging.....	97
Figure 4-12. Comparison of simulation performance according to: (a) flow models; (b) friction models.....	98
Figure 4-13. Predicted velocity obtained from four solvers for second pigging	100
Figure 4-14. Comparison of prediction performance of solvers	101
Figure 4-15. Difference between the Stoner-MOC and MOC-FVM hybrid models	103
Figure 4-16. PIG velocity differences in the friction models: (a) Tuned friction model; (b) Weighted friction model	105
Figure 5-1. A two-stage simulation methodology for modeling speed excursion considering fluid composition.....	109
Figure 5-2. Phase diagram for $\text{CH}_4 + \text{H}_2$ mixture.....	110
Figure 5-3. Phase diagram for $\text{CO}_2 + \text{N}_2$ mixture	112
Figure 5-4. Simulation results for H_2 pipeline pigging according to pressure.	115
Figure 5-5. Comparison of H_2 and Natural gas pipeline pigging.....	116
Figure 5-6. Phase diagram of $\text{CH}_4\text{-H}_2$ including simulation results	116
Figure 5-7. Simulation results for CO_2 pipeline pigging according to pressure	117
Figure 5-8. Comparison of CO_2 and Natural gas pipeline pigging.....	118
Figure 5-9. Phase diagram of $\text{CO}_2\text{-N}_2$ including simulation results.....	118

Nomenclature

Roman symbols

A	Area of inner pipe cross-section [m ²]
C	Speed of sound [m/s]
c'	Preconditioned speed of sound [m/s]
c'_{un}	Unsteady preconditioned speed of sound [m/s]
C_c	Convection heat transfer coefficient [W/m ² K]
C_v	Specific heat at constant volume [J/kgK]
d_o	Internal diameter of pipe [m]
d_i	Inner diameter of wall thickness change [mm]
d_s	Outer diameter of sealing disc [mm]
d_c	Outer diameter of spacer disc [mm]
D	Internal diameter of pipe [m]
D_i	i -th actual PIG velocity from field pigging data [m/s]
D_s	Body force Source term [-]
E	Total energy [J]
e	Internal energy per unit mass [J/kg]
F	Darcy friction coefficient [-]
f	Darcy-Weisbach friction factor [-]
f_h	Friction force of fluid flowing in the pipeline [bar]
F_{chwt}	Maximum friction when a PIG passes wall thickness change section [bar]
F_c	Convective flux vector [-]
F_d	Dynamic friction of PIG [bar]
F_{di}	Dynamic friction at the i -th speed excursion [bar]
F_f	Friction force between PIG and pipe [bar]
F_p	Driving force of PIG [bar]
F_s	Static friction force of PIG [bar]

F_v	Viscous flux vector [-]
g	Gravity acceleration [m/s^2]
H	Total enthalpy [J]
k	Roughness of pipe [mm]
k_{bend}	Friction coefficient of bends in weighted friction model
k_{chwt}	Friction coefficient of wall thickness variations in weighted friction model
L	Characteristic length [m]
L_{pig}	PIG length [m]
L_p	Position of pressure sensor [m]
L_{pipe}	Pipeline length [m]
L_{wt}	Linepack length [m]
M	Mass flow rate [kg/s]
m	Hydraulic mean radius of pipe [m]
m_p	Mass of PIG [kg]
n	Number of sample [-]
O_i	i -th simulated PIG velocity [m/s]
p	Flow pressure [Pa]
P_1	Pressure at PIG tail [Pa]
P_2	Pressure at PIG nose [Pa]
P_{out}	Outlet pressure [atm]
q	Compound rate of heat inflow per unit of pipe wall [w/m^2]
Q	Vector of primitive variables [-]
Q_{air}	Air flowrate [l/min]
R	Gas constant [J/kgK]
R_b	Radian of bend angle
S	Perimeter of pipe [m]

t	Physical time [s]
t_0	Initial wall thickness [mm]
t_{build}	Build-up time [s]
t_{chwt}	Changed wall thickness [mm]
t_s	thickness of sealing disc [mm]
$t_{recovery}$	Recovery time [s]
T	Flow temperature [K]
T_{ext}	Seabed temperature [K]
u, v, w	Velocity component of x, y, z axis [m/s]
U	Contravariant velocity [m/s]
v_{air}	Air flow velocity [m/s]
v_{se}	Maximum speed excursion [m/s]
v_p	Velocity of PIG [m/s]
v_{av_pig}	Average PIG velocity [m/s]
$V_{f,max}$	Maximum air velocity [m/s]
V_{co}	Cut-off velocity [m/s]
V_{un}	Unsteady velocity [m/s]
w	Weight parameter [-]
W	Vector of conservative variables

Greek Letters

α	Inclination angle of pig [-]
α_d	decay constant [-]
α_s	Interference of sealing disc [%]
β_s	Clamping rate of sealing disc [%]
γ	Ratio of specific heat [-]
γ_{wt}	Wall thickness change ratio [%]

ν	Kinetic viscosity of flow [m^2/s]
ρ	Fluid density [kg/m^3]
δ_s	Thickness ratio of sealing disc [%]
τ	Pseudo time [-]
τ_{xx}	Shear stress [N/m^2]
θ	Slope of pipe [$^\circ$]
Φ	Viscous flux for total energy [-]
φ_{er}	Excursion ratio [-]
$\varphi_{friction}$	Friction increase ratio [-]
Γ	System preconditioning matrix
λ	Eigenvalues of Euler equation [m/s]

Abbreviations

AAE	Average Absolute Error
ALE	Arbitrary Lagrangian Eulerian
CCS	Carbon Capture and Storage
CFD	Computational Fluid Dynamics
CFL	Courant-Friedrichs-Lewy
CRM	Coefficient of Residual Mass
EGR	Error Growth Ratio
ERR	Error Reduction Ratio
EPDM	Ethylene Propylene Diene terpolymer
FVM	Finite Volume Method
GCL	Geometric Conservation Law
MAE	Mean Absolute Error
MAPE	Mean Absolute Percentage Error
MFL	Magnetic Flux Leakage
MOC	Method of Characteristics

ODE	Ordinary Differential Equation
PDE	Partial Differential Equation
PIG	Pipeline Inspection Gauge
PVC	Polyvinyl Chloride
RMSE	Root Mean Square Error
SE	Speed Excursion

Chapter 1. Introduction

1.1. Research background

Pipelines are the safest and most cost-efficient method for transporting large amounts of natural gas from gas reserves to major markets. Safety is the first priority in transporting natural gas to avoid fatal accidents in urban areas. Currently, a pipeline inspection gauge (PIG) is a widely used tool in oil and gas industry for flow assurance and pipeline integrity. The role of PIG in terms of flow assurance is mainly used to remove deposits in pipes such as wax and hydrates. This type of PIG is called a mechanical PIG. Recently, intelligent PIG or smart PIG, which can inspect long-distance piping with non-destructive inspection technology and new propulsion system, is being utilized in the industry. This study begins with the problem of operating an Intelligent PIG in a single-phase gas pipeline network.

Since the PIG is driven by the force of the fluid, the operating conditions of the inlet and outlet are the main variables that determine the PIG behavior. It is also significantly different from normal pigging in that long linepacks are created on the front and back of the PIG because it operates within a pipeline network. This line pack also acts as a key variable in determining PIG behavior. Most pigging operations in gas pipelines are performed at regular flow rates at normal operating pressures, with PIG speeds typically in the 2-5 m/s range [64, 76, 77].

However, pigging in low-pressure and low-flow gas pipelines is very difficult because of speed excursions that rapidly increase the PIG velocity. Predicting and Mitigating speed excursions is an important challenge during the gas pipeline pigging process.

When a speed excursion occurs, the data acquisition efficiency of the MFL (Magnetic Flux Leakage) system attached to the PIG decreases significantly when driving at 5 m/s or more, and the meaning of the inspection disappears. When driving at 10 m/s or more, the risk of structural impact between PIG and pipeline greatly increases [65, 71].

Some studies have been conducted to simulate and predict PIG velocity. In early research on pigging models, the basic steady-state pigging model in multiphase flow [2, 44], and transient pigging simulation with the method of characteristics (MOC) [24, 38] were studied. The computational fluid dynamics (CFD) approach was used to study the fluid term [1, 18, 82], whereas the friction term was mainly studied with theoretical models and driving cup experiments [9, 16, 36, 42]. For modeling PIG dynamics in natural gas pipelines, the method of characteristics (MOC) has been proposed for solving the transient gas flow equations, and the Runge–Kuta method has been proposed for the dynamic equations of PIGs [34, 35]. Based on their proposed MOC model, additional numerical studies related to pigging simulations have been performed [4, 10, 14, 15, 49, 79]. Furthermore, flow-governing equations such as the Euler equation or other simplified equations are solved using the MOC or finite volume method (FVM) numerical schemes. Furthermore, studies related to multiphase flow analysis in gas-liquid mixture pipeline pigging [48] and local two-dimensional flow analysis around the bypass PIG have been conducted [3].

In general, the PIG velocity can be simulated using a commercial multiphase flow simulator widely used in the oil and gas industry [13, 25, 43, 83], and has been also used to validate their pigging model [8, 22, 48]. In most of the existing pigging simulation studies, the friction was assumed to be constant, and the previous studies did not focus on speed excursion due to friction variation [39, 25, 10, 49, 14, 15, 28,

20, 31, 66, 67, 74, 75, 87, 88, 89, 90]. Friction is generally estimated based on empirical findings [78], field experience [23], and guesswork with a high degree of uncertainty [11, 27, 36]. O'Donoghue (1996) proposed a simplified wall force model that includes the geometric and material properties of the sealing disk [42]. Although this model is the first physical equation-based friction model, friction is relatively underestimated [16, 17, 19, 42, 50]. A two-dimensional linear and non-linear friction model for contact force simulation was proposed as a method of finite element (FE) calculation of the sealing disk [47, 50, 81, 84, 85, 86]. However, it is difficult to include the FE calculations in the existing PIG models.

Some experimental studies have been conducted for PIG dynamics. Research related to PIG dynamics has mostly focused on engineering simulations to predict the dynamics [1, 10, 18, 20, 28, 34, 35, 39, 49, 68]. Only a few papers have addressed the speed excursion phenomenon during natural gas pipeline pigging [19, 26, 32]. Researchers have conducted experiments on bypass pigging technology [5, 6, 7, 19, 21, 30, 52, 69, 73] to investigate PIG dynamics. A few studies have focused on the friction and resistance of PIG [12, 33, 47, 50].

Despite growing demand for CO_2 and H_2 pipelines, most previous studies have been limited range to natural gas pipeline pigging. Integrity assessment of CO_2 and H_2 pipeline with a 'smart PIG' is also viable, but very few inspections runs with smart PIG are reported [60, 61, 62, 63]. Inspection pigging of CO_2 and H_2 pipelines is not routinely done and regarded as more difficult than natural gas pipeline pigging.

This study began with the fundamental question of why speed excursions occur, how they relate to main variables, and whether they can be simulated and predicted. The dissertation consists of three main parts to present various models, solvers and

methodologies that can predict the unstable behavior of PIG such as velocity excursions through modeling, simulation and experiment. The main goal of the current PhD project is to gain a better basic understanding of the physics of speed excursions in gas pipelines to improve engineering models used in industry for pigging operations. In the industry, PIGs have been used for decades, but little research on speed excursion phenomenon has been conducted. Therefore, pigging operations with speed excursions rely heavily on the rule of thumb that low pressure and low flow cause excessive speed excursion and that friction of PIG should be reduced to reduce speed excursion. However, few studies have done the effect of pressure and flow rate on speed excursion and are not very well understood as they depend on the operator's experience. The emphasis in our study will be on speed excursion phenomenon. The results can be used to implement the engineering design tools used to predict the speed excursion and PIG velocity in natural gas pipeline.

In the Chapter 2, two novel friction models of pipeline inspection gauges were proposed to simulate and predict speed excursions occurring in the total distance ratio of a pipeline generated by numerous bends and changes in wall thickness. These two friction models are tuning models based on field data to simulate speed excursions due to frictional variation, and can be strategically selected according to the purpose of the simulation. These results mean that the speed excursion at the total distance ratio can be simulated and predicted with high accuracy using the proposed friction models. Therefore, these two novel friction models would provide insights for the operators to simulate and predict the dynamics of the PIGs in their pipeline networks.

In the Chapter 3, speed excursion due to changes in wall thickness were experimented to investigate the mechanism of speed excursion and the relationship

between speed excursion and main variables as flowrate, wall thickens change, and linepack length. The research questions in this chapter are as follows:

- What is the mechanism and process of speed excursion?
- What is the relationship between speed excursion and main variable?
- Does speed excursion increase at low flowrate?
- Does line pack affect speed excursion?
- Is it a linear relationship or a non-linear relationship?

In the Chapter 4, as a follow-up study of the Chapter 2, four pigging solvers that were developed by employing different combinations of flow and friction models were proposed. The research questions in this chapter are as follows:

- Which solver has the best simulation and predictive performance?
- In fluid parts, does the hybrid-based solver perform better than stoner-based solver?
- How much does the simulation accuracy and predictability change depending on the flow model?
- How different are the analysis times for different flow models?
- In friction model parts, does the weighted-based solver perform better than tuned-based solver?
- How much does the simulation accuracy and predictability change depending on the friction model?
- How different are the analysis times for different friction models?

The three chapters covered modeling, simulation, and to get better understanding and insight for speed excursion, and carried out research that could be a starting point for speed excursion as shown in the Figure 1-1. In chapter 4, interest in CCS and hydrogen is increasing, so as a further study, Industrial application on pigging

simulation of CO₂ and hydrogen transport pipelines using the solvers proposed in the three chapter.

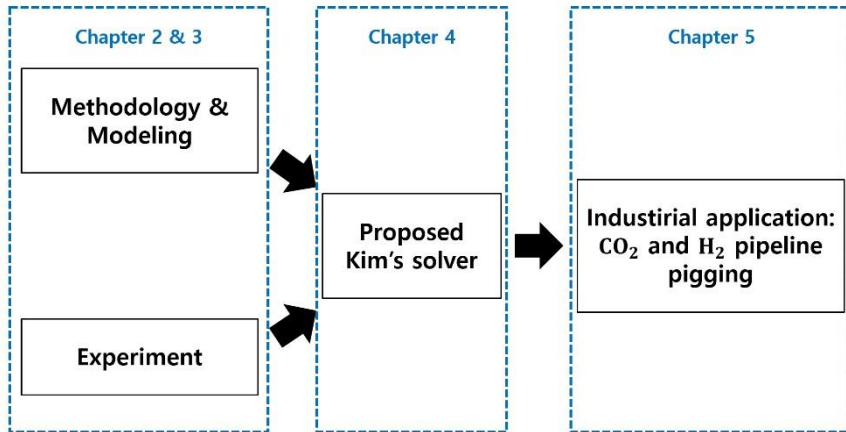


Figure 1-1. Scope of the PhD thesis

Chapter 2. Modelling and simulation of pigging in natural gas pipeline*

2.1. Introduction

Natural gas is an important energy source to lower the carbon emission and to bridge to zero-carbon energy society. Long-distance transportation of natural gas relies on the technical advances of liquefaction and natural gas storage under cryogenic conditions. However, the distribution of natural gas requires the pipeline network to efficiently connect the storage sites to the customers, including households and commercial buildings. The natural gas pipeline is operating under high, medium, and low-pressure conditions depending on the distance from the compression junction, thus the safe operation of the pipeline is the highest priority to avoid fatal accidents in urban area. As the pipeline failure is mostly started from the small cracks on the pipeline surface, there have been efforts to develop the pipeline's inspection technologies. Among them, pipeline inspection gauges (PIGs) are extensively used for the maintenance of long pipelines. According to the industry, pigging in high-pressure pipelines is generally performed stably, but pigging in low-pressure/low-flowrate pipelines is unstable due to speed excursion, which indicates sudden acceleration of PIG [45].

Speed excursion is mainly caused by gas compressibility and friction variation. In our field pigging data of low-pressure/low-flowrate gas pipelines, speed excursion has been frequently observed, which mainly occurs when the PIG passes through sections where friction increases instantaneously, such as bends and changes in wall thickness. In general, it is recommended that the velocity of the PIG be in the range of 2–5 m/s in natural gas pipelines, but speed excursions over 5 m/s frequently occur, which reduces the safety and inspection efficiency.

* This chapter is partially adapted from Speed excursion simulation of PIG using improved friction models in *Journal of Natural Gas Science and Engineering* 97 (2022) 104371 with authors S. Kim, K. Yoo, B. Koo, D. Kim, H. Yoo, and Y. Seo. (<https://doi.org/10.1016/j.jngse.2021.104371>).

According to existing studies, various studies have been conducted to simulate and predict PIG velocity. In the equation of motion of the PIG, the fluid and friction terms are the main uncertainties. The computational fluid dynamics (CFD) approach was used to study the fluid term [1, 18], whereas the friction term was mainly studied with theoretical models and driving cup experiments [9, 16, 36, 42].

For modeling PIG dynamics in natural gas pipelines, the method of characteristics (MOC) has been proposed for solving the transient gas flow equations, and the Runge–Kuta method has been proposed for the dynamic equations of PIGs [34, 35]. Based on their proposed MOC model, additional numerical studies related to pigging simulations have been performed [4, 10, 14, 15, 49]. In addition, various numerical models for pigging simulations have been developed. A numerical model of a PIG with the continuity and linear momentum equation for a compressible gas flow [20], two- and three-dimensional numerical models of PIG dynamics for gas pipelines [39], and pigging simulation in multiphase pipelines [28] have been developed. Speed control simulations and experiments using the PIG bypass valve have been also studied to prevent speed excursions [5, 32, 37].

In general, the PIG velocity can be simulated using a commercial multiphase flow simulator widely used in the oil and gas industry [13, 25, 43], and has been also used to validate their pigging model [8, 22, 48]. However, the current pigging model in the commercial pigging simulator often fails to simulate the locally occurring speed excursion in detail, because it is difficult to reflect the variations in friction force between the PIG and pipe wall that occur when passing through bends and variations in wall thickness.

In most of the existing pigging simulation studies, the friction was assumed to be constant, and the previous studies did not focus on speed excursion due to friction variation [39, 25, 10, 49, 14, 15, 28, 20, 31]. A literature survey reveals very few papers that address the speed excursion of PIG that occurs when a PIG passes through bends or wall thickness changes. The objective of the analysis to be presented in this paper is to propose two novel friction models that can simulate and

predict the speed excursion when PIG passes through bends or wall thickness changes, and to show the applicability and performance of the models through the error evaluation.

The first friction model is an extension of previous studies that assume friction force to be constant. This first model adopted the dynamic friction table in which the friction constant can be entered as many times as the number of occurrences of speed excursion. Friction variation due to bends and wall thickness changes can be simulated by tuning values in the dynamic friction table. The second friction model utilizes a linear equation for friction variation caused by changes in wall thickness and pipe bends, then weight parameters are applied to determine the influence of each factor. This approach has not been considered in previous PIG studies. The two proposed friction models were validated in detail using a fairly large amount of field pigging data from the Korea Gas Corporation (KOGAS).

The main difference between the first and second friction model is the level of detail and predictability of the speed excursion simulation. In the first friction model, called tuned friction model, speed excursion simulation is possible with high accuracy, but the modeling requires significant amount of time while its predictability may decrease when the operating conditions change, such as gas flow rate and pressure. To compensate for the shortcomings of the first friction model, a second friction model, called weighted friction model, was developed. This model simulates the speed excursions caused by all bends and changes in wall thickness in detail, and therefore the speed excursion can be predicted for future pigging operation even if the input conditions change. However, its accuracy may be slightly lower than that of the first model. These two friction models are tuning models based on field data, which can be strategically selected according to the purpose of the simulation and will provide insights for the operators to design the pigging of the natural gas pipeline network.

2.2. Model description

2.2.1 PIG dynamic model

A schematic of a PIG moving in a pipeline is shown in Figure 2-1. The dynamic equation (2.1) of the PIG are derived from Newton's second law and are divided into two terms as follows:

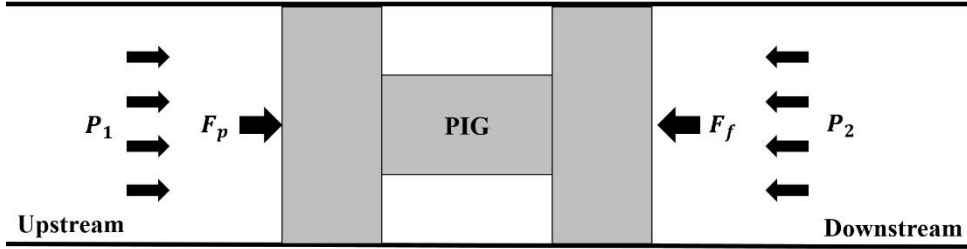


Figure 2-1. Schematic of conventional PIG

$$m_p \frac{dv_p}{dt} = F_p - F_f = (P_1 - P_2)A - F_f \quad (2.1)$$

Where m_p is the PIG mass, v_p is the PIG velocity, F_p is the driving force of PIG, F_f is the friction force between PIG and pipe wall, P_1 is the pressure at PIG tail, P_2 is the pressure at PIG nose, and A is the area of inner pipe cross-section.

In the equation (2.1), it can be observed that the PIG velocity is determined by the balance between the driving force resulting from the differential pressure at the rear and front of the PIG and the friction force between the PIG and pipeline wall. In the case of differential pressure, it can be calculated using the fluid model applied to the numerical model. In this study, referring to previous studies [34, 35], the transient gas flow equations are solved by the MOC, and then the Runge–Kuta method is used to solve the dynamic equation of a PIG.

2.2.2 Gas flow model

The gas flow in the pipeline was modeled as a one-dimensional unsteady flow model using method of characteristics(MOC). MOC is a numerical technique that converts the governing equation of fluid in the form of partial differential equation into the form of ordinary differential equation. Although the accuracy is slightly lower than other numerical model, it is a widely used for a one-dimensional unsteady flow models that require many calculations, such as long pipelines. In Figure 2-2, we defined a simplified governing equation with several assumptions, and the PDE form of the governing equation is converted into an ODE form that can calculate flow variables. At the time step of t_j , the equations for the forward characteristic line and the backward characteristic line at each grid point are solved to calculate the flow variable to the next time step t_{j+1} .

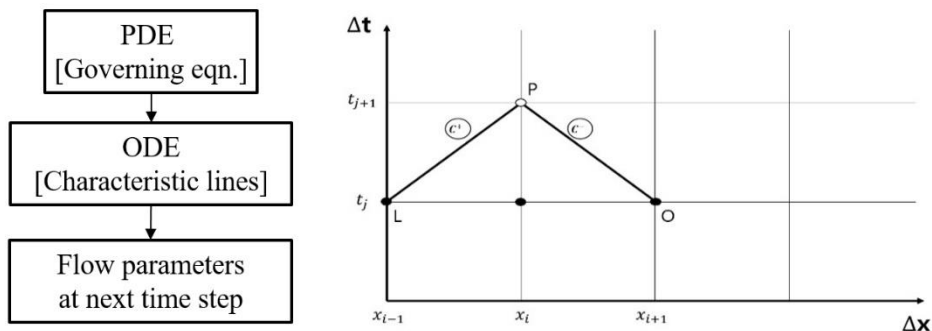


Figure 2-2. Backward and forward characteristic lines using method of characteristics (MOC).

The natural gas flow in the pipeline was assumed as following.

- (1) The inner fluid is an ideal gas and is single-phase.
- (2) The internal diameter of the pipeline is a constant
- (3) To ignore the effect of gravity, the center line of the pipeline is placed on the horizontal line.

(4) The friction factor is a function of wall roughness, and Reynolds number.
Steady state values are used in transient calculation.

(5) The flow of gas is quasi-steady heat flow.

In this model, the gas density is the main concern, which is dependent on the temperature and pressure of the gas composition. The first assumption simplifies gas density calculations using the ideal gas law. To model the unsteady flow, four governing equations, continuity, momentum, state equation, and energy equations (2.2)-(2.5) are as follows.

$$\frac{\partial \rho}{\partial t} + u \frac{\partial \rho}{\partial x} + \rho \frac{\partial u}{\partial x} = 0 \quad (2.2)$$

$$\frac{\partial p}{\partial x} + \rho u \frac{\partial u}{\partial x} + \rho \frac{\partial u}{\partial t} + \frac{f_h}{A} = 0 \quad (2.3)$$

$$\frac{p}{\rho} = RT = (\gamma - 1)C_v T \quad (2.4)$$

$$\frac{\partial}{\partial t} \left[\rho \left(e + \frac{u^2}{2} \right) \right] + \frac{\partial}{\partial x} \left[\rho u \left(e + \frac{u^2}{2} \right) \right] + \frac{\partial}{\partial x} (\rho u) - \frac{qS}{A} = 0 \quad (2.5)$$

Where ρ is the fluid density, u is the flow velocity, p is the flow pressure, f_h is the friction force of fluid flowing in the pipeline, R is the gas constant, T is the flow temperature, γ is the ratio of specific heat, C_v is the specific heat at constant volume, e is the internal energy per unit mass, q is the compound rate of heat inflow per unit of pipe wall, and S is the perimeter of pipe.

The nonlinear hyperbolic partial differential equations (2.2)-(2.5) are transformed to ordinary differential equations using the MOC. The Transformed ordinary differential equations (2.6)-(2.8) are as follows.

$$\frac{du}{dt} + \frac{c}{\gamma p} \frac{dp}{dt} = \frac{\gamma - 1}{c} \frac{q}{\rho m} + \frac{f_h}{\rho A} \left(\frac{u(\gamma - 1)}{c} - 1 \right) \text{ along } \frac{dx}{dt} = u + c \quad (2.6)$$

$$\frac{du}{dt} - \frac{c}{\gamma p} \frac{dp}{dt} = -\frac{\gamma-1}{c} \frac{q}{\rho m} - \frac{f_h}{\rho A} \left(\frac{u(\gamma-1)}{c} + 1 \right) \text{ along } \frac{dx}{dt} = u - c \quad (2.7)$$

$$\frac{du}{dt} - c^2 \frac{dp}{dt} = (\gamma-1) \left(\frac{q}{m} + \frac{f_h u}{A} \right) \text{ along } \frac{dx}{dt} = u \quad (2.8)$$

Where the parameter m , c , q , and f_h can be calculated by the equations (2.9)-(2.12). The value of friction force of fluid flowing in the pipeline, f_h can be calculated as shown in the reference [46].

$$m = \frac{A}{S} \quad (2.9)$$

$$c = \sqrt{\gamma p / \rho} \quad (2.10)$$

$$q = C_c (T_{ext} - T) \quad (2.11)$$

$$f_h = \frac{1}{8} \pi d f \rho u^2 \quad (2.12)$$

Where m is the hydraulic mean radius of pipe, c is the wave speed, C_c is the convection heat transfer coefficient, and T_{ext} is the seabed temperature.

The fluid variables p , u , and ρ are solved at each location x and time t . The sampling distance and time are chosen under the CFL stability condition (2.13).

$$\Delta t < \frac{\Delta x}{u + c} \quad (2.13)$$

Figure 2-3 shows the relationship between fluid variables ρ , p , and u at the time step t_{j-1} and at the following time step t_j . At time step t_{j-1} , variable ρ , p , and u at grid points S, M, and R are obtained from linear interpolation of the data on O, N and L. Subsequently, the gas flow parameters at point p can be derived from previous calculated grid points S, M, and R. Then, we integrate the equations (2.6)-(2.8) along the corresponding characteristic lines dx/dt to get the desired variables through the equations. From linear interpolation, equations (2.14)-(2.16)

can be derived, and finally the desired variables will be obtained through the equations (2.17)-(2.19).

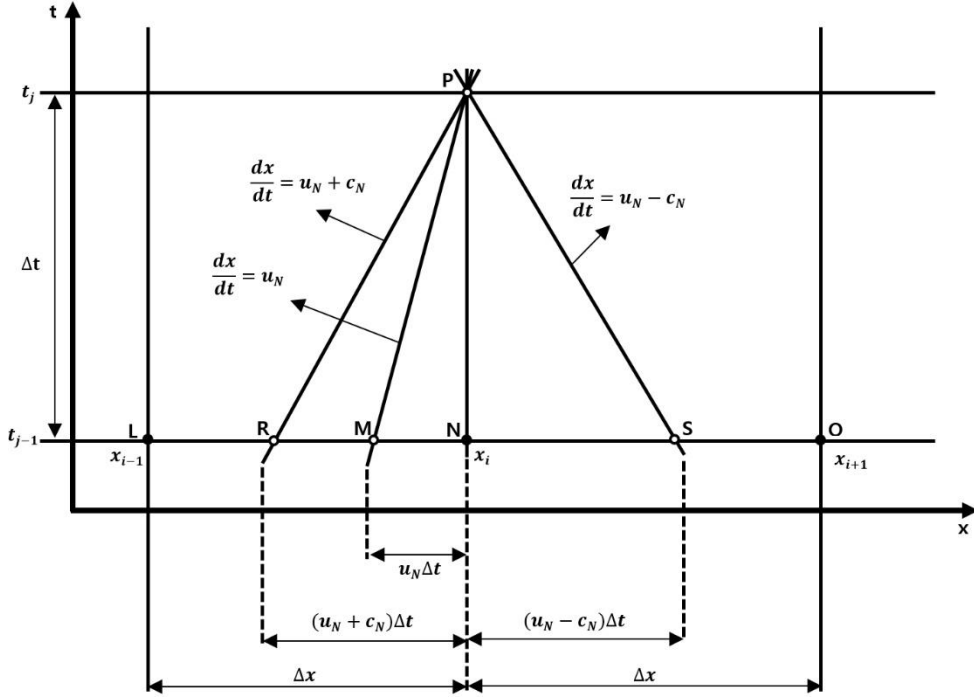


Figure 2-3. Characteristic lines used in MOC.

$$X_R = X_N + (X_L - X_N) \frac{(u_N + c_N)\Delta t}{\Delta x} \quad (2.14)$$

$$X_M = X_N + (X_L - X_N) \frac{u_N \Delta t}{\Delta x} \quad (2.15)$$

$$X_S = X_N - (X_O - X_N) \frac{(u_N - c_N)\Delta t}{\Delta x} \quad (2.16)$$

$$p_P = \frac{\gamma}{\frac{c_R}{p_R} + \frac{c_S}{p_S}} \left[(u_R - u_S) + \frac{c_R + c_S}{\gamma} + (E_{1R} - E_{2S})\Delta t \right] \quad (2.17)$$

$$u_P = u_R + \frac{c_R}{\gamma p_R} (p_R - p_P) + E_{1R} \Delta t \quad (2.18)$$

$$\rho_P = \rho_M + \frac{1}{c_M^2} [p_P - p_M - E_{3M} \Delta t] \quad (2.19)$$

$$E_{1R} = \frac{\gamma - 1}{c_R} \frac{qS}{\rho_R A} + \left(\frac{F_f}{\rho A} + g \sin \theta \right) \left[\frac{u_R (\gamma - 1)}{c_R} - 1 \right] \quad (2.20)$$

$$E_{2S} = \frac{\gamma - 1}{c_S} \frac{qS}{\rho_S A} - \left(\frac{F_f}{\rho A} + g \sin \theta \right) \left[\frac{u_S (\gamma - 1)}{c_S} + 1 \right] \quad (2.21)$$

$$E_{3M} = (\gamma - 1) \frac{qS}{A} + \frac{F_f}{\rho_M A} + g \sin \theta (\gamma - 1) u_M \rho_M \quad (2.22)$$

2.3. Novel friction models

The friction force in the dynamic equation of a PIG can be basically modeled by applying a static friction force when the PIG is stationary, and a dynamic friction force when it is moving, as shown in Figure 2-4. Speed excursion occurs owing to the difference between the static and dynamic friction forces. In most previous studies, pigging simulations were performed by inputting static and dynamic friction forces as constants shown in the equation (2.23). However, the friction model in the previous studies can only simulate the speed excursion that occurs in the initial stage, and it is difficult to simulate numerous speed excursions occurring in the total distance ratio due to bends and wall thickness variations. To overcome this limitation, in this study, two models that can express friction changes during pigging were proposed.

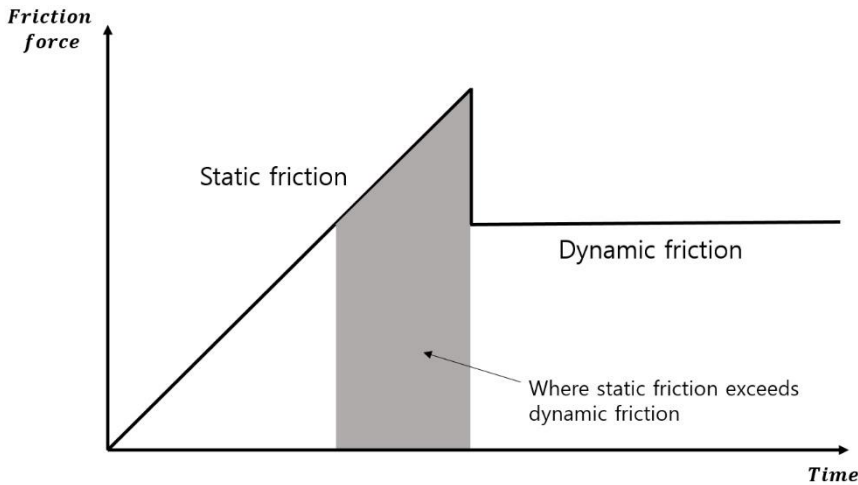


Figure 2-4. Friction force of basic friction model when PIG starts to move

$$F_f = \begin{cases} F_s & \text{if } v_p = 0 \\ F_d & \text{if } v_p \neq 0 \end{cases} \quad (2.23)$$

2.3.1 Tuned friction model

The first friction model, called tuned friction model, uses a dynamic friction table coupled with an exponential dynamic friction model to simulate the instantaneous increase in friction force when the PIG passes a bend or variation in wall thickness. The dynamic friction table is a constant table of the dynamic friction force at the locations where speed excursions will occur. This model requires field pigging data because the location and velocity of the speed excursion must be specified in advance. Figure 2-5 shows an example of the range to which the constant friction force of the dynamic friction table and the friction force calculated from the exponential friction model are applied. When the PIG passes through the bend or wall thickness variation, the friction force set in the dynamic friction table is applied. Otherwise, the friction force calculated from the exponential dynamic friction model or the default dynamic friction force is applied, which can be selected by user.

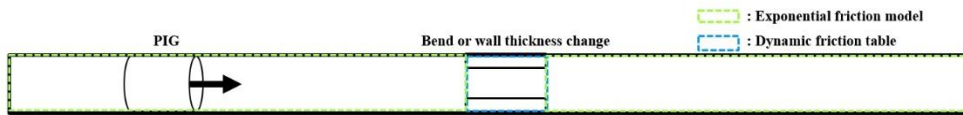


Figure 2-5. Range of dynamic friction table and exponential friction model

Figure 2-6 and equation (2.24) show how the friction force of the tuned friction model is applied. When the PIG starts to move, the first speed excursion is calculated based on the friction variation between F_s and F_d . The speed excursions that occur as the PIG passes through the bends and wall thickness changes after departure can be calculated based on the friction variation between F_d , and F_i ($F_{d1}, F_{d2}, F_{d3} \dots$). Where F_d is the dynamic friction force when PIG is at a constant velocity, and F_{d1} is the dynamic friction force at the first speed excursion, F_{d2} is the dynamic friction force at the second speed excursion, and F_{di} is the dynamic friction force at the i -th speed excursion.

$$F_f = \begin{cases} F_s & \text{if } v_p = 0 \\ F_d, F_{d1}, F_{d2}, F_{d3} \dots F_{di} & \text{if } v_p \neq 0 \end{cases} \quad (2.24)$$

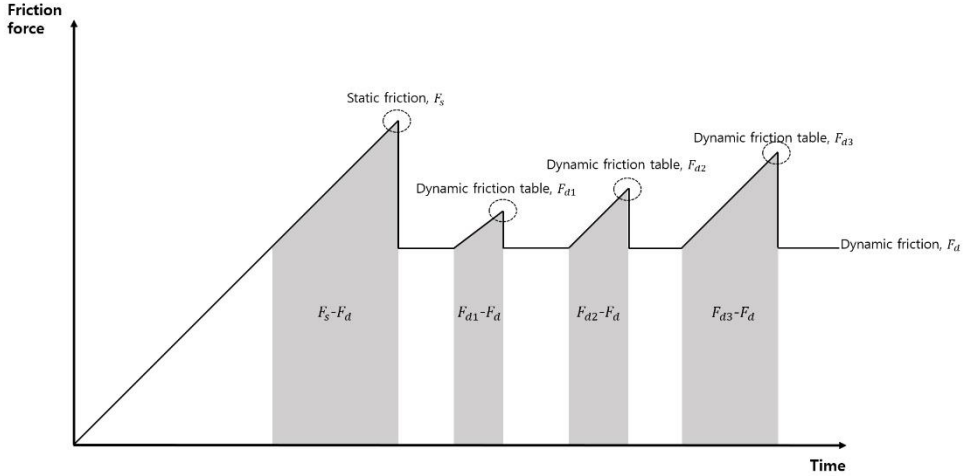


Figure 2-6. Calculation method of friction variation caused by bends and wall thickness changes in tuned friction model

F_d is estimated based on field data, however, F_{di} should be found by tuning the values that can best simulate the field PIG velocity. The friction force of F_d can be used by selecting the constant friction force set by default or the friction force calculated from the exponential model (2.25). The friction force of an object showing stick–slip motion is a function of velocity, and when the friction force decreases from static to dynamic friction, it exhibits exponential decay as a function of velocity [29]. To simulate the motion of the PIG in a manner similar to the real one, F_d was calculated using an exponential friction model.

$$F_f = F_d + (F_s - F_d)e^{-\alpha_d * |v_p|} \quad (2.25)$$

Where F_f is the friction force between PIG and pipe, F_d is the dynamic friction of PIG, F_s is the static friction of PIG, α is the decay constant, and F_s is the PIG velocity.

Figure 2-7 shows the simulation algorithm using the tuned friction model. Based on the field pigging data, the simulation was performed by inputting the initial estimated friction in the dynamic friction table. If the simulation result applying the initial estimated friction does not agree well with the field pigging data, the error can be reduced by tuning the estimated friction again.

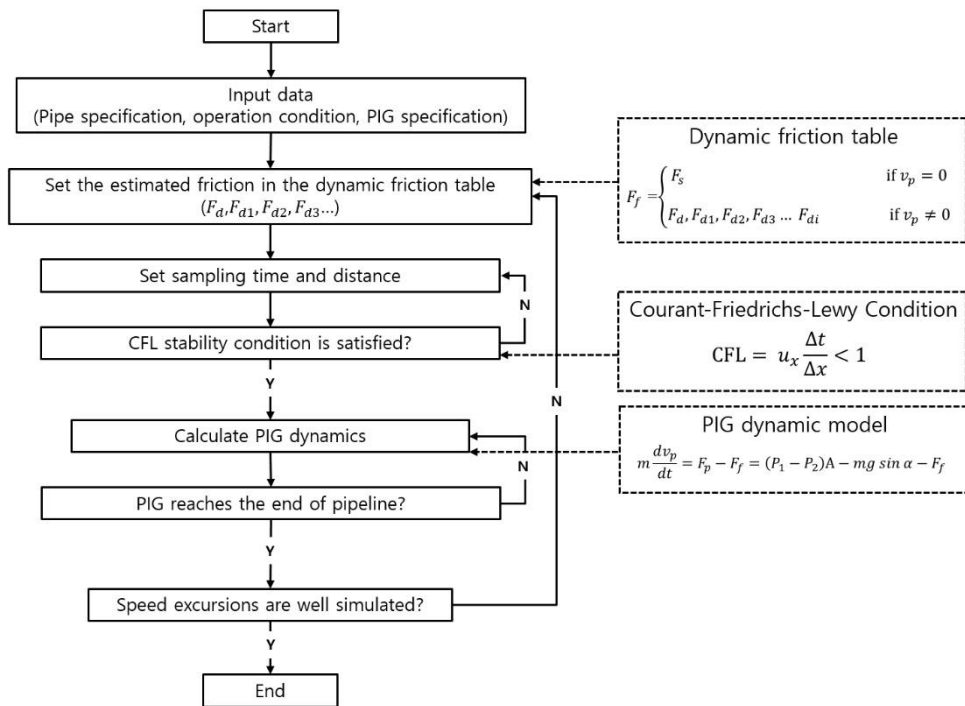


Figure 2-7. Flowchart of simulation algorithms for tuned friction model

2.3.2 Weighted friction model

The second friction model, called weighted friction model, uses the linear equation of friction variation due to bends and changes in wall thickness and weight parameters to determine the influence of each factor. Figure 2-8 shows how the model calculates friction using a network.

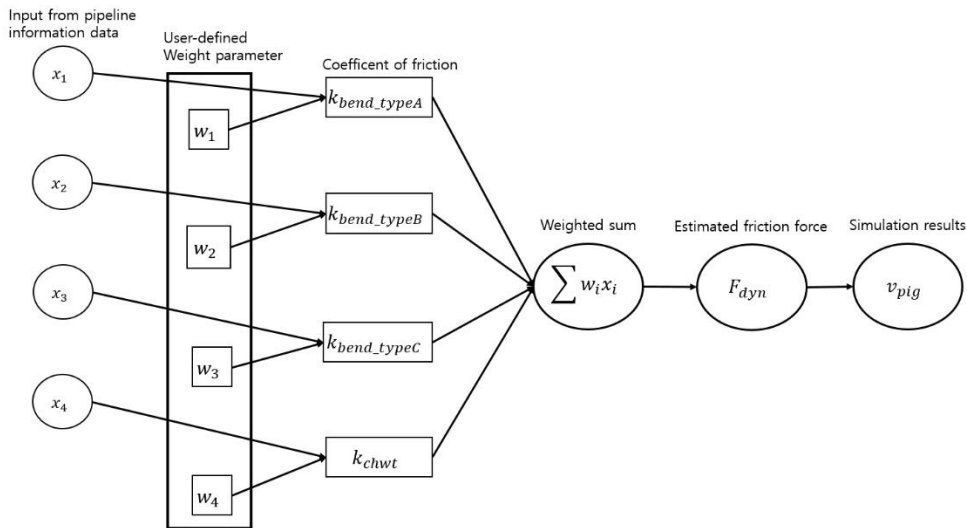


Figure 2-8. Schematic network for weighted friction model

This model has been proposed to use the field pigging data directly as an input to the linear equations, where the weight parameters are applied to determine the influence of each variable on the friction force. The amounts of added friction due to bends and changes in wall thickness are determined using the weight parameters. The bend angle and wall thickness data are loaded from the field data and then directly used as input values in the linear friction equations. In our field data, tree angles (Type A, B, and C) of bends and some wall thickness changes were observed, which were identified as the main parameters influencing the friction fluctuations.

However, if there are additional causes for the friction variation, they can be included in the model as additional parameters. In addition, by composing the formula with the increased wall thickness of the default wall thickness, it is possible

to reflect the additional friction caused by all the changes in wall thickness. The linear equations (2.26)-(2.30) for the weighted friction model are as follows:

$$F_f = F_d(1 + k_{bend} + k_{chwt}) \quad (2.26)$$

$$k_{bend_typeA} = w_1 * R_{b_typeA} \quad (2.27)$$

$$k_{bend_typeB} = w_2 * R_{b_typeB} \quad (2.28)$$

$$k_{bend_typeC} = w_3 * R_{b_typeC} \quad (2.29)$$

$$k_{chwt} = w_4 * \left(\frac{t_{chwt}}{t_0} \right) \quad (2.30)$$

Where k_{bend} is the friction coefficient of bends, k_{chwt} is the friction coefficient of wall thickness variations, R_b is the radian of bend angle, w is the weight parameter, t_0 is the initial wall thickness, and t_{chwt} is the changed wall thickness.

From the field pigging data, it was shown that when the PIG passed through bends, the friction force changed significantly depending on the angle of the bend. On the other hand, the changed wall thickness had a relatively small effect on the friction force than the bend angle. Therefore, three weight parameters were constituted to adjust the friction according to the bend angle as shown in equations (2.27)-(2.29), and the variations in wall thickness was constituted by one weight parameter as shown in equation (2.30).

Figure 2-9 shows the simulation algorithm using the weighted friction model. This algorithm simulates all the bends and wall thickness changes in the pipeline by fetching the bend and wall thickness data in the pipeline information data. The user needs to determine empirically the initial weight parameters by estimating the influence of each degree of bend and change in wall thickness on the friction force. If the simulation result applying the initial weight parameters does not agree well with the field pigging data, the error can be reduced by adjusting the weight parameters.

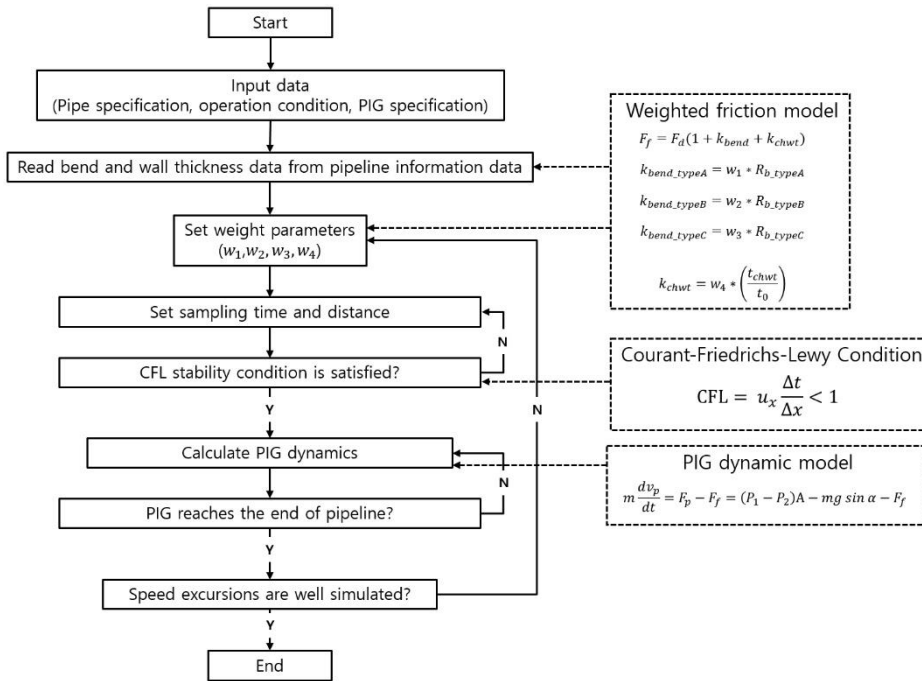


Figure 2-9. Flowchart of simulation algorithms for weighted friction model

2.4. Validation

To validate the proposed friction models, we introduce four error evaluation equations that calculate the error between the field pigging data and the simulation results of the proposed models. The simulation results were compared with the field pigging data for three different routes obtained by the KOGAS. The average absolute error (AAE) is a widely used quantitative evaluation method. As shown in equation (2.31), the difference between the field data and numerical solution is expressed as an absolute value, and the values are summed and divided by the number of observations. The root mean squared error (RMSE) is also a quantitative error that shows the difference between the field data and numerical solution (2.32). In particular, when the RMSE method is used, the greater the deviation of the error is, the larger the values. Along with these methods, the coefficient of residual mass (CRM) is used to show the extent to which the numerical solution of the model is under or overestimated compared to the observed value (2.33). If the CRM is more than 0 or less than 0, it indicates that the numerical solution is under or overestimated, respectively [40]. The mean absolute percentage error (MAPE) is a measure of simulation and prediction accuracy of models in statistics (2.34). It usually expresses the accuracy of models as a ratio.

For comparing the actual PIG velocity and simulated PIG velocity, the error was calculated using the linear interpolation method with an interval of 0.1 m in the pigging distance.

$$\text{AAE (Absolute Average Error)} = \frac{\sum_{i=1}^n |D_i - O_i|}{n} \quad (2.31)$$

$$\text{RMSE (Root Mean Squared Error)} = \sqrt{\frac{\sum_{i=1}^n (D_i - O_i)^2}{n}} \quad (2.32)$$

$$\text{CRM(Coefficient of Residual Mass)} = \frac{[\sum_{i=1}^n O_i - \sum_{i=1}^n D_i]}{\sum_{i=1}^n O_i} \quad (2.33)$$

$$\text{MAPE(Mean Absolute Percentage Error)} = \frac{100}{n} \sum_{i=1}^n \frac{|D_i - O_i|}{D_i} \quad (2.34)$$

Where D_i is the i -th actual PIG velocity from field pigging data, and O_i is the i -th simulated PIG velocity, and n is number of samples.

To validate the proposed friction model, the simulation results were compared with the field pigging data of three pipeline routes obtained by the KOGAS. The field pigging data of the two routes, Route-A and Route-B, were compared with the simulation results using the tuned friction model. Figure 2-10 shows partial field pigging data up to first 61.4 % of the total length of Route-A. The distance ratio on the x-axis indicates the ratio of the PIG travel distance to the total length of Route-A. The Route-A pipeline is correspond to the low-pressure and low-flowrate operating conditions. High-speed excursions (SE no.1, and no.4) were observed near 0.37 and 21.26 % of total travel distance, and small speed excursions (SE no.2, no.3, and no.5) were observed at 9.86, 11.93, and 51.81 % of total travel distance.

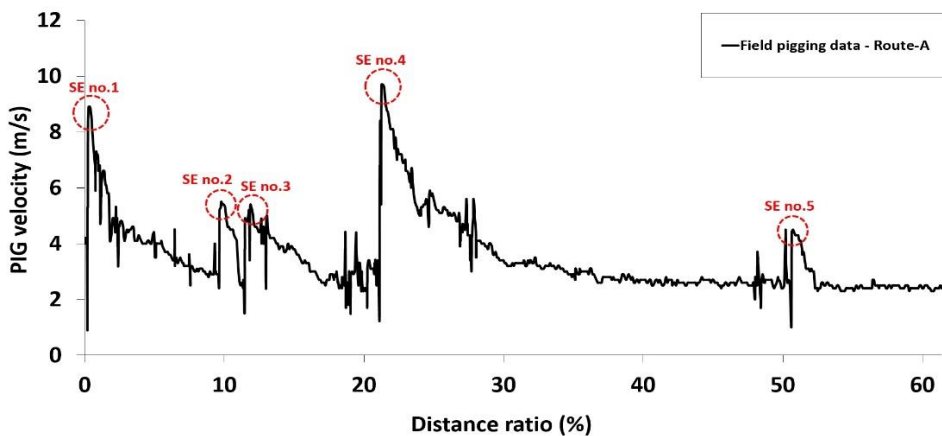


Figure 2-10. Field pigging data of Route-A

The Route-B pipeline is also corresponded to the low-pressure and low-flowrate operating conditions and three high-speed excursions (SE no.1, no.2 and no.3) were observed near 0.39, 43.93, and 77.79 % of total travel distance. In Route-C, pigging was performed under different flow conditions two times. The 1st pigging results were compared with the simulation results using the weighted friction model. Then, the speed excursions were predicted for the 2nd pigging operation conditions by adopting the weight parameters determined from the 1st pigging results. The estimated PIG velocity ratio was compared to the 2nd pigging operation data.

2.5. Results and discussion

2.5.1 Simulation of Route-A and Route-B

The operating conditions, PIG's specification, static friction, and default dynamic friction were entered based on the field pigging data. The friction values that need to be entered into the dynamic friction table of the tuned friction model are listed in Table 2-1. The initial F_{di} of the dynamic friction table that simulate speed excursion was also estimated based on field pigging data. If the simulation result applying the initial estimated friction does not agree well with the field pigging data, the error can be reduced by tuning the estimated friction again. Through several tuning processes, the dynamic friction table values in Table 2-1 were found.

In the field pigging data, local velocity fluctuation occurs more frequently because of the numerous bends and variations in wall thickness, so more friction values should be entered into the dynamic friction table for a detailed simulation. In this study, a speed excursion of approximately 5 m/s or more was considered for validation purposes. For the case of Route-A, the values of F_{d1} , F_{d2} , F_{d3} , and F_{d4} were entered into the dynamic friction table to simulate the occurrence of four speed excursions. In the case of Route-B, two speed excursions were observed over 5 m/s, and thus the values of F_{d1} and F_{d2} were entered in the dynamic friction table.

Table 2-1. Dynamic friction table of the tuned friction model for each route

Parameter	Route-A	Route-B	Unit
Static friction, F_s	0.85	1.2	bar
Default dynamic friction, F_d	0.365	0.365	bar
Dynamic friction table, F_{d1}	0.58	1	bar
Dynamic friction table, F_{d2}	0.58	1.48	bar
Dynamic friction table, F_{d3}	0.8	-	bar
Dynamic friction table F_{d4}	0.52	-	bar

Figure 2-11 shows the simulation results of Route-A using the tuned friction model. It can be observed that the average PIG velocity and speed excursions are well simulated, but a slight error occurs in the distance ratio where the speed is decelerated after the speed excursion. In order to reduce the error occurring in the deceleration distance ratio, it is necessary to input detailed boundary conditions such as operating pressure, flowrate, linepack length. However, the constant boundary is assumed in this route because of insufficient field data.

Table 2-2 shows error evaluation in total distance ratio of pipeline, and Table 2-3 shows speed excursion error for Route-A. The evaluation results suggested that the AAE and RMSE were 0.61 and 0.97, respectively, which were larger than expected. However, the MAPE for speed excursions showed a high accuracy of 3%. This result means that the deceleration distance ratio could not be simulated with high accuracy due to insufficient field data, but the speed excursion can be simulated well. Because the CRM result is 0.12, the numerical solution is underestimated compared to the field pigging data, suggesting more accurate prediction is required for the deceleration of the PIG.

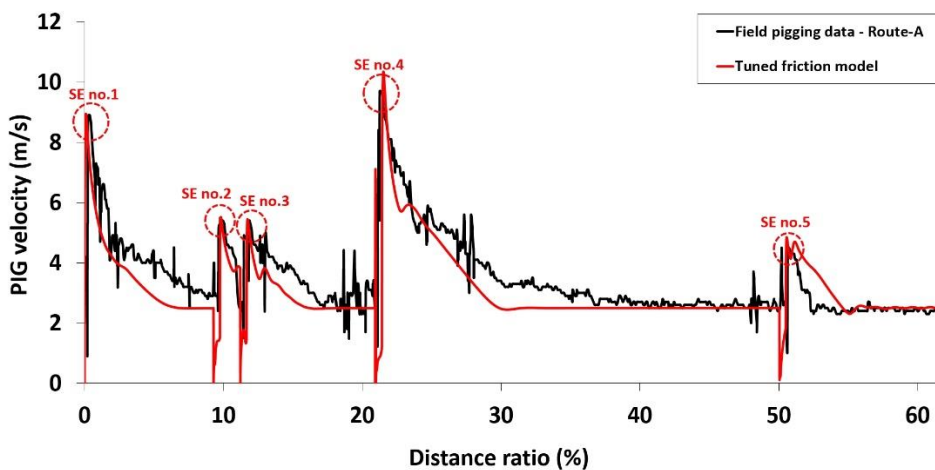


Figure 2-11. Simulated PIG velocity using the tuned friction model - Route-A

Table 2-2. Error evaluation in total distance ratio of pipeline – Route-A

Error model	Value	Criteria
AAE [m/s]	0.61	< 1 m/s
RMSE	0.97	-
CRM	0.12	CRM > 0 underestimate CRM < 0 overestimate

Table 2-3. Speed excursion error using the tuned friction model – Route-A

SE no.	Distance ratio (%)	PIG velocity		Error rate (%)
		Field pigging data (m/s)	Simulation (m/s)	
1	0.37	8.9	8.93	0.33
2	9.86	5.5	5.48	0.36
3	11.93	5.4	5.44	0.74
4	21.26	9.7	10.3	6.2
5	51.81	4.5	4.83	7.3
MAPE (%)				3

Figure 2-12 shows the simulation results of Route-B using the tuned friction model. In this route, detailed boundary conditions were entered due to sufficient field data. Therefore, it was able to simulate the average speed and speed excursion well in total distance ratio. Table 2-4 shows error evaluation in total distance ratio of pipeline, and Table 2-5 shows speed excursion error for Route-B. In the table, it was confirmed that the AAE and RMSE were 0.33 and 0.54, respectively, which was relatively lower than the error of Route-A. Also, the MAPE for speed excursions showed a high accuracy of 0.79%. Because the CRM result is 0.0044, the numerical solution is slightly underestimated compared to the field pigging data. These error result

shows that average speed and speed excursion of PIG can be simulated with high accuracy due to the detailed boundary conditions.

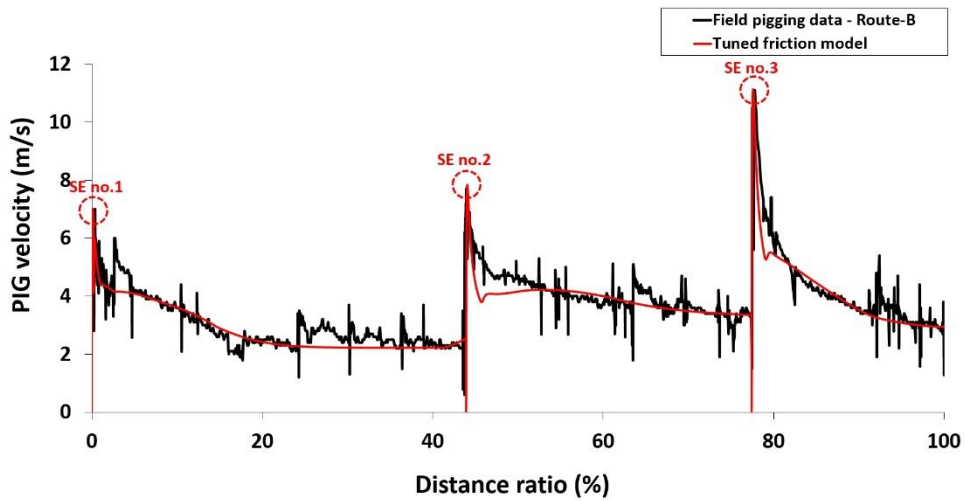


Figure 2-12. Simulated PIG velocity using the tuned friction model - Route-B

Table 2-4. Error evaluation in total distance ratio of pipeline – Route-B

Error model	Value	Criteria
AAE [m/s]	0.33	< 1 m/s
RMSE	0.54	-
CRM	0.0044	CRM > 0 underestimate CRM < 0 overestimate

Table 2-5. Speed excursion error using the tuned friction model – Route-B

SE no.	Distance ratio (%)	PIG velocity		Error rate (%)
		Field pigging data (m/s)	Simulation (m/s)	
1	0.39	7	6.99	0.14
2	43.93	7.64	7.79	1.96
3	77.79	11.06	11.09	0.27
MAPE (%)				0.79

2.5.2 Simulation and prediction of Route-C

The operating conditions, static friction, and default dynamic friction were entered based on the field pigging data. To simulate the speed excursion with a weighted friction model, it is necessary to determine the weight parameters considering the influence of each variable on the friction. The influences of the bends and wall thickness of Route-C on the friction and weight parameters are listed in Table 2-6. When passing through a bend of Type A, the friction is instantaneously increased by 20% compared to the default dynamic frictional force; in the bend of Type B, it is increased by 32%, and in the bend of Type C, it is increased by 51%.

In the case of increased friction due to variation in wall thickness, the default wall thickness is the straight pipe's wall thickness, and the friction increases instantaneously by 30%, 37%, and 40% owing to increases in wall thickness of 2.4, 5.6, and 7.2 mm, respectively. The increase in friction for each variable was determined using the weight parameter. In Route-C, pigging was performed twice under different operating conditions. Using the weight parameter determined from the 1st pigging operation, simulation was performed to observe whether the field pigging data for 2nd pigging could be matched.

Table 2-6. Friction increase by weight parameter for each variable

Variable	Weight parameter	Route-C		Friction increase (%)
		1st pigging	2nd pigging	
Type A bend	w_1	0.5	0.5	20
Type B bend	w_2	0.41	0.41	32
Type C bend	w_3	0.33	0.33	51
Increase of 2.4 mm wall thickness				30
Increase of 5.6 mm wall thickness	w_4	0.25	0.25	37
Increase of 7.2 mm wall thickness				40

The simulation results of Route-C in the 1st pigging using the weighted friction model are shown in Figure 2-13 (a). For this route, detailed boundary conditions were entered due to sufficient field data. Despite the numerous bends and changes in wall thickness in the total distance ratio, it can be observed that the field pigging data and the average PIG velocity of the simulation agree well.

However, the error of AAE and RMSE of 1st pigging simulation are shown in Table 2-7 as 0.51 and 0.81, which are relatively higher than the error results of Route-B. The reason is that the larger local error was calculated since the numerous speed excursions due to all bends and wall thickness changes in the total distance ratio were simulated. The MAPE for speed excursions showed a relatively higher accuracy of 5.73% as shown in Table 2-8. This means that the weighted friction model generates a relatively higher error, but the error rate of 5.73% is a reasonable error because it generates an average error of about 0.24 m/s.

The result of predicting speed excursion by inputting the weight parameters determined in the 1st pigging simulation to the 2nd pigging operation conditions is

shown in Figure 2-13 (b). Despite the different operating conditions in 1st and 2nd pigging, the average PIG velocity and speed excursion of 2nd pigging were able to predict similarly to the accuracy of the 1st pigging simulation. The AAE and RMSE of the 2nd pigging simulation are shown in Table 2-7 as 0.56 and 0.85, which are very similar to the error values of the 1st pigging simulation. The MAPE of 2nd pigging is shown in Table 2-9 as 7.25%, which value slightly increased compared to the MAPE of the 1st simulation, but it is also reasonable because it generates an average error of 0.36 m/s.

These obtained results suggest that the speed excursions can be predicted very well even under the different operating conditions once the weight parameters are specified for the route.

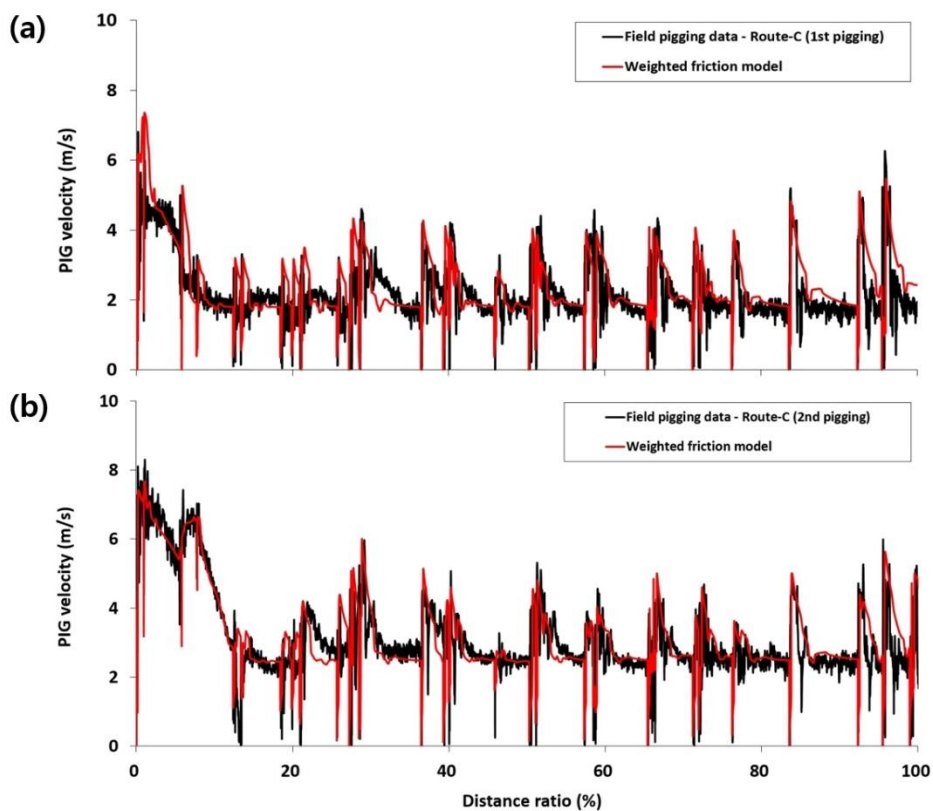


Figure 2-13. Prediction of PIG velocity for future pigging using the weighted friction model - (a) simulated PIG velocity at the 1st pigging (b) predicted PIG velocity at the 2nd pigging.

Table 2-7. Error evaluation in total distance ratio of pipeline – Route-C (1st and 2nd pigging)

Case	Error model	Value	Criteria
1st pigging simulation	AAE [m/s]	0.51	< 1 m/s
	RMSE	0.81	-
	CRM	-0.0052	CRM > 0 underestimate CRM < 0 overestimate
2nd pigging simulation	AAE [m/s]	0.56	< 1 m/s
	RMSE	0.85	-
	CRM	-0.00134	CRM > 0 underestimate CRM < 0 overestimate

**Table 2-8. Speed excursion error of 1st pigging using weighted friction model –
Route-C**

SE no.	Distance ratio (%)	PIG velocity		Error rate (%)
		Field pigging data (m/s)	Simulation (m/s)	
1	1.0	7.33	7.36	0.38
2	5.9	5.251	5.23	0.36
3	7.8	3.2833	3.13	4.58
4	12.5	2.9	3.18	9.66
5	18.7	3.05	3.17	3.93
6	20.1	2.9	3.17	9.24
7	21.3	3.25	3.15	3.20
8	25.9	3.22	3.13	2.80
9	27.5	3.91	4.00	2.28
10	28.6	4.55	4.24	6.75
11	36.4	4.18	4.25	1.72
12	40.0	4.2	3.75	10.67
13	46.3	2.79	2.82	1.08
14	51.1	4.03	3.83	4.99
15	57.6	3.93	3.89	1.02
16	58.7	4.55	3.84	15.60
17	66.3	4.33	3.78	12.77
18	76.5	3.78	3.98	5.29
19	83.6	5.17	4.80	7.25
20	92.3	4.92	5.11	3.76
21	95.5	6.23	5.41	13.09
MAPE (%)			5.73	

**Table 2-9. Speed excursion error of 2nd pigging using weighted friction model
– Route-C**

SE no.	Distance ratio (%)	PIG velocity		Error rate (%)
		Field pigging data (m/s)	Simulation (m/s)	
1	1.0	8.06	7.66	4.91
2	5.9	7.40	6.42	13.24
3	7.8	7.03	6.63	5.66
4	12.5	3.53	3.39	3.97
5	18.7	3.06	2.95	3.59
6	20.1	3.59	3.26	9.16
7	21.3	4.05	4.20	3.68
8	25.9	4.03	4.37	8.44
9	27.5	4.55	5.05	11.04
10	28.6	5.95	6.00	0.84
11	36.4	4.58	5.12	11.79
12	40.0	5.03	4.59	8.78
13	46.3	2.77	2.72	1.81
14	51.1	5.27	4.76	9.68
15	57.6	3.86	3.58	7.25
16	58.7	4.54	4.03	11.24
17	66.3	4.53	4.96	9.56
18	76.5	3.58	3.61	0.84
19	83.6	4.77	5.00	4.92
20	92.3	5.24	4.40	16.07
21	95.5	5.98	5.63	5.82
MAPE (%)			7.25	

2.5.3 Comparison of the proposed models

In order to compare the differences between the two proposed friction models, the simulation results using the tuned friction model and weighted friction model were compared for the 1st pigging result of Route-C. As seen in Figure 2-14 (a) and (b), it can be seen that both friction models fit the field data well.

However, in the speed excursion error as shown in Table 2-10, the performance of the friction models is slightly different. The MAPE of the tuned friction model and the weighted friction model. The MAPE of the tuned friction model and the weighted friction model and were 5.2% and 5.73%, respectively. The tuned friction model has higher accuracy because the friction could be adjusted individually, while the weighted friction model has a relatively larger error because the friction was adjusted as a group through the weight parameters.

The obtained results suggest that the operators are able to choose the appropriate friction model considering the objective of the PIG simulation. For the case of analyzing the speed excursion with high accuracy, it is recommended to choose the tuned friction model as all friction force that cause speed excursions can be tuned through a dynamic friction table. For the case of predicting the speed excursion, it is recommended to choose the weighted friction model because once the weight parameters are specified, speed excursion can be quickly simulated, including all bends and wall thickness variations in the total distance ratio of the pipeline. In addition, it was confirmed speed excursion prediction is possible even if the operating conditions change as shown in Figure 2-13.

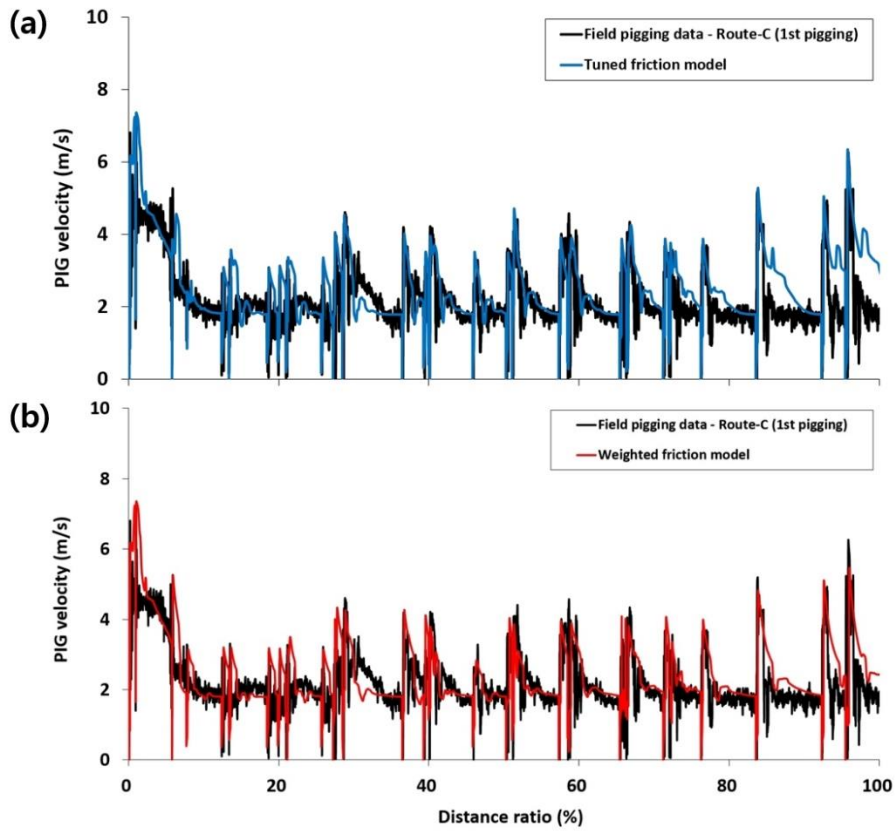


Figure 2-14. Comparison of tuned friction model and weighted friction model.

(a) Simulated PIG velocity with tuned friction model. (b) Simulated PIG velocity with weighted friction model

Table 2-10. Comparison of speed excursion error between tuned friction model and weighted friction model

SE no.	Distance ratio (%)	Field	Tuned friction model		Weighted friction model	
		pigging data (m/s)	Simulation (m/s)	Error rate (%)	Simulation (m/s)	Error rate (%)
1	1.0	7.33	7.36	0.41	7.36	0.38
2	5.9	5.25	4.55	13.35	5.23	0.36
3	7.8	3.28	2.80	14.72	3.13	4.58
4	12.5	2.9	3.05	5.17	3.18	9.66
5	18.7	3.05	3.04	0.33	3.17	3.93
6	20.1	2.9	3.11	7.24	3.17	9.24
7	21.3	3.25	3.32	2.15	3.15	3.20
8	25.9	3.22	3.34	3.73	3.13	2.80
9	27.5	3.91	4.03	3.07	4.00	2.28
10	28.6	4.55	4.49	1.32	4.24	6.75
11	36.4	4.18	3.98	4.78	4.25	1.72
12	40.0	4.2	3.89	7.38	3.75	10.67
13	46.3	2.79	2.96	6.09	2.82	1.08
14	51.1	4.03	3.47	13.90	3.83	4.99
15	57.6	3.93	3.88	1.27	3.89	1.02
16	58.7	4.55	3.89	14.51	3.84	15.60
17	66.3	4.33	4.25	1.85	3.78	12.77
18	76.5	3.78	3.87	2.38	3.98	5.29
19	83.6	5.17	5.25	1.62	4.80	7.25
20	92.3	4.92	5.04	2.40	5.11	3.76
21	95.5	6.23	6.33	1.61	5.41	13.09
MAPE (%)			5.2		5.73	

2.5.4 Linepack effect on simulation results

Overall, the simulation results of Section 2 showed a large error in the deceleration section, showing a MAE error of 0.5 to 0.6 m/s. We found that the linepack accuracy has a significant effect on the deceleration section results. Figure 2-15 (a) and (b) showed the simulation results according to linepack accuracy. If the linepack at the rear of the PIG is entered excessively, overestimated results are shown in the deceleration section. On the other hand, if the linepack on the rear of the PIG is entered insufficiently, underestimated results are shown in the deceleration section. Therefore, in order to reduce errors, it is necessary to enter the correct linepack value based on field data. However, in the case of a pipeline network, it is difficult to accurately estimate the linepack value, so an approximate linepack can be found through a parametric study.

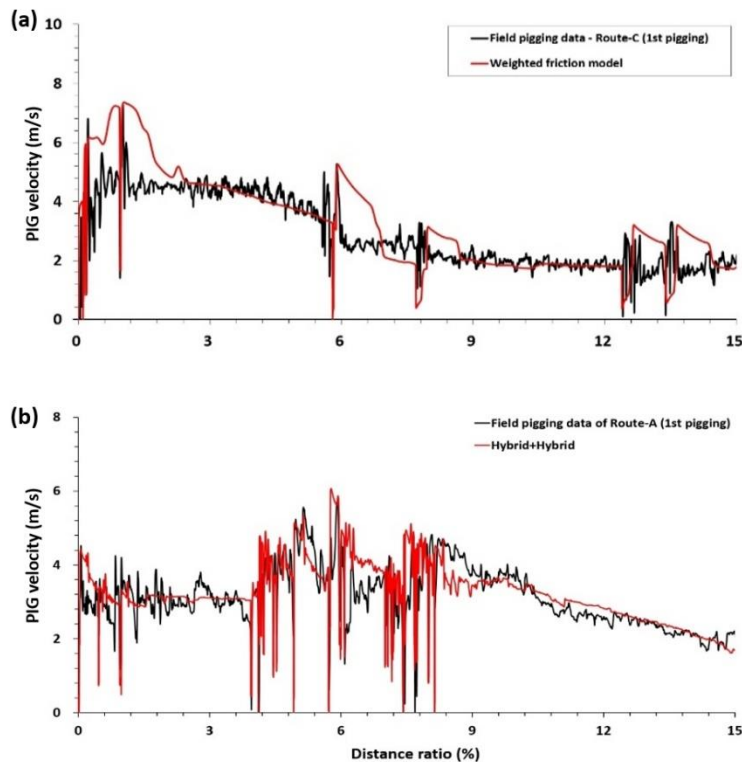


Figure 2-15. Simulation accuracy according to linepack (a) Low accuracy (b) High accuracy

2.6. Summary

This study proposed two novel friction models of pipeline inspection gauges (PIGs) to simulate and predict speed excursions occurring in the total distance ratio of a pipeline generated by numerous bends and changes in wall thickness. These two friction models are tuning models based on field data to simulate speed excursions due to frictional variation, and can be strategically selected according to the purpose of the simulation. These results mean that the speed excursion at the total distance ratio can be simulated and predicted with high accuracy using the proposed friction models. Therefore, these two novel friction models would provide insights for the operators to simulate and predict the dynamics of the PIGs in their pipeline networks. The main conclusions and further research are as follows:

- a) The first proposed model, the tuned friction model, has high accuracy because it can directly input the friction force at the locations where speed excursions occur. In addition, all friction forces can be individually tuned. However, modeling may require significant time because it is necessary to tune the friction of numerous bends and wall thickness variations. In addition, if the operating conditions are changed, the simulation results and field pigging data may deviate; therefore, the friction force must be adjusted again. This model can simulate speed excursion with high accuracy, but the prediction accuracy decreases when the input conditions change.
- b) The second proposed model, the weighted friction model, shows slightly lower accuracy than that of the tuned friction model. Because the simulation is performed by determining the influence of the bends and variations in wall thickness with weight parameters, it may be different from the field conditions. However, once the weight parameters are specified, speed excursion can be quickly simulated, including all bends and wall thickness variations in the total distance ratio. In addition, it was confirmed speed excursion prediction is possible even if the operating conditions change.

Therefore, this model is suitable for use in the field because it is possible to predict the speed excursion of routes where pigging has been performed even only once in the past.

- c) Further research is needed to reduce the error between the actual pigging data and the simulation results. To reduce the speed excursion error, the weight parameters of the weighted friction model and the dynamic friction table of the tuned friction model should be optimized. It is necessary to find the value that generates the minimum error of speed excursion that occurs in the total distance ratio using the optimization technique. To reduce the AAE and RMSE, the error occurring in the distance ratio where the speed is decelerated after the speed excursion occurs should be reduced. Therefore, it is necessary to consider the gravitational term in PIG dynamics owing to the pipeline elevation and utilize detailed field operation data for the boundary condition.

Finally, it was assumed that the error due to the one-dimensional model of gas flow would not be large because the non-bypass PIG was adopted in this study. However, since the one-dimensional model of gas flow may differ from the actual flow, improvement is needed to reduce the error caused by the flow model part.

2.7. Acknowledgement

This chapter is partially adapted from Speed excursion simulation of PIG using improved friction models in *Journal of Natural Gas Science and Engineering* 97 (2022) 104371 with authors S. Kim, K. Yoo, B. Koo, D. Kim, H. Yoo, and Y. Seo. (<https://doi.org/10.1016/j.jngse.2021.104371>). This work was supported by Development of Next Generation Pipeline Robot Technology for the Long-Distance Inspection of the Low Pressure/the Low Flow of Gas Pipelines (RD 2019-0251) research project from Korea Gas Corporation (KOGAS).

Chapter 3. Experiment investigation on speed excursion of PIG due to friction variation in natural gas pipeline**

3.1. Introduction

Pipelines are the safest and most cost-efficient method for transporting large amounts of natural gas from gas reserves to major markets. Safety is the first priority in transporting natural gas to avoid fatal accidents in urban areas. Currently, a pipeline inspection gauge (PIG) is used to detect defects and clean deposits in pipelines. Most pigging operations in gas pipelines are performed at normal operating pressures with regular flow rates, and the PIG velocity is generally in the range of 2–5 m/s. However, pigging in low-pressure and low-flowrate gas pipelines is very difficult due to speed excursion, which rapidly increases the PIG velocity. Mitigating speed excursions is an important challenge during the gas pipeline pigging process [45].

The main causes of the speed excursion are the gas compression at the rear end and the change in the friction force at the front end of the PIG. Speed excursions may lead to potential inspection data loss and are dangerous due to their high acceleration. A speed excursion of over 5 m/s can reduce the data acquisition efficiency, and a speed excursion of over 15 m/s can largely impact the PIG body and pipe wall [41].

Research related to PIG dynamics has mostly focused on engineering simulations to predict the dynamics [1, 10, 18, 20, 28, 34, 35, 39, 49]. Only a few papers have addressed the speed excursion phenomenon during natural gas pipeline pigging [19, 26, 32].

Researchers have conducted experiments on bypass pigging technology [5, 6, 7, 19,

** This chapter is partially adapted from Experimental study on speed excursion of PIG due to friction variation in natural gas pipeline in Journal of Natural Gas Science and Engineering with authors S. Kim, J. Jeong, K. Yoo, H. Yoo, and Y. Seo (<https://doi.org/10.1016/j.jngse.2022.104659>).

21, 30, 52]to investigate PIG dynamics. A few studies have focused on the friction and resistance of PIG [12, 33, 47, 50]. Experimental studies have mostly focused on investigating the intrinsic mechanisms of pigging, but fundamental studies on speed excursion phenomenon due to friction variations during natural gas pipeline pigging have not been conducted. Therefore, pigging operations with speed excursions rely heavily on this rule of thumb. This study is the first to conduct a lab-scale experiment to study the effects of friction variation during gas pipeline pigging on speed excursion. We aim to investigate the mechanism of speed excursion and the relationship between speed excursion and main variables as flowrate, wall thickens change, and linepack length. Moreover, the equation of friction increase ratio according to the wall thickness change ratio was proposed from the experimental results. The results were validated by our in-house pigging solver within 8.5% error of speed excursion.

3.2. Experimental system

3.2.1 Speed excursion experimental system

Based on the schematic of the speed excursion experimental system shown in Figure 3-1, the experimental setup was designed and constructed to measure the differential pressure and speed excursions of the PIG.

A feature of this setup is the detachable wall thickness change section to generate speed excursions due to friction variations. The first and second wall thickness change sections were installed on the horizontal pipeline at 4.5 m and 9 m from the starting position, respectively. The friction of these sections can be controlled by adjusting the inner diameter of the flanges as shown in Figure 3-2(b). Two flanges are installed 4.5 m, and 9 m from the Inlet, and these lengths are defined as linepack length.

A high-speed camera (Photron, FASTCAM Mini UX50) was installed near the wall thickness change sections to measure the peak PIG velocity during speed excursions.

The horizontal pipeline system installed in the laboratory and the wall thickness change section installed on the horizontal pipeline are shown in Figures 3-2(a) and 3-2(b), respectively.

A pipeline with an inner diameter of 50.8 mm and a total length of 24.1 m was made of transparent PVC material to visually analyze the speed excursion process. Five pressure sensors (Wika, A-10) were installed to measure the differential pressure of the PIG. The location of each sensor is listed in Table 3-1. Table 3-1 shows the properties of the speed excursion experimental system, where the outlet pressure is 1 atm, and the maximum air velocity can be controlled up to 6 m/s. Details regarding the materials used for the experimental system are listed in Table 3-2.

The experimental procedure is as follows. First, the air pressurized by the compressor is stored in the buffer tank and undergoes a pressure stabilization process. Air is then stably supplied to the horizontal pipeline system through precise flow

adjustment using a mass flow controller (MFC, Brooks SLA5853S). The designed PIG for the experiment was placed into the launcher, and the required gas flow rate was set for pigging preparation. The master valve is adjusted so that the flow goes to the rear of the PIG to start the PIG, and differential pressure is formed to move the PIG.

The differential pressure that causes all movements from the start of the PIG is measured using five pressure sensors. The speed excursion that occurs when passing through the wall thickness change is measured using a high-speed camera. Data is acquired using the LabVIEW software.

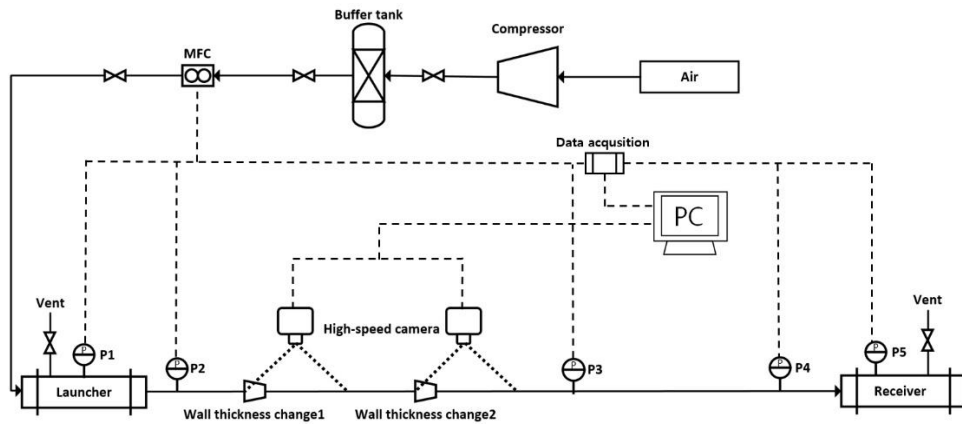


Figure 3-1. Schematic of speed excursion experimental system

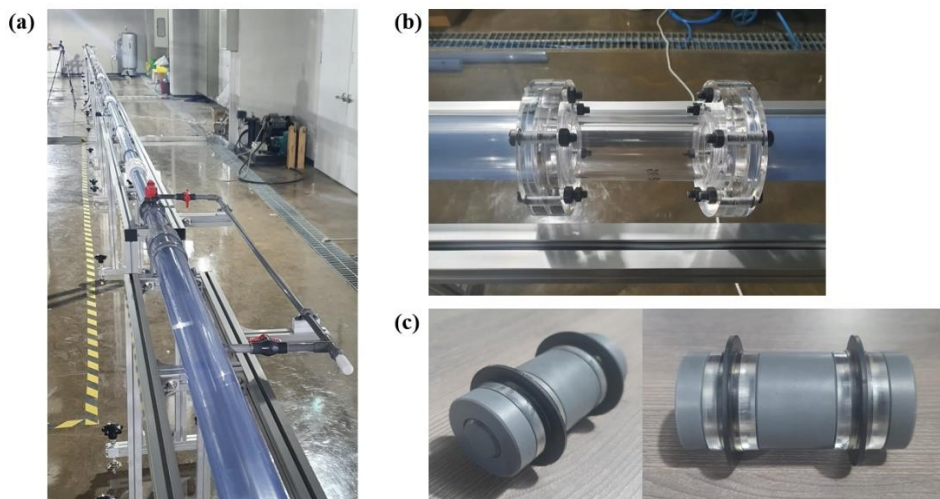


Figure 3-2. Experimental apparatus (a) Horizontal pipeline system (b) Wall thickness change section (c) Experimental pig

Table 3-1. Properties of speed excursion experimental system

Property	Symbol	Value	Unit
Pipeline length	L_{pipe}	24.1	m
Inner diameter of pipe	d_o	50.8	mm
Inner diameter of wall thickness change	d_i	49.8	mm
		48.8	
Outlet pressure	P_{out}	1	atm
Max. air velocity	$V_{f,max}$	6	m/s
Position of P1	L_{p1}	0.2	m
Position of P2	L_{p2}	2.5	m
Position of P3	L_{p3}	10	m
Position of P4	L_{p4}	16.5	m
Position of P5	L_{p5}	19.5	m
Linepack length of Wall thickness change 1	L_{wt1}	4.5	m
Linepack length of Wall thickness change 2	L_{wt2}	9	m
PIG mass	m_{pig}	0.153	kg
PIG length	L_{pig}	90	mm

Table 3-2. Materials used in speed excursion experimental system

Structure	Material
PIG body	PVC
Sealing disk	EPDM
Clamping disk	Perspex
Spacer disk	Perspex
Pipe	PVC
Wall thickness change section	PVC

3.2.2 Wall thickness change section

A schematic of the change in wall thickness is shown in Figure 3-3. The wall thickness change sections were installed on the horizontal pipeline. The friction of these sections was controlled by adjusting the inner diameter d_i of the flanges. The wall thickness change ratio, γ_{wt} , is defined in Equation (3.1). In our previous field pigging study [26], the wall thickness change ratio was in the range 0.9%~3%. Based on these calculations, 49.8 mm and 48.8 mm were selected as inner diameter d_i value for 1.97% and 3.94% of γ_{wt} .

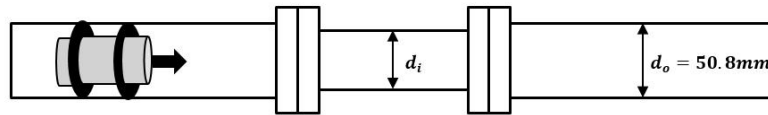


Figure 3-3. Schematic of wall thickness change section

$$\gamma_{wt} = \left(1 - \frac{d_i}{d_o}\right) * 100\% \quad (3.2)$$

3.2.3 Design of experimental PIG

The experimental PIG with all design dimensions is shown in Figure 3-4. The PIG was designed with structural parameters (3.2)–(3.4) suggested by a previous study [50]. The low-friction PIG was designed to minimize the contact force between the sealing and pipe wall. Its structural parameters are listed in Table 3-3.

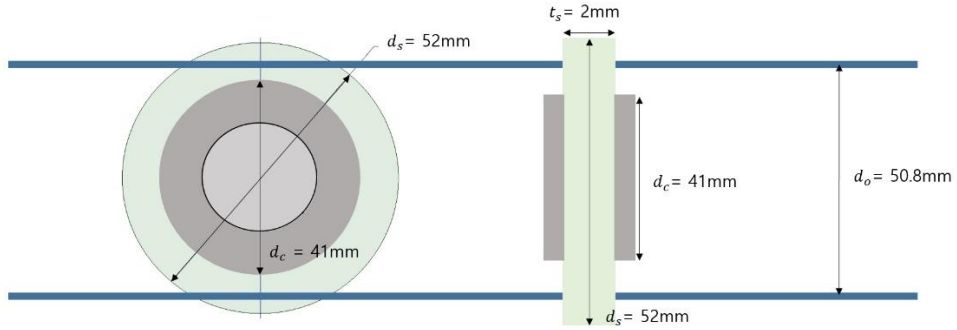


Figure 3-4 Experimental PIG with all design dimensions

$$\alpha_s = \frac{d_s - d_o}{d_o} * 100\% \quad (3.2)$$

$$\beta_s = \frac{d_c}{d_s} * 100\% \quad (3.3)$$

$$\delta_s = \frac{t_s}{d_s} * 100\% \quad (3.4)$$

Table 3-3. Structural parameters of experimental PIG

Parameter	Equation	Value (%)
Interference	$\alpha_s = \frac{d_s - d_o}{d_o} * 100\%$	2.4
Clamping rate	$\beta_s = \frac{d_c}{d_s} * 100\%$	78.8
Thickness ratio	$\delta_s = \frac{t_s}{d_s} * 100\%$	3.8

Where d_o is the Internal diameter of pipe, d_s is the outer diameter of sealing disc, d_c is the outer diameter of spacer disc, and t_s is the thickness of sealing disc.

3.3. Results and discussion

The influence on the speed excursion of the airflow rate Q_{air} , wall thickness change ratio γ_{wt} , and linepack length L_{wt} were studied in detail to investigate the relationship between to investigate the relationship between speed excursion and main variables as flowrate. The controllable variables used in the experiment are listed in Table 3-4.

Table 3-4. Controllable variables for speed excursion experiment

Experimental variable	Range of variation	Unit
Q_{air}	25, 50, 75, 100, 150, 200, 250, 300, 350, 400, 450, 500, 550, 600, 650	l/min
γ_{wt}	1.97, 3.94	%
L_{wt}	4.5, 9	m

Note: Q_{air} is airflow rate, γ_{wt} is wall thickness change ratio, and L_{wt} is linepack length

Section 3.1 describes the mechanism of speed excursion and explains the measurement and comparison to investigate the speed excursion phenomenon. Sections 3.2, 3.3, and 3.4 discuss the relationship between the variables and speed excursion based on the experimental results. Finally, in Section 3.5, the numerical simulation results are presented along with formulas derived from the experimental results.

3.3.1 Mechanism of speed excursion

This section describes the mechanism of speed excursion and measurements and analyses the results. Based on differential pressure in Figure 3-5 (a), a typical mechanism and process of speed excursion due to friction variations can be derived 5 phases: (i) stable behavior, (ii) build-up phase, (iii) Pre-speed excursion phase, (iv) Speed excursion phase, and (v) Recovery phase. The PIG exhibited stable behavior until it encountered friction variation.

In the build-up phase, the PIG speed decreased as the PIG encountered a section where the friction and differential pressure increased, as the fluid was compressed at the rear of the PIG. During this process, the PIG moved slowly and was positioned at the end of this section; at this time, the peak differential pressure was achieved.

The period in which the maximum differential pressure was reached is defined as the pre-speed excursion phase. When the PIG passed through the friction increase section, the increased friction was momentarily removed, and the force on the PIG was unbalanced. The rear of the PIG was pushed by a force by the compressed fluid, generating the maximum differential pressure. However, the resistance force was removed from the front of the PIG. Therefore, the difference in force caused the PIG to accelerate instantaneously, defined as the speed excursion phase. As the PIG moved at a higher velocity, a large volume was created at the rear of the PIG; the differential pressure was quickly released to fill this volume. The PIG stopped when the pressure dropped below the dynamic differential pressure. As it returned to the dynamic differential pressure, the PIG returned to its normal velocity. This phase was defined as the recovery phase.

Photographic images of the speed excursion patterns at the wall thickness change were captured at 500 fps using a high-speed camera to visually analyze the speed excursion process, as shown in Figure 3-5(b). Through this mechanism, four major measurement values—build-up time at the build-up phase, peak differential at the pre-speed excursion phase, speed excursion velocity at the speed excursion phase, and recovery time at the recovery phase—were measured and compared to

investigate the speed excursion phenomenon based on the mechanism of speed excursion.

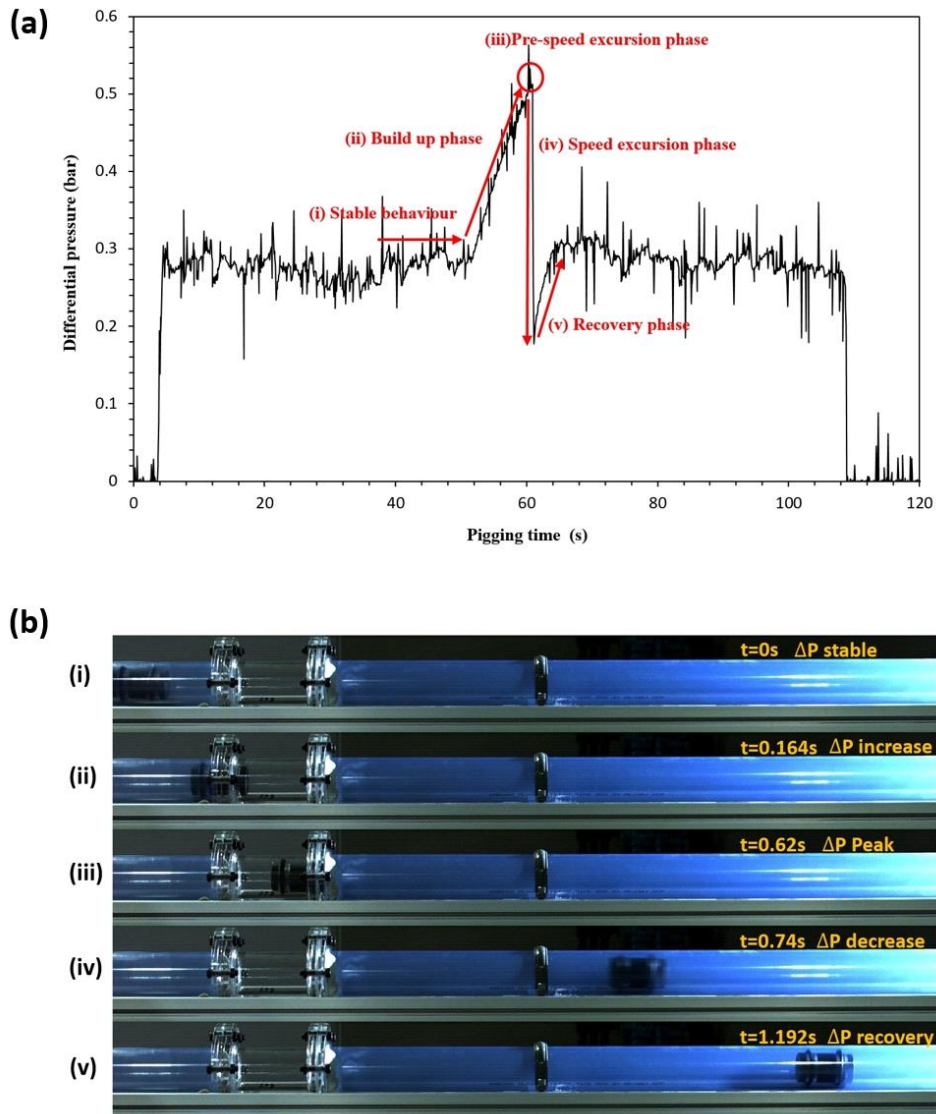


Figure 3-5. (a) Mechanism of speed excursion. (b) Speed excursion process based on the differential pressure is displayed through: (i) Stable behavior, (ii) Build-up phase, (iii) Pre-speed excursion phase, (iv) Speed excursion phase, and (v) Recovery phase.

3.3.2 Effect of flowrate

The experimental results of the average PIG velocity according to the flow velocity were compared with the results of other studies [7, 19] to validate our experiment, as shown in Figure 3-6.

The PIG velocity should be equal to the upstream flow velocity when it has no bypass hole. Our experimental results showed a linear relationship with the flow velocity and followed the Idelchik relation. In addition, our experimental system can be considered well-designed as our results were consistent with the results of other experimental studies.

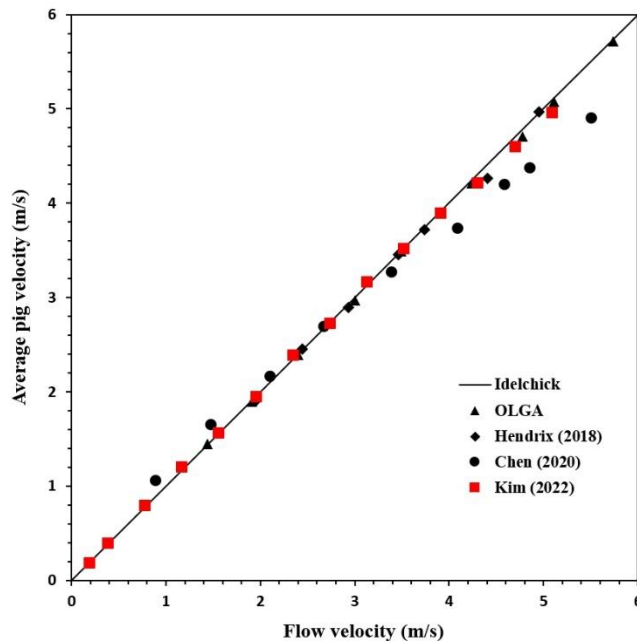


Figure 3-6. Measured average PIG velocity as function of flow velocity

Table 3-5. Fitting formula, R-squared, and covariance of the average PIG velocity according to the flow velocity

Reference	Fitting formula	R ²	Covariance
Idelchik	$v_{av_pig} = v_{air}$	1	6.67
OLGA	$v_{av_pig} = 1.0022v_{air} - 0.0247$	0.9998	3.3
Hendrix (2018)	$v_{av_pig} = 0.9933v_{air} - 0.0115$	0.9976	0.96
Chen (2020)	$v_{av_pig} = 0.9558v_{air} - 0.0434$	0.99	4.48
Kim (2022)	$v_{av_pig} = 0.9762v_{air} - 0.0305$	0.9995	2.51

Figure 3-7(a) shows the measured speed excursions according to the flow velocity for $\gamma_{wt} = 1.97\%$ and $L_{wt} = 4.5$ m. As seen in Figure 3-7(a) the speed excursion had a linear relationship with the flow velocity. However, the excursion ratio, which indicates the excursion speed compared to the average speed, was an exponential function. It increased rapidly at a low flow velocity, as shown in Figure 3-7(b). These results indicate that low-flowrate pigging produces relatively low-speed excursions but can be a risky operation because of the rapid increase in the excursion ratio (Figure 3-7(e), and Movie 1). However, high-flowrate pigging caused high-speed excursion; thus, it can also be a risky operation due to high-speed excursion (Figure 3-7(f) and Movie 2).

Figure 3-7(c) and (d) show the build-up and recovery time according to the flow velocity. Both showed an exponential curve that increased rapidly at low flow velocities. These results indicate that pigging behavior is significantly unstable owing to the long buildup and recovery times during low-flow pigging. All the experimental results in Figure 3-7 show that pigging below 1 m/s is very dangerous due to speed excursions.

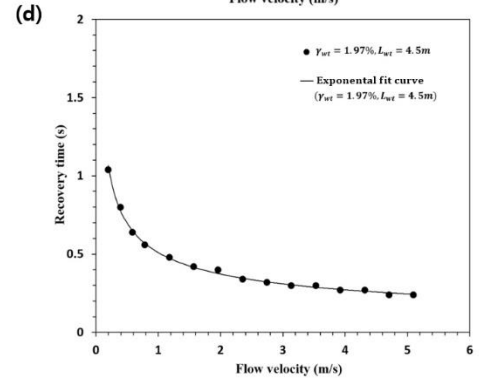
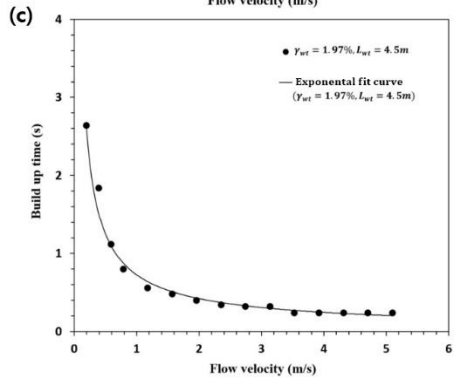
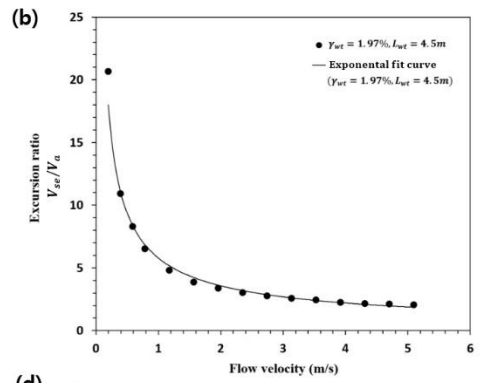
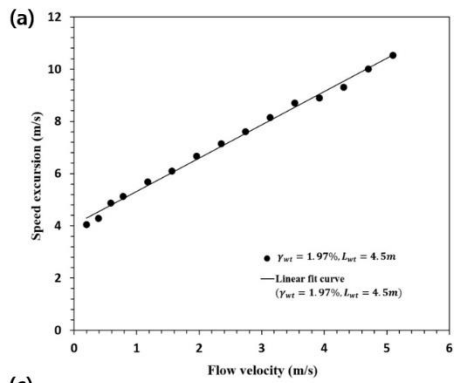




Figure 3-7. Speed excursion versus flow velocity with $\gamma_{wt} = 1.97\%$, and $L_{wt} = 4.5$ m are shown for: (a) Speed excursion, (b) Excursion ratio, (c) Build up time, (d) Recovery time, (e) Speed excursion phase at low flowrate, $v_{air} = 0.392$ m/s, and (f) Speed excursion phase at high flowrate, $v_{air} = 3.136$ m/s.

3.3.3 Effect of Wall thickness change

This section presents the results of adjusting the wall thickness change ratio γ_{wt} on the speed excursion. The black and red lines in Figure 3-8(a) represent the observed speed excursion at $\gamma_{wt} = 1.97\%$ and $\gamma_{wt} = 3.94\%$, respectively. The red line showed a linear relationship even though friction increased due to wall thickness change. However, due to the increase in friction, the speed excursion increased from approximately 46% to 110%. The rate of increase increased as the flow rate decreased. The phenomenon of low-speed excursion at relatively low friction is observed in Figure 3-8(e) and Movie 3. High-speed excursion at relatively high friction is observed in Figure 3-8(f) and movie 4.

In the excursion ratio in Figure 3-8(b), the red line is an exponential curve even when the friction increases owing to the wall thickness change. The excursion ratio dramatically increased as the flow rate decreased. Both the build-up time and recovery time results in Figures 3-8(c) and 3-8(d) show an exponential curve that rapidly increases at low flow rates due to increased friction. These results indicate that the PIG behavior becomes more unstable with the increased friction.

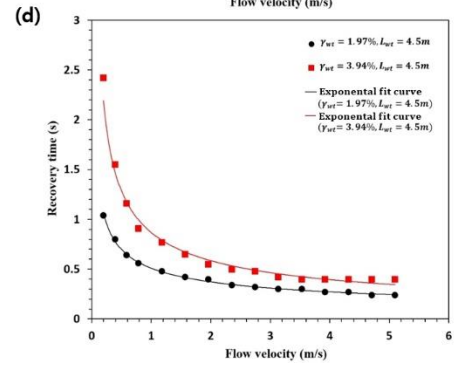
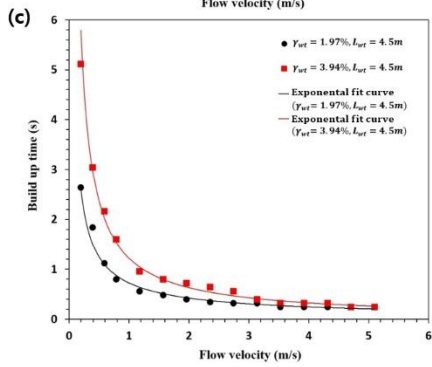
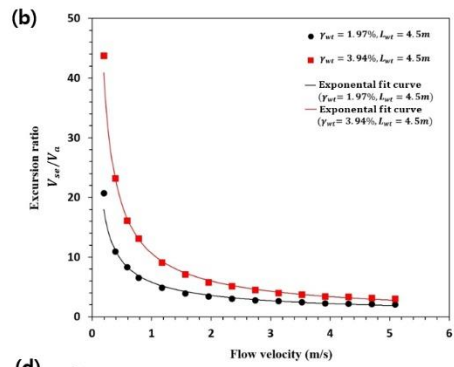
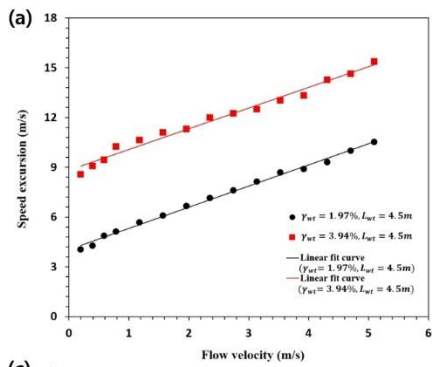


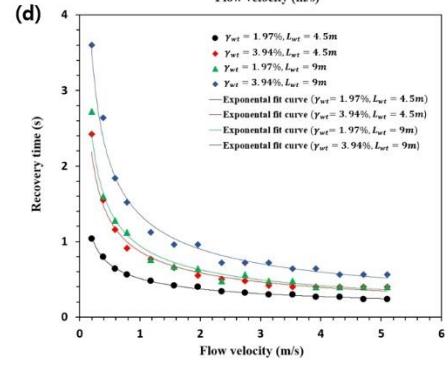
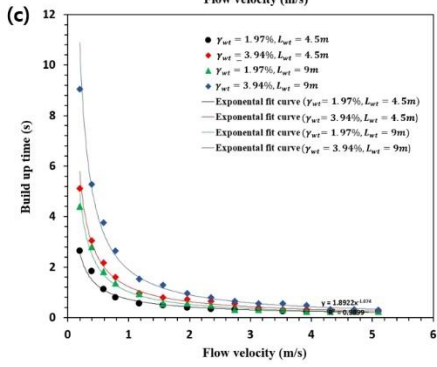
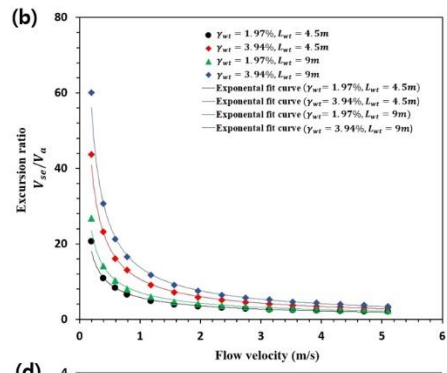
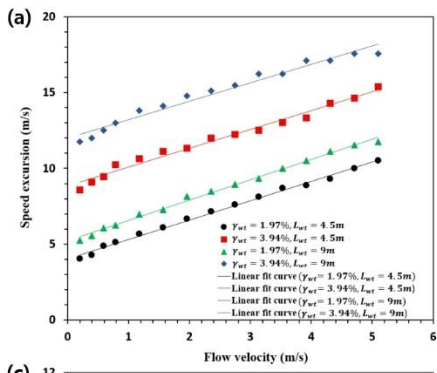


Figure 3-8. Comparison of speed excursion of $\gamma_{wt} = 1.97\%$, and $\gamma_{wt} = 3.94\%$ is shown for: (a) Speed excursion, (b) Excursion ratio, (c) Build-up time, (d) Recovery time, (e) Speed excursion phase at low friction, $\gamma_{wt} = 1.97\%$, and (f) Speed excursion phase at high friction, $\gamma_{wt} = 3.94\%$,

3.3.4 Effect of Linepack

This section discusses the effect of linepack on speed excursion by linepack length L_{wt} . The black and red lines in Figure 3-9(a) are the observed speed excursions for $L_{wt} = 4.5$ m. The green and blue lines are the observed speed excursions for $L_{wt} = 9$ m. The green and blue lines are linear, but higher speed excursions occur as the linepack length increased even under the same friction conditions, as shown in Figure 3-9(a) and (b). The phenomenon of low-speed excursion at a relatively short linepack length is observed in Figure 3-9(e) and 5, and the high-speed excursion at a relatively long linepack length is observed in Figure 3-9(f) and 6. These results indicate that the linepack length is the main factor in the speed excursion.

In addition, both the build-up time and recovery time results in Figure 3-9(c) and (d) show an exponential curve that rapidly increases at low flow rates due to increased linepack length, indicating that PIG behavior is more unstable due to increased linepack length. This phenomenon is also an important finding, indicating that the linepack length is a major factor in pigging behavior. Thus, linepacks should be considered as important variables affecting speed excursion and behavior in long-distance pipeline pigging.



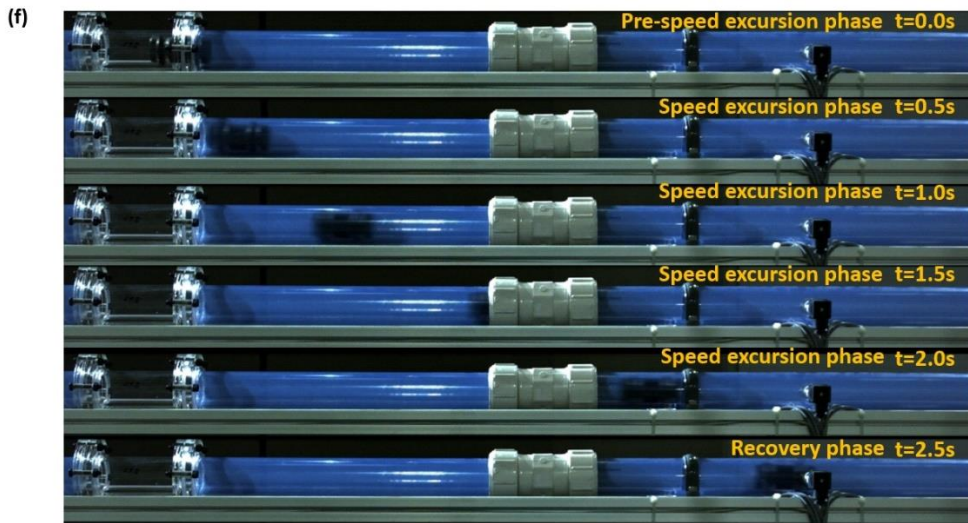


Figure 3-9. Comparison of speed excursion of $L_{wt} = 4.5$ m, and $L_{wt} = 9$ m is shown for: (a) Speed excursion, (b) Excursion ratio, (c) Build-up time, and (d) Recovery time. Speed excursion phase at short linepack length, $L_{wt} = 4.5$ m and long linepack length, $L_{wt} = 9$ m is shown in (e) and (f), respectively.

The fitting formula and coefficient of determination of the relationship between the experimental results and the flow rate are given in Table 3-6. These fitting formulas have the potential to be reflected in the pigging model with speed excursions in the gas pipeline network, as shown in Equation (3.11).

Table 3-6. Fitting formula of experimental results and flowrate

Result	γ_{wt}	L_{wt}	Fitting formula	R^2
Speed excursion	1.97%	4.5 m	$v_{se} = 1.273v_{air} + 4.0458$	0.995
	3.94%	4.5 m	$v_{se} = 1.341v_{air} + 5.2213$	0.995
	1.97%	9 m	$v_{se} = 1.2439v_{air} + 8.8352$	0.9816
	3.94%	9 m	$v_{se} = 1.2155v_{air} + 12.008$	0.9705
Excursion ratio	1.97%	4.5 m	$\varphi_{er} = 5.7906v_{air}^{-0.696}$	0.9912
	3.94%	4.5 m	$\varphi_{er} = 7.0974v_{air}^{-0.735}$	0.9924
	1.97%	9 m	$\varphi_{er} = 10.633v_{air}^{-0.827}$	0.9973
	3.94%	9 m	$\varphi_{er} = 13.759v_{air}^{-0.863}$	0.9989
Build-up time	1.97%	4.5 m	$t_{build} = 0.7256v_{air}^{-0.784}$	0.9831
	3.94%	4.5 m	$t_{build} = 1.0203v_{air}^{-0.969}$	0.9886
	1.97%	9 m	$t_{build} = 1.2228v_{air}^{-0.954}$	0.9878
	3.94%	9 m	$t_{build} = 1.8922v_{air}^{-1.074}$	0.9899
Recovery time	1.97%	4.5 m	$t_{recovery} = 0.5099v_{air}^{-0.453}$	0.9957
	3.94%	4.5 m	$t_{recovery} = 0.8679v_{air}^{-0.568}$	0.9826
	1.97%	9 m	$t_{recovery} = 0.9416v_{air}^{-0.588}$	0.982
	3.94%	9 m	$t_{recovery} = 1.3547v_{air}^{-0.591}$	0.9873

3.3.5 Numerical simulation

This section includes the experimental results of the friction increase ratio according to the wall thickness change ratio and numerical simulation by applying the experimental results to the weighted friction model proposed by [26]. The weighted friction model in the previous study can be seen in Equations (3.6)–(3.10) [26]. Equations (3.6)–(3.9) and (3.10) represent the friction increase ratio by the bend angle and by changing the wall thickness, respectively. The friction increase ratio according to the wall thickness change ratio was obtained from the data in Table 3-7. It showed a linear relationship, as shown in Figure 3-10. This experimental result can be used to derive Equation (3.11) from Equation (3.10).

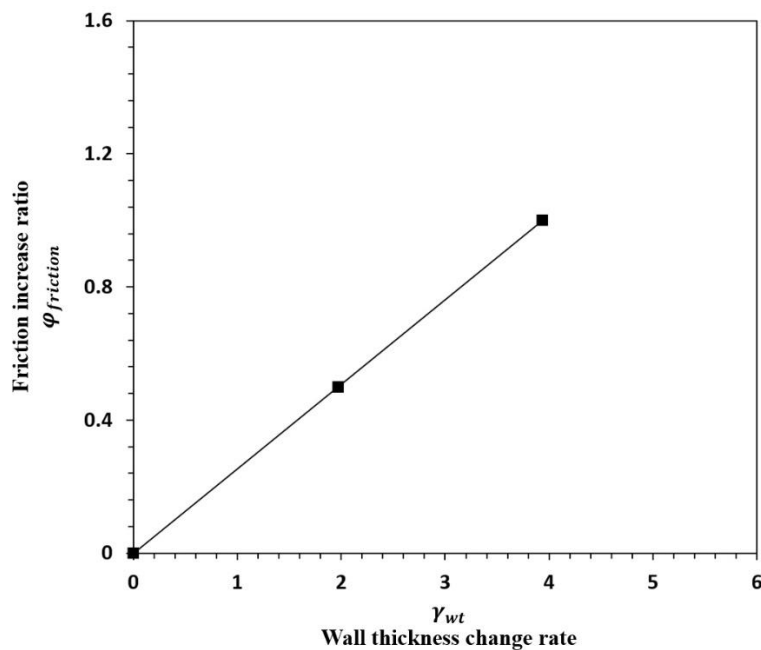


Figure 3-10. Friction increase ratio according to wall thickness change ratio

$$\varphi_{friction} = \left(\frac{F_{chwt}}{F_d} \right) - 1 \quad (3.5)$$

$$F_f = F_d(1 + k_{bend} + k_{chwt}) \quad (3.6)$$

$$k_{bend_typeA} = w_1 * R_{b_typeA} \quad (3.7)$$

$$k_{bend_typeB} = w_2 * R_{b_typeB} \quad (3.8)$$

$$k_{bend_typeC} = w_3 * R_{b_typeC} \quad (3.9)$$

$$k_{chwt} = w_4 * \left(\frac{t_{chwt}}{t_0} \right) \quad (3.10)$$

Where $\varphi_{friction}$ is the friction increase ratio, F_d is the dynamic friction of PIG, F_{chwt} is the maximum friction when a PIG passes wall thickness change section, k_{bend} is the friction coefficient of bends, k_{chwt} is the friction coefficient of wall thickness variations, R_b is the radian of bend angle, w is the weight parameter, t_0 is the initial wall thickness, and t_{chwt} is the changed wall thickness.

Table 3-7. Fitting formula of friction increase ratio and wall thickness change ratio

Result	Fitting formula	R^2
Friction increase ratio	$\varphi_{friction} = 0.254\gamma_{wt}$	1

$$k_{chwt} = 0.254 \left(\frac{d_o - t_{chwt} * 2}{d_o - t_0 * 2} \right) \quad (3.11)$$

Where γ_{wt} is the wall thickness change ratio, d_o is the internal diameter of pipe, t_0 is the initial wall thickness, and t_{chwt} is the changed wall thickness.

Pigging under the experimental conditions listed in Table 3-8 was simulated using our in-house pigging solver to validate the proposed equation (3.11). The in-house solver is almost the same as the solver proposed by [26] except for the application of equation (3.11). The weight parameters w_1, w_2 , and w_3 were set to zero to remove the effect on the bends; only the effect due to the wall thickness change was

considered. The simulation results of Kim's solver using the proposed equation (3.11) of wall thickness change are shown in Figure 3-11. Figure 3-11(a) shows the differential pressure results. The results are consistent with the experimental result. Additionally, the speed excursion results shown in Figure 3-11 (b) was 15.6 m/s for Kim's solver, and the experimental result was 16.7 m/s, showing an error of about 6.54%. Maximum error between Kim's solver and experiment value for speed excursion is 8.5% in Table 3-9.

Table 3-8. Numerical parameters for simulation using Kim's solver

Parameter	Value	Unit
d_o	0.0528	m
L_{pipe}	24.1	m
k	0.0015	mm
P_{out}	1	atm
Q_{air}	250	l/min
T	15	°C
ρ	1.1883	kg/m ³
m_{pig}	135	g
F_d	0.29	bar
t_o	1	mm
t_{chwt}	2	mm
L_{wt}	9	m
w_1	0	-
w_2	0	-
w_3	0	-

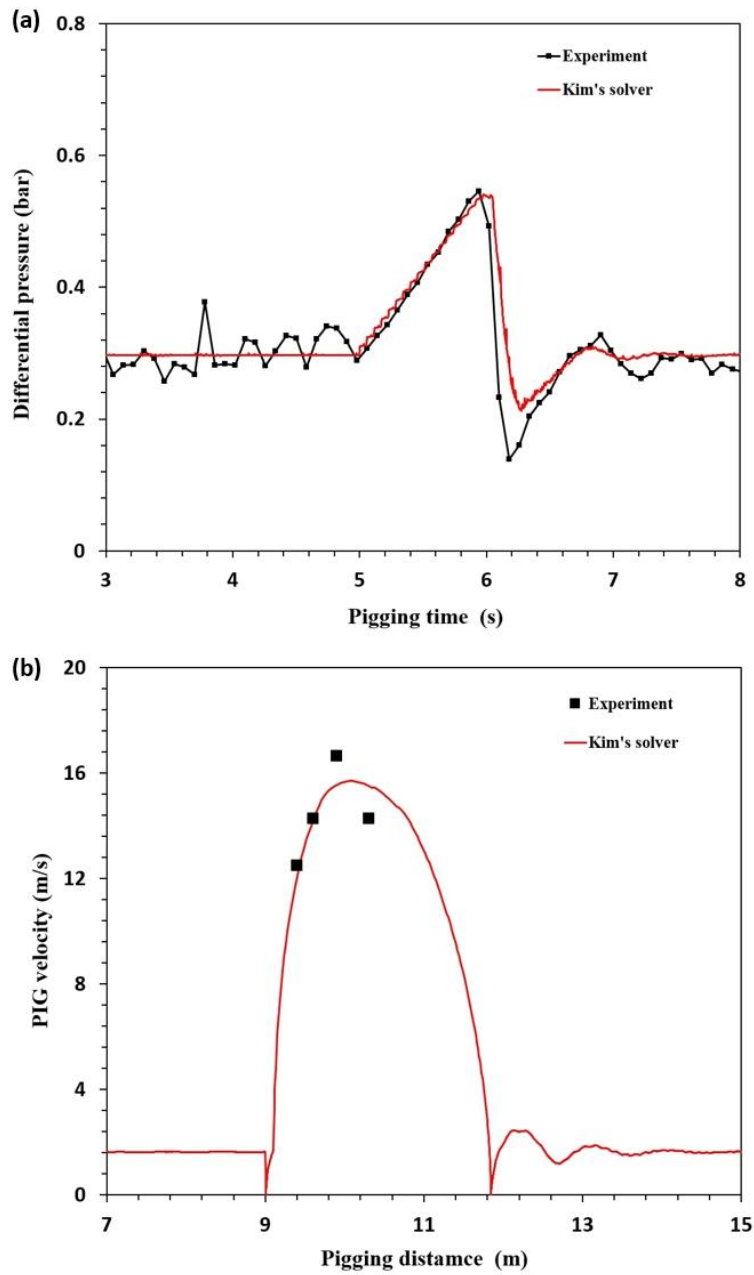


Figure 3-11. Results using Kim's solver by applying the proposed equation of wall thickness change (a) Differential pressure (b) Speed excursion

Table 3-9. Speed excursion error between experiment and Kim’s solver

Pigging distance (m)	Experiment (m/s)	Kim’s solver (m/s)	Error (%)
9.4	12.5	12.1	3.2
9.6	14.3	14.3	0.18
9.9	16.7	15.6	6.54
10.3	14.3	15.5	8.5

3.4. Summary

This study experimented on speed excursion due to changes in wall thickness to investigate the mechanism of speed excursion and the relationship between speed excursion and main variables as flowrate, wall thickens change, and linepack length. Based on the differential pressure measurement results, the speed excursion process was divided into four phases: build-up phase, pre-speed excursion phase, speed excursion phase, and recovery phase. The PIG behavior was analyzed based on the results of these five phases.

The flow velocity has a linear relationship with the speed excursion, but the excursion ratio has an exponential curve that rapidly increases at low flow velocity. These results indicate that low-flow pigging produces relatively low-speed excursions but can be risky because of the rapid increase in the excursion ratio. The build-up and recovery times also showed an exponential curve that increased rapidly at low flow velocities. These results indicate that pigging behavior is significantly unstable owing to the long buildup and recovery times during low-flow pigging.

When the wall thickness change ratio increased from 1.94% to 3.94%, the increase in friction caused the speed excursion to increase from 46% to 110%, showing a linear relationship. The rate of increase was higher as the flow rate decreased. In the excursion ratio result, an exponential curve was obtained even when the friction increased due to the wall thickness change. The excursion ratio dramatically increased as the flow rate decreased. The build-up time and recovery time results

showed an exponential curve that rapidly increased at low flow rates due to increased friction. These results indicate that the PIG behavior is more unstable due to increased friction, especially at low flow rates.

When the linepack length changed from 4.5 m to 9 m, higher-speed excursions occurred as the linepack length increased, even under the same friction conditions. These results are important as they indicate that the linepack length is the main factor in the speed excursion.

Finally, the equation of friction increase ratio according to the wall thickness change ratio was proposed from the experiment and was validated by Kim's solver within 8.5% error.

3.5. Acknowledgement

This chapter is partially adapted from Experimental study on speed excursion of PIG due to friction variation in natural gas pipeline in *Journal of Natural Gas Science and Engineering* with authors S. Kim, J. Jeong, K. Yoo, H. Yoo, and Y. Seo (<https://doi.org/10.1016/j.jngse.2022.104659>). This work was supported by Development of Next Generation Pipeline Robot Technology for the Long-Distance Inspection of the Low Pressure/the Low Flow of Gas Pipelines (RD 2019-0251) research project from Korea Gas Corporation (KOGAS)

Chapter 4. Speed excursion predictions of PIG in natural gas pipeline using pigging solvers based on flow and friction model combinations

4.1. Introduction

The role of natural gas as clean energy is growing, and the rapid increase in gas consumption has clearly led to more construction of natural-gas pipeline transportation systems. Natural-gas pipeline networks operate under numerous pressure and flow conditions, and the safe operation of pipelines is the top priority to prevent fatal accidents in populated areas. Therefore, it is essential to ensure pipeline integrity, and pipeline inspection gauges (PIGs) are generally employed in the industry to inspect the pipeline wall thickness and defects. As PIG is a passive gauge that works on the principle of pressure difference between the front and rear of the PIG, the operating conditions of the pipeline and fluid properties are the main factors that influence the PIG behavior.

A sudden acceleration of pigging velocity, mainly due to gas compressibility and friction variation in natural-gas pipeline networks, is called speed excursion and is frequently observed in our field pigging data, as shown in Figure 4-1. According to the pipeline pigging industry, speed excursions are a major concern that causes unstable behavior of PIG during natural-gas pipeline pigging [45]. The black and blue lines in Figure 4-1 show the pig velocities of first and second operations, respectively, from our field data. These operations were performed under different pressure and flow conditions along Route-A, and it could be verified that the speed excursions occurred constantly owing to pipeline bends and wall thickness changes.

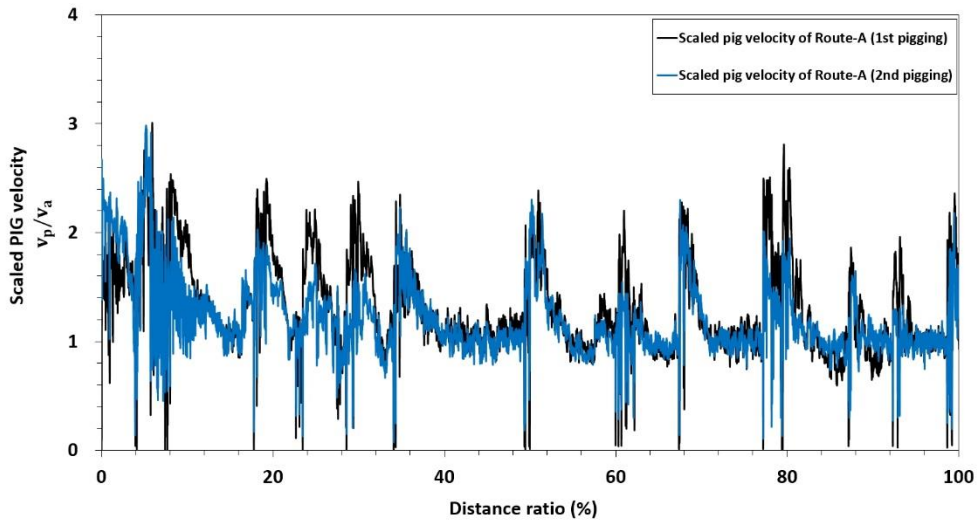


Figure 4-1. Field pigging data of Route-A (1st & 2nd pigging).

In addition, from our pigging operation experience, speed excursions greater than or equal to approximately 10 m/s frequently occur at low-pressure operating conditions, which greatly reduce safety and inspection efficiency of pigging. To predict the unstable behavior of PIG in advance and to ensure the inspection efficiency and safety of pigging, a pigging solver capable of simulating and predicting speed excursions with high precision is essential for operators.

Several studies have been performed to predict the behavior of PIGs. In early research on pigging models, the basic steady-state pigging model in multiphase flow [2, 44], and transient pigging simulation with the method of characteristics (MOC) [24, 38] were studied. The MOC is the most widely used and validated method for pipeline analysis of unsteady fluids and has been generally adopted for fluid analysis in other pigging studies [4, 10, 14, 15, 34, 35, 49].

The equation of motion of PIG can be divided into a fluid part and a friction part that are employed to calculate the driving force and friction between the PIG and pipe wall, respectively. An accurate prediction of the pressure difference across the PIG is important for estimating the driving force that propels the PIG. In most cases, the system is approximated to be a one-dimensional system for flow analysis related

to natural-gas pipelines. Furthermore, flow-governing equations such as the Euler equation or other simplified equations are solved using the MOC or finite volume method (FVM) numerical schemes. Furthermore, studies related to multiphase flow analysis in gas-liquid mixture pipeline pigging [48] and local two-dimensional flow analysis around the bypass PIG have been conducted [3].

The role of friction in the equation of motion is important and has a significant influence on the prediction accuracy. However, the role of friction is not clearly understood, and few models can estimate the friction variation owing to pipeline bends and wall thickness changes. Friction is generally estimated based on empirical findings, field experience [23], and guesswork with a high degree of uncertainty [11, 27, 36]. O'Donoghue (1996) proposed a simplified wall force model that includes the geometric and material properties of the sealing disk [42]. Although this model is the first physical equation-based friction model, friction is relatively underestimated [16, 17, 19, 42, 50]. A two-dimensional linear and non-linear friction model for contact force simulation was proposed as a method of finite element (FE) calculation of the sealing disk [47, 50]. However, it is difficult to include the FE calculations in the existing PIG models.

Although various studies have been conducted on pigging, few studies have focused on the unstable behavior of PIG owing to the speed excursion phenomenon in natural-gas pipelines. OLGA is a dynamic simulation tool that is widely used in the industry and has been used in various pigging studies [8, 13, 22, 25, 43]. However, this commercial tool has limitations in modeling speed excursion by friction variation owing to bends and wall thickness changes in detail.

Therefore, in our previous study [26], we had proposed two novel friction models to predict speed excursions by friction variations and validated the proposed friction models with field pigging data. However, the flow model adopted in the previous study was a one-dimensional Euler-based MOC model, which was employed in other simulation studies [4, 10, 14, 15, 34, 35, 49]. In future studies, it will be necessary to improve the flow model to reduce the error between the simulation results and

field data.

This study presents four pigging solvers that employ a combination of two novel flow models and two friction models proposed in our previous study [26]. In the dynamic model of the PIG, the Stoner-based MOC and MOC-FVM hybrid models were considered for the fluid part, and the tuned friction model and the weighted friction model were considered for the friction part. The simulation and prediction performances of solvers are evaluated by comparing the results of each solver with field pigging data. This study aims to characterize the proposed friction and flow models and identify the simulation and prediction performances of each solver for speed excursions. As the flow and friction models applied to each solver are different, the simulation and prediction performances will be different, which can be identified through performance evaluation.

The Stoner-MOC solver exhibited slightly less simulation accuracy; however, it computed four times faster than the MOC-FVM hybrid solver. Conversely, the MOC-FVM hybrid solver exhibited better simulation and prediction accuracies. Furthermore, the tuned friction model exhibited better simulation accuracy, and the weighted friction model exhibited better prediction performance. Therefore, the hybrid tuned-based solver performed the best in terms of simulation accuracy, and the hybrid weight-based solver performed the best in terms of prediction accuracy. As the differences in simulation and prediction performances of solvers due to the combinations of proposed flow and friction models were verified, the flow model and friction model can be strategically combined to develop a solver corresponding on the usage requirements.

4.2. Dynamic model and solver

A schematic of the forces acting on a PIG moving in an inclined pipeline is shown in Figure 4-2. The equation of motion of PIG, as expressed in Eq. (4.1), consists of three terms, and the main uncertainties that determine the PIG behavior are the fluid and friction terms.

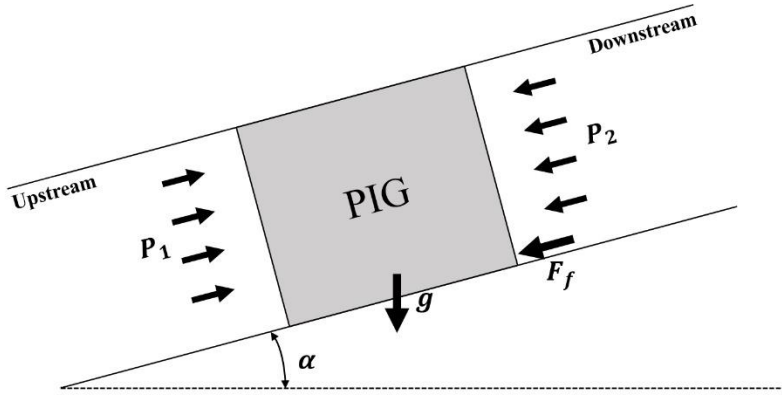


Figure 4-2. PIG moving in an inclined pipeline.

$$m \frac{dv_p}{dt} = F_p - F_g - F_f = (P_1 - P_2)A - mg \sin \alpha - F_f, \quad (4.3)$$

where P_1 and P_2 represent the pressure values exerted on the head and tail of a PIG, respectively. Both pressure values were determined from the flow analysis. Assuming that the sealing of the PIG is proper, the flow region can be separated as downstream and upstream sections, which are the regions ahead of and behind the PIG, respectively. Therefore, we performed a flow analysis with an upstream section that included the flow region from the pipeline inlet to the PIG tail and with a downstream section that included the flow region from the PIG head to the pipeline outlet.

To conduct the pigging analysis without supply interruption, the pressure and mass flow rates at the inlet and outlet boundaries received time-varying values in the form of a table, and the boundary condition of the surface that was in contact with the PIG

was modeled as a moving wall. In this study, two different flow solvers were used: the conventional MOC-based flow solver, which enables fast analysis, and a novel MOC-FVM hybrid flow solver. In the MOC-based flow solver, the Stoner equation, which is a simplified form of a one-dimensional Euler equation, was solved by employing prominent MOC schemes based on several assumptions. The MOC-FVM hybrid solver combines an MOC numerical scheme and a density-based FVM to guarantee calculation accuracy, while minimizing the increase in computational cost.

To simulate the speed excursion by friction variation, two friction models, which are tuning models based on field data [26], were applied to the friction term. The core of the tuned friction model is a dynamic friction table, which is used to estimate the friction variation by employing the friction constant. The peak friction that causes the speed excursion can be determined by tuning the friction in the dynamic friction table. The core of the weighted friction model is a linear equation for friction variation owing to pipeline bends and wall thickness changes. The influence of each variable on friction can be determined by the weight parameters in the linear equations. The four pigging solvers were developed by employing different combinations of the two novel flow models and two friction models as listed in Table 4-1. By comparing the results of each solver, the simulation and prediction performances according to the flow and friction models were evaluated to characterize the four pigging solvers.

Table 4-1. Pigging solver list based on flow and friction model combinations

Solver no.	Flow model	Friction model
Solver 1	Stoner-MOC	Tuned friction
Solver 2	MOC-FVM Hybrid	Tuned friction
Solver 3	Stoner-MOC	Weighted friction
Solver 4	MOC-FVM Hybrid	Weighted friction

4.2.1 Stoner-MOC

4.2.1.1 Governing equations

In this study, the Stoner equation, which is widely used in unsteady flow analysis in natural-gas pipelines, was used as the governing equation for MOC analysis. The Stoner equation was derived from the Euler equation by simplifying the convective acceleration term with an insignificant effect of the velocity gradient and adopting an isothermal assumption. The vector form of the Stoner equation can be expressed as

$$\mathbf{U}_t + \mathbf{F}\mathbf{U}_x = \mathbf{J} \quad (4.2)$$

Where $\mathbf{U} = \begin{bmatrix} p \\ M \end{bmatrix}$, $\mathbf{F} = \begin{bmatrix} 0 & C^2/A \\ A & 0 \end{bmatrix}$, and $\mathbf{J} = \begin{bmatrix} 0 \\ -\frac{fC^2M|M|}{2pDA} - \rho g A \sin\theta \end{bmatrix}$

Where p is the pressure of natural gas, M is the mass flow rate, C is the speed of sound, D is the inner diameter of pipe, f is the Darcy-Weisbach friction factor, and θ is the slope of pipe.

\mathbf{J} is a source term matrix that represents the viscous wall friction and gravitational force acting on the gas. The Darcy–Weisbach empirical equation was used according to the viscous wall friction, and Haaland’s approximate formula was used to determine the Darcy-Weisbach friction factor f .

4.2.1.2 Methods of characteristics

The characteristic form of the Stoner equation (Eq. (4.2)) can be expressed for the MOC as

$$\begin{cases} \frac{1}{A} \frac{dM}{dt} + \frac{1}{C} \frac{dp}{dt} + pg \sin \theta + \frac{fC^2 M |M|}{2DA^2 P} = 0 & \frac{dx}{dt} = +C \\ \frac{1}{A} \frac{dM}{dt} - \frac{1}{C} \frac{dp}{dt} + pg \sin \theta + \frac{fC^2 M |M|}{2DA^2 P} = 0 & \frac{dx}{dt} = -C \end{cases} \quad (4.3)$$

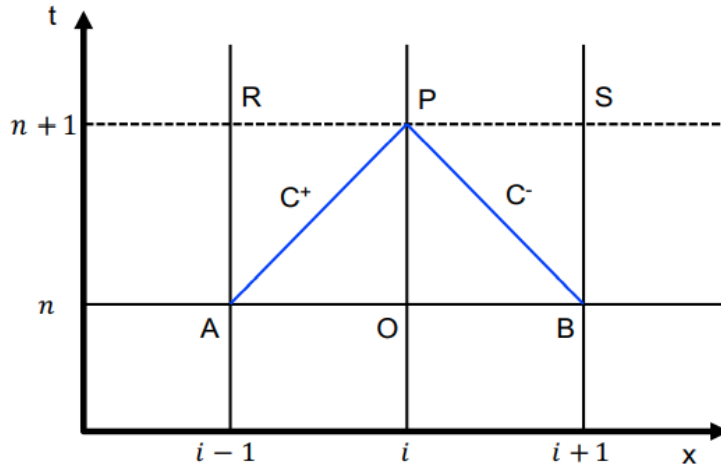


Figure 4-3. Schematic of characteristic lines of MOC and space-time grid configuration.

Figure 4-3 shows the positive and negative characteristic lines of MOC and space-time grid configuration. The grid points satisfying the Courant–Friedrichs–Lewy (CFL) condition for the previous, current and next time steps, where two characteristic lines coincide, are represented by points A, P, and B, respectively. The discretization forms of Eq. (4.4) can be expressed as follows:

$$\left\{ \begin{array}{l} P_P - P_A + \frac{C}{A}(M_P - M_A) + \frac{fC^2\Delta x}{DA^2(P_P + P_A)} \frac{e^s - 1}{s} \left(\frac{M_P + M_A}{2} \left| \frac{M_P + M_A}{2} \right| \right) \\ \quad + \frac{P_P^2}{P_A + P_P} (e^s - 1) - \rho g \sin\theta \\ -(P_P - P_B) + \frac{C}{A}(M_P - M_B) + \frac{fC^2\Delta x}{DA^2(P_P + P_B)} \frac{e^s - 1}{s} \left(\frac{M_P + M_B}{2} \left| \frac{M_P + M_B}{2} \right| \right) \\ \quad + \frac{P_P^2}{P_B + P_P} (e^s - 1) - \rho g \sin\theta \end{array} \right. \quad (4.4)$$

Where P is the pressure of natural gas, M is the mass flow rate, C is the speed of sound, D is the inner diameter of pipe, f is the Darcy-Weisbach friction factor, and θ is the slope of pipe, and s is the perimeter of pipe.

Hence, the Stoner equation, which is a partial differential equation, becomes an ordinary differential equation. Thus, the fluid variables, including the pressure and mass flow rates, can be computed. Because the isothermal speed of sound is not constant, interpolation is necessary to satisfy the CFL condition. Therefore, linear interpolation for space was employed in this study.

4.2.2 MOC-FVM Hybrid

4.2.2.1 Solver configuration

A schematic of general solver configuration is shown in Figure 4-4. The regions calculated using the hybrid solver were divided into four sections. It consists of two FVM analysis regions that are distinguished by the direction of the PIG: one in the head-ward direction and one in the tail-ward direction. However, MOC analysis regions surround the FVM region and cover the entire computational domain between the ends of the FVM regions and pipes. The length and number of grids in each FVM and MOC analysis area can be individually adjusted. In the computational domain shown in Figure 4-4, there is a sliding domain, which is marked with gray dashed lines, containing both FVM regions and an empty space where a PIG is placed. If the PIG starts to move, the FVM domains track PIG's speed, and all grid elements in the sliding domain are moved at the same speed as the PIG, so that the sliding domain travels through the MOC computational domain.

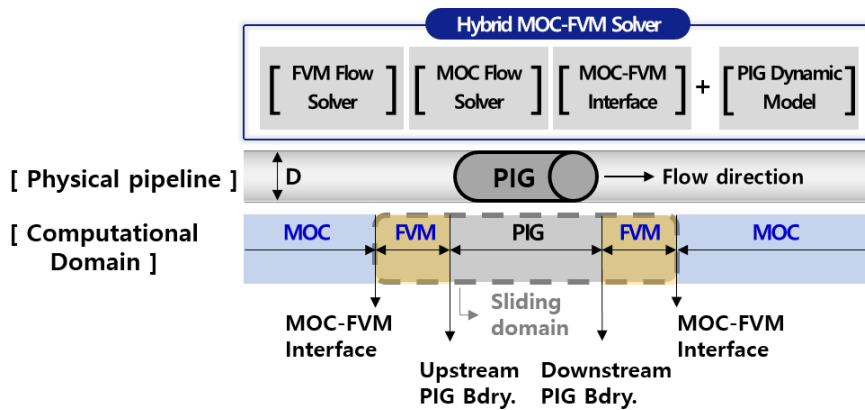


Figure 4-4. General solver configuration.

4.2.2.2 Governing equations

The governing equations applied in the FVM domain of the hybrid solver are a compressible Reynolds-averaged Euler equation, which can be derived from the following Navier–Stokes equation:

$$\frac{\partial}{\partial t} \oint_{\Omega} \mathbf{W} d\Omega + \oint_{d\Omega} [(\mathbf{F}_c - \mathbf{F}_v) \cdot \mathbf{n}] dS = \int_{\Omega} \mathbf{D} d\Omega \quad (4.5)$$

The vector of conservative variables \mathbf{W} and the convective flux tensor \mathbf{F}_c are given by

$$\mathbf{W} = [\rho \quad \rho u \quad \rho v \quad \rho w \quad \rho E]^T \quad (4.6)$$

$$\mathbf{F}_c = \begin{bmatrix} \rho u & \rho v & \rho w \\ \rho u^2 + p & \rho uv & \rho uw \\ \rho vu & \rho v^2 + p & \rho vw \\ \rho wu & \rho wv & \rho w^2 + p \\ \rho uH & \rho vH & \rho wH \\ \rho \gamma_v u & \rho \gamma_v v & \rho \gamma_v w \\ \rho \gamma_g u & \rho \gamma_g v & \rho \gamma_g w \end{bmatrix} \quad (4.7)$$

and \mathbf{F}_v indicates the viscous flux tensor

$$\mathbf{F}_v = \begin{bmatrix} 0 & 0 & 0 \\ \tau_{xx} & \tau_{xy} & \tau_{xz} \\ \tau_{yx} & \tau_{yy} & \tau_{yz} \\ \tau_{zx} & \tau_{zy} & \tau_{zz} \\ \Phi_x & \Phi_x & \Phi_x \\ 0 & 0 & 0 \\ 0 & 0 & 0 \end{bmatrix} \quad (4.8)$$

4.2.2.3 System preconditioning

In general, numerical methods for compressible flows provide good stability and convergence characteristics for the transonic and supersonic flow regimes. However, at low speeds, the system stiffness resulting from disparate convective and acoustic velocities leads to a deterioration of the convergence rates. By altering the acoustic speed of the system, the convergence rates can be made independent of the Mach number such that all system eigenvalues are of the same order. The governing equation (4.5) are preconditioned by pre-multiplying the time derivative term using the preconditioning matrix introduced by Weiss and Smith [53], as follows:

$$\Gamma \frac{\partial}{\partial \tau} \int_{\Omega} \mathbf{Q} d\Omega + \oint_{d\Omega} [(\mathbf{F}_c - \mathbf{F}_v) \cdot \mathbf{n}] dS = \int_{\Omega} \mathbf{D} d\Omega + \int_{\Omega} \mathbf{D}_T d\Omega \quad (4.9)$$

where \mathbf{Q} indicates the primitive variable vector given by

$$\mathbf{Q} = [p \quad u \quad T]^T \quad (4.10)$$

and the preconditioning matrix Γ is

$$\left[\begin{array}{ccc} \frac{1}{\beta} & 0 & \frac{\partial \rho}{\partial T} \\ u & \rho & \frac{\partial \rho}{\partial T} u \\ H^* & 0 & \frac{\partial \rho}{\partial T} H + \rho \frac{\partial h}{\partial T} \end{array} \right] \quad (4.11)$$

With,

$$H^* = \frac{H}{\beta} + \rho \frac{\partial h}{\partial p} - 1 \quad (4.12)$$

If $\frac{1}{\beta} = \frac{\partial \rho}{\partial p}$, Γ becomes $\frac{\partial W}{\partial Q}$, resulting in a non-preconditioned system in the primitive form. The eigenvalues of the preconditioned system in Eq. (4.9) are given by

$$\lambda \left(\Gamma^{-1} \frac{\partial \mathbf{F}}{\partial \mathbf{Q}} \right) = U, U' - d, U' + d \quad (4.13)$$

where

$$U' = \frac{1}{2} \left(1 + \frac{c'^2}{c^2} \right) U \quad (4.14)$$

$$d = \frac{1}{2} \sqrt{\left(1 - \frac{c'^2}{c^2} \right)^2 U^2 + 4c'^2} \quad (4.15)$$

Here, $U (\equiv n_x u)$ is the contravariant velocity component normal to the surface element dS . The speed of sound c can be expressed as

$$c^2 \equiv \left. \frac{\partial p}{\partial \rho} \right|_s = \frac{\rho \frac{\partial h}{\partial T}}{\rho \frac{\partial \rho}{\partial p} \frac{\partial h}{\partial T} + \frac{\partial \rho}{\partial T} \left(1 - \rho \frac{\partial h}{\partial p} \right)} \quad (4.16)$$

The relation between $\frac{1}{\beta}$ and c' is then given by

$$\frac{1}{\beta} = \frac{1}{c'^2} - \frac{\frac{\partial \rho}{\partial T} \left(1 - \rho \frac{\partial h}{\partial p} \right)}{\rho \frac{\partial h}{\partial T}} \quad (4.17)$$

The preconditioned speed of sound c' is then given by

$$c' = \min\left(c, \max\left(\sqrt{u^2 + v^2 + w^2}, V_{co}\right)\right) \quad (4.18)$$

In Eq. (4.18), V_{co} is a cutoff value that is typically used to prevent the pre-conditioned speed of sound from becoming zero near the stagnation region (where the local velocity magnitude is zero). The cut-off parameter V_{co} is generally specified as $V_{co} = kV_{\infty}$, where V_{∞} is the freestream velocity, and k is set to one in this study. The cut-off parameter V_{co} should have a non-zero value; otherwise, the pre-conditioned speed of sound becomes zero as mentioned above and this could lead to a floating-point error. For supersonic flows, the preconditioned speed of sound becomes the local speed of sound turning off system preconditioning. Because the system preconditioning destroys the temporal accuracy of the governing equations, Eq. (4.9) is restricted to steady-state calculations with pseudo-time τ . For unsteady computations, the dual time-stepping method was employed, wherein the preconditioned pseudo-time derivative term was introduced in addition to the physical time derivative in Eq. (4.1) and can be expressed as

$$\Gamma \frac{\partial}{\partial \tau} \int_{\Omega} \mathbf{Q} d\Omega + \frac{\partial}{\partial t} \oint_{\Omega} \mathbf{W} d\Omega + \oint_{d\Omega} [(\mathbf{F}_c - \mathbf{F}_v) \cdot \mathbf{n}] dS = \int_{\Omega} \mathbf{D}_s d\Omega \quad (4.19)$$

where t denotes the physical time, and τ is the pseudo-time used in the sub-iteration procedure, thereby the physical time-step size is not affected by the stiffness of the system, whereas the convergence of the inner iterations in pseudo-time is optimized by judicious selection of the preconditioning method (or design of the preconditioned speed of sound, c'). To calculate unsteady flows with a large physical time step Δt , Eq. (4.18) is employed. However, it is suboptimal for intermediate and small-time steps, resulting in an unsatisfactory convergence behavior. To overcome this, Venkateswaran and Merkle [54] proposed a preconditioning method that considers the effect of Strouhal number through von Neumann stability analysis of the dual time-stepping method. The resulting unsteady preconditioning parameter is given by

$$V_{un} = \frac{L}{\pi\Delta t} = \frac{L}{\pi\Delta t} \times V = Str \times V \quad (4.20)$$

where L represents characteristic length, and Δt represents the physical time step size. The characteristic length is generally considered as the problem domain size, which is a representative scale of the lowest wavenumber. Considering Eq. (4.20), the preconditioned speed of sound c' for unsteady flows is given by

$$c'_{un} = \min\left(c, \max\left(\sqrt{u^2 + v^2 + w^2}, V_{co}, V_{un}\right)\right) \quad (4.21)$$

For steady flows or low Strouhal number flows with a large time step, V_{co} is larger than V_{un} ; consequently, the preconditioned speed of sound is the same as in Eq. (4.18). For an intermediate-time step, the unsteady velocity (V_{un}) can be larger than the local velocity, and unsteady preconditioning occurs. As the time step decreases for high Strouhal number flows, the unsteady velocity can completely turn off the system preconditioning, thus reverting the preconditioned speed of sound c_0 to the original speed of sound c . This corresponds to a physical situation wherein a pressure wave propagates with respect to the original speed of sound. Thus, Eq. may ensure optimal convergence for inner iterations at all flow speeds and for all values of time step sizes.

4.2.2.4 Sliding domain

For ALE (Arbitrary Lagrangian Eulerian) method, as the entire FVM domain moves through the MOC computational domain with the speed of the PIG in the MOC-FVM hybrid PIG solver, the arbitrary Lagrangian Eulerian (ALE) method was applied to the flow solver to accurately simulate the movement of the grid. The general Euler equation in a conservative form without grid movement can be expressed as

$$\frac{\partial \mathbf{W}}{\partial t} + \nabla \cdot \mathbf{F}(\mathbf{W}) = 0 \quad (4.22)$$

where \mathbf{U} is the conservative variable vector and $\mathbf{F}(\mathbf{U})$ is a convective flux vector. With respect to the control volume variation with time, the integral form of the governing equation can be expressed as follows:

$$\frac{\partial \mathbf{W}}{\partial t} + \nabla \cdot \mathbf{F}(\mathbf{W}) = 0 \quad (4.23)$$

For GCL condition, numerical errors may occur during the grid movements and could deteriorate the calculation accuracy if they continue to accumulate during long-running pigging simulations. To prevent errors induced by grid elements, the geometric conservation law (GCL) must be considered during the grid movement and deformation processes. According to the GCL condition, a specific system is fully independent of grid motion and can only be determined from the flow governing equations. In this study, a modified SOD shock tube problem analysis was performed to rigorously verify the ALE method that satisfied the GCL condition within the FVM grid.

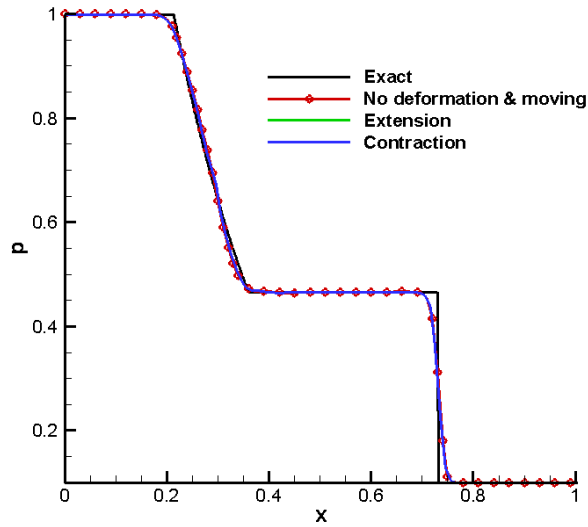


Figure 4-5. Comparison of pressure distribution along the x-axis.

In Figure 4-5, the black solid line represents the reference data (exact solution), and the red solid line and symbol represent the analysis results when there is no grid deformation or movement. The green solid line indicates the grid extension and expands from a value of 0.3 on the x-axis, which is a non-dimensionalized length, and the blue solid line indicates the grid contraction and reduces from the same value on the x-axis ($x = 0.3$). The above results indicate that the movement of the grid did not affect the flow analysis result by always satisfying the conservation, even when the movement and deformation of the grid occurred.

4.2.2.5 Solver interface

The interface between the FVM and MOC calculation domains is depicted in Figure 4-6, and the data between the two flow domains were transferred to the area where the two domains overlapped. The following describes the data transfer in the downstream pipe as an example. For the interface located in the downstream region, the two grid points closest to the right boundary of the FVM region were selected as donor nodes to transfer the flow property to the FVM boundary ghost cell boundary (fringe cell). Two different flow properties of the two donor locations were transferred to the fringe point via linear interpolation. As the FVM calculation domain has second-order spatial accuracy, two boundary ghost cells were required. Therefore, four donor nodes were required as two pairs of nodes. Conversely, at the boundary of the downstream MOC region, the flow properties of the two FVM donor cells adjacent to the end of the MOC domain are transferred to the fringe boundary node.

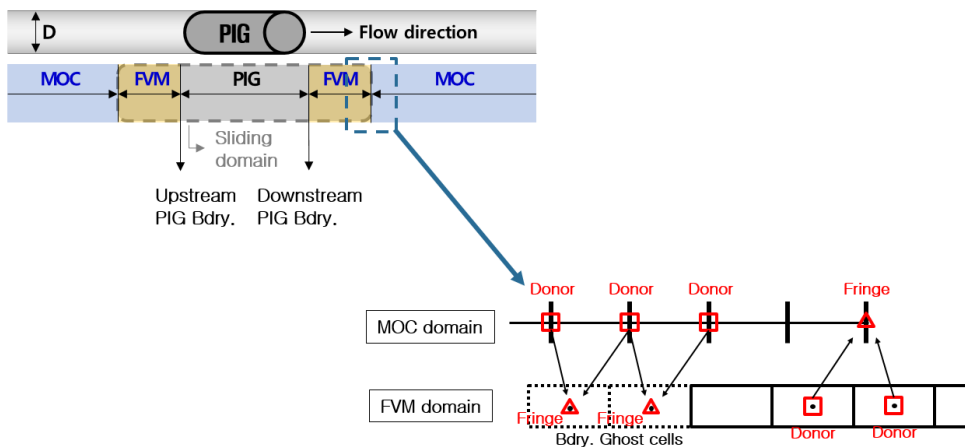


Figure 4-6. Interface between FVM and MOC computation regions.

4.2.3 Tuned friction model

A dynamic friction table that reflects the friction variation was adopted in this friction model. This method inputs the friction constants into the dynamic friction table at all points where speed excursion occurs, as shown in Figure 4-7, and the speed excursion can be calculated by the difference between F_{di} and F_d as expressed in Eq. (4.24).

To use this model, the field data of speed excursions and occurrence locations are required to input the dynamic friction table. F_d is obtained from the field pigging data, but all values of F_{di} must be determined by adjusting the values that best simulate the field-PIG velocity. The simulation algorithm of the tuned friction model is shown in Figure 4-9 (a), which shows the tuning process for determining F_{di} in the dynamic friction table. The initial F_{di} values were entered empirically, and the final friction values were determined through the tuning process.

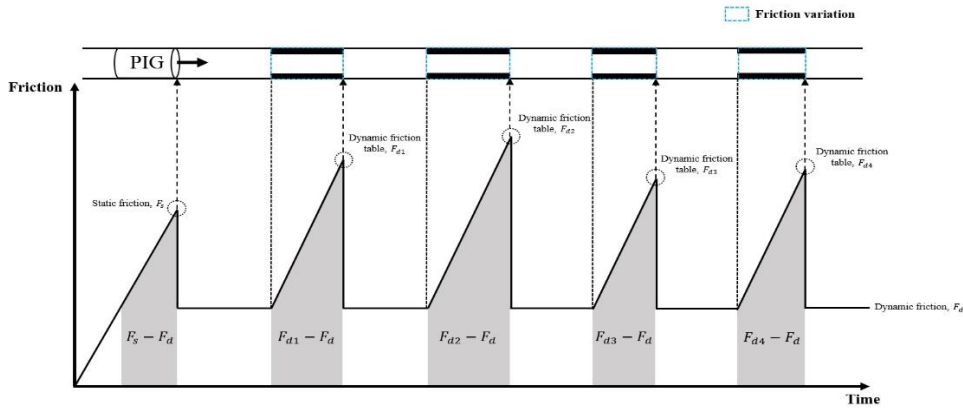


Figure 4-7. Schematic of the tuned friction model

$$F_f = \begin{cases} F_s & \text{if } v_p = 0 \\ F_d, F_{d1}, F_{d2}, F_{d3}, F_{d4} \dots F_{di} & \text{if } v_p \neq 0 \end{cases} \quad (4.24)$$

4.2.4 Weighted friction model

The core of this friction model is a linear equation for the friction variation owing to pipeline bends and wall thickness changes. The influence of each variable on friction can be determined by the weight parameters in the linear equations. The angle of the bends and the change in wall thickness can be obtained from field pigging data, and these are directly applied as inputs to linear equations (Eqs. (4.25–4.29)). The user should determine the weight parameters by considering the effect of each variable on friction. The network for the overall computational scheme for this model is shown in Figure 4-8.

From the field data, it was observed that three bend angles (types A, B, and C) and some wall thickness change affected the friction variation; therefore, three weight parameters were adopted to calculate the friction according to the angle of bends (Eqs. (4.26–4.28)), and one weight parameter was adopted to adjust the wall thickness changes as expressed in Eq. (4.29). As the weight parameter can determine the additional friction force of each variable, it is necessary to determine the weight parameters to employ this model. Therefore, the initial weight parameters were entered empirically, and the final weight parameters were determined through the tuning process shown in Figure 4-9 (b).

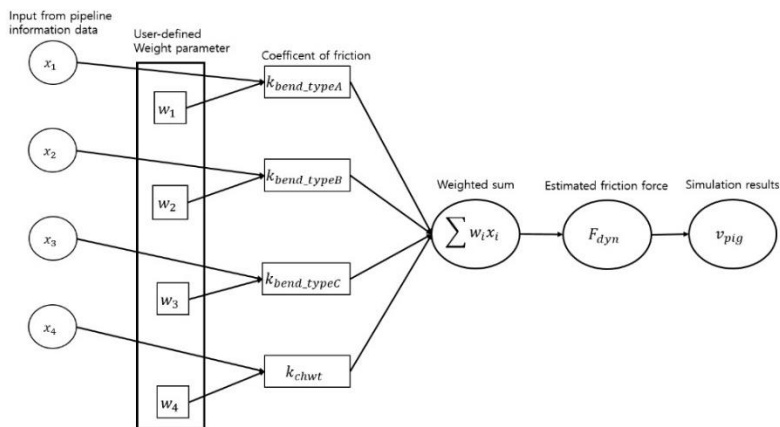


Figure 4-8. Calculation scheme of weighted friction model

$$F_f = F_d(1 + k_{bend} + k_{chwt}) \quad (4.25)$$

$$k_{bend_typeA} = w_1 * R_{b_typeA} \quad (4.26)$$

$$k_{bend_typeB} = w_2 * R_{b_typeB} \quad (4.27)$$

$$k_{bend_typeC} = w_3 * R_{b_typeC} \quad (4.28)$$

$$k_{chwt} = w_4 * \left(\frac{t_{chwt}}{t_0} \right) \quad (4.29)$$

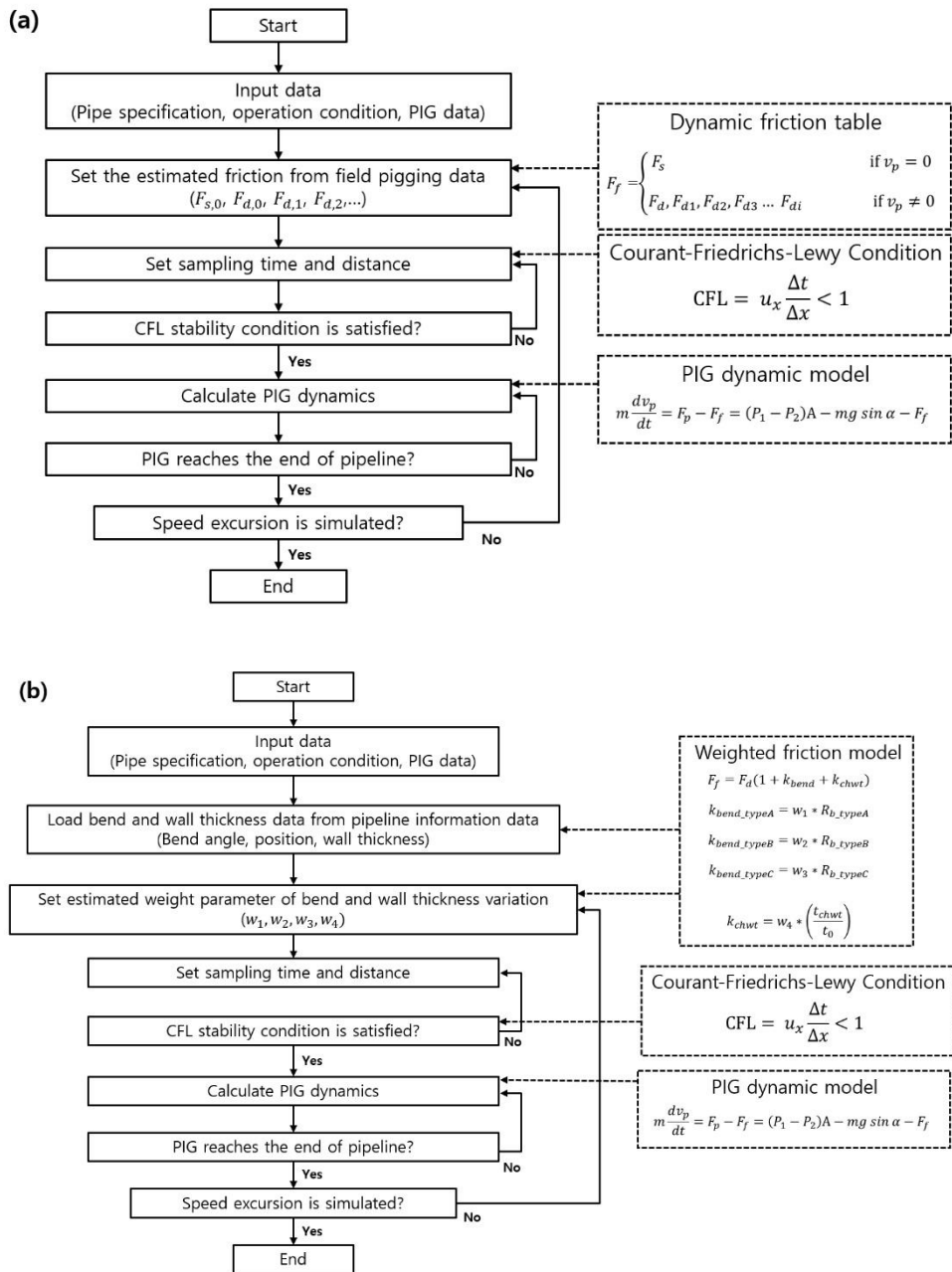


Figure 4-9. Simulation algorithms for: (a) Tuned friction model; (b) Weighted friction model

4.3. Solver evaluation method

The field pigging data that was simulated and predicted by each solver is shown in Figure 4-1. First and second pigging data had different pressure and flow conditions, while the rest of the conditions were the same. The results of the four solvers were compared with the field pigging data using the following error evaluation equations:

$$MAE [m/s] = \frac{\sum_{i=1}^n |D_i - O_i|}{n} \quad (4.30)$$

$$ERR(\%) = \frac{MAE_o - MAE_i}{MAE_o} \quad (4.31)$$

$$EGR(\%) = \frac{MAE_i - MAE_o}{MAE_o} \quad (4.32)$$

$$CRM = \frac{[\sum_{i=1}^n O_i - \sum_{i=1}^n D_i]}{\sum_{i=1}^n O_i} \quad (4.33)$$

First, the error between the results of the solvers and field data was calculated using the mean absolute error (MAE), which is expressed in Eq. (4.30). This value shows an intuitive difference between the predictions and the field data. To evaluate the performance of each solver with MAE, the increase or decrease in MAE is expressed as a percentage using the error reduction rate (ERR), as expressed in Eq. (4.31), and error growth rate (EGR), as expressed in Eq. (4.32). The higher the performance, the higher the ERR, and the lower the performance, the higher the EGR. Additionally, coefficient of residual mass (CRM), which is a measure of the tendency of the model to overestimate or underestimate the measured value, can be expressed in Eq. (4.33). A positive CRM value indicates that the numerical solution is underestimated, and a negative CRM value indicates that the numerical solution is overestimated [40]. By adopting a linear interpolation method, the field data and the results of the solvers were compared with approximately 60,000 data at 0.1 m intervals in pigging distance.

4.4. Results and discussion

This section presents the simulation and prediction results for each solver, including the solver performance evaluation. Section 4.4.1 presents the simulation results for the first pigging velocity from each solver, and Section 4.4.2 presents the prediction results for the second pigging velocity from each solver. In Section 4.4.3, the differences between the Stoner-MOC and MOC-FVM hybrid models are analyzed and described, and in Section 4.4, the differences between the tuned and weighted friction models are analyzed and described.

As the flow and friction models applied to each solver were different, the required numerical input was also different. Figure 4-10 (a) shows the dynamic friction table of the tuned friction model. The friction values were determined through several field-data-based tuning processes. These friction values were used as friction inputs for solvers 1 and 2, based on the tuned friction model. However, to use solvers 3 and 4 based on the weighted friction model, the weight parameters must be determined. The weight parameters were determined based on field data, as listed in Table 4-2, through several tuning processes.

Figure 4-10 (b) shows the relative elevation of Route-A, which was used as an input for all solvers to calculate the gravitational force in the dynamic equation of the PIG. Figure 4-10(c) and (d) show the scaled pressure and flowrate derived from the first pigging field data, which were used as input values for the first pigging simulation in all solvers.

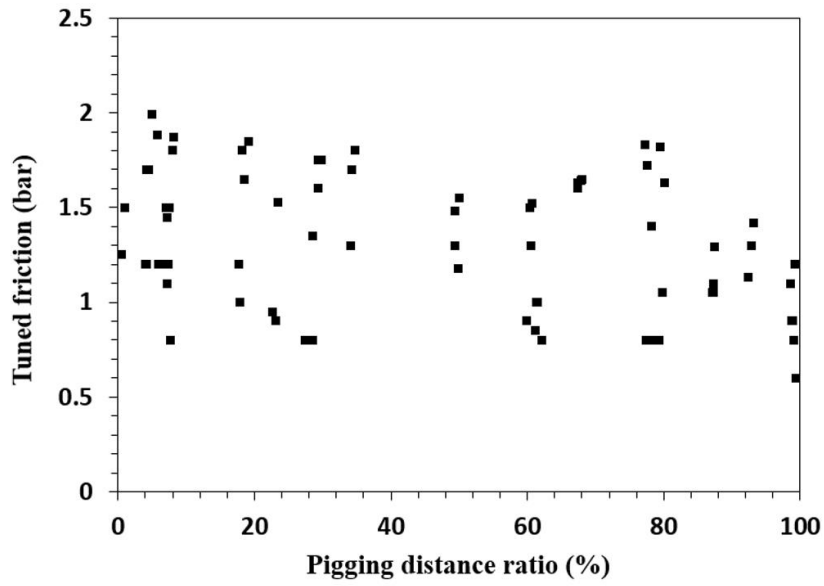


Figure 4-10. Numerical inputs for simulation: (a) Tuned friction in the dynamic friction table

Table 4-2. Friction values for weighted friction model

Variable	Unit	Value
F_s	bar	0.533
F_d	bar	0.365
w_1	-	5.27
w_2	-	3.09
w_3	-	1.67
w_4	-	0.34

4.4.1 Simulation performance of the solvers

The simulated PIG velocities obtained from each solver for first pigging are shown in Figure 4-11. It was verified that the PIG velocities simulated by all the solvers were in good agreement with the field pigging data.

However, if the difference in the field pigging data and the simulated PIG velocity is precisely compared at 0.1 m interval using the MAE equation, it can be seen that the simulation performance between solvers is different, as given in Table 4-3.

Through MAE evaluation, it was verified that Solver 2, composed of the MOC-FVM hybrid and tuned friction models, showed the highest accuracy as shown in Figure 4-12 (a), and Solver 3, composed of Stoner-MOC and the weighted friction models, showed the lowest accuracy, as shown in Figure 4-12 (b).

When using the MOC-FVM hybrid instead of the Stoner-MOC in the flow model, it was verified that the MAE error was clearly reduced, as shown in Figure 4-12 (a), which means that the MOC-FVM hybrid model shows higher simulation performance. However, the error slightly increased when the weighted friction model was adopted, as shown in Figure 4-12 (b), which means that the tuned friction model shows higher simulation performance. Therefore, the MOC-FVM hybrid model for the flow part and the tuned friction model for the friction part showed better simulation performances; hence, Solver 2 showed the highest simulation performance.

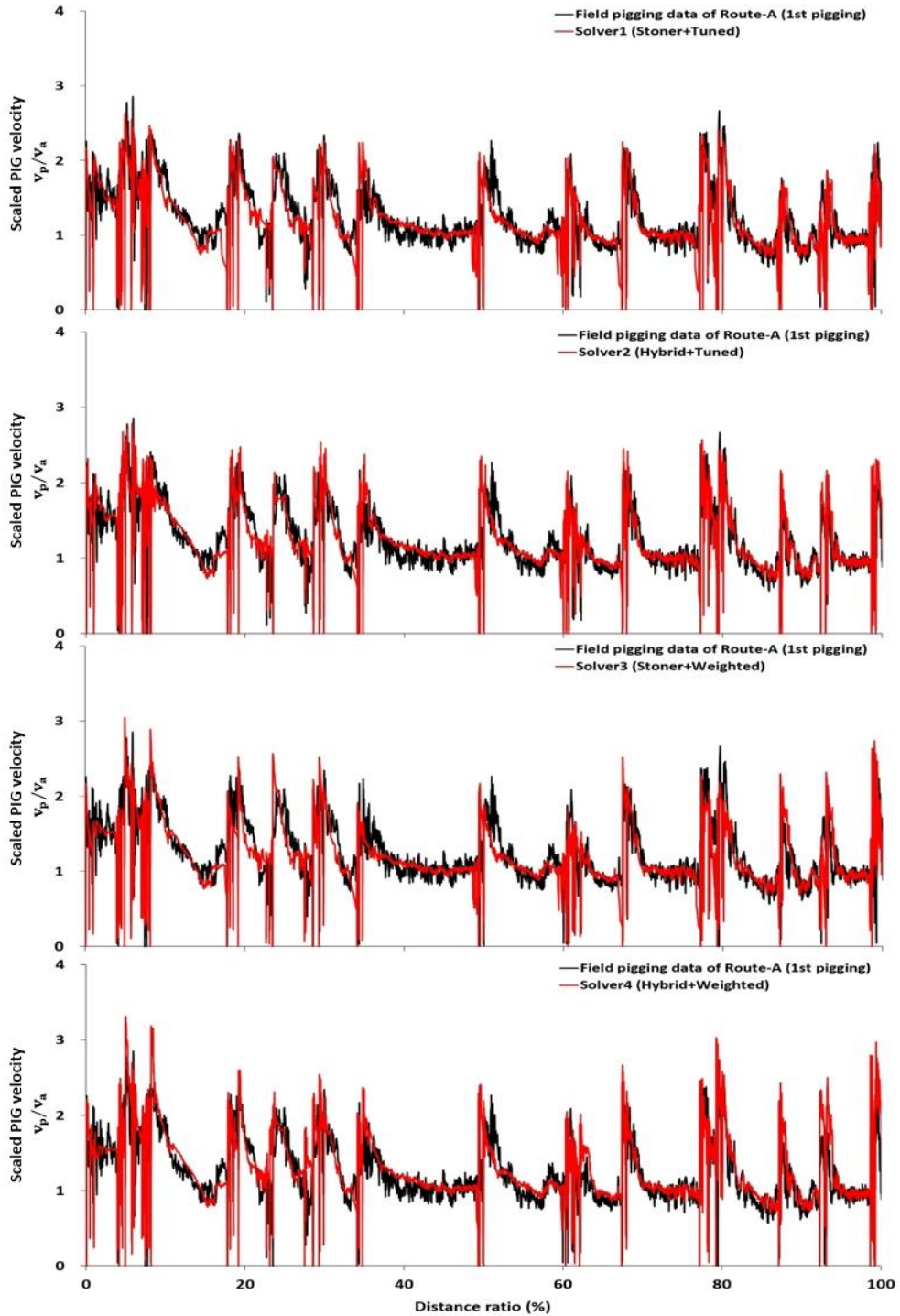


Figure 4-11. Simulated PIG velocities obtained from four solvers for first pigging.

Table 4-3. Simulation performance of solvers through error evaluation

Error model	Solver 1	Solver 2	Solver 3	Solver 4	Criteria
MAE [m/s]	0.464	0.428	0.471	0.444	< 1 m/s
CRM	0.0163	-0.02128	0.0082	-0.0705	CRM>0 underestimate CRM<0 overestimate

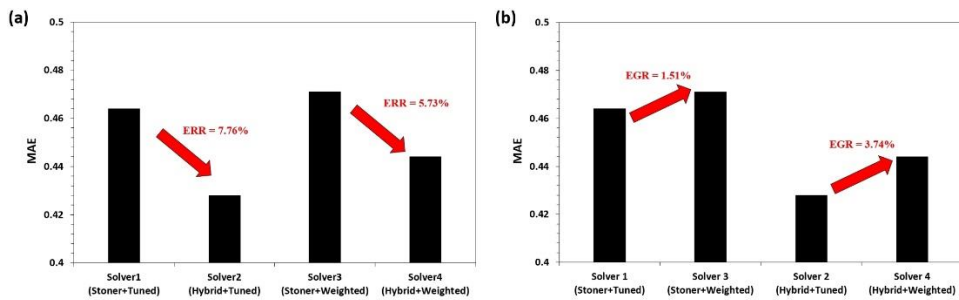


Figure 4-12. Comparison of simulation performance according to: (a) flow models; (b) friction models.

4.4.2 Prediction performance of the solvers

The predicted PIG velocities obtained from the four solvers for second pigging are shown in Figure 4-13. It was verified that the PIG velocities predicted by all the solvers were in good agreement with the field pigging data. However, on comparing the MAE of the solvers as given in Table 4-4, it can be seen that there is a difference in the prediction performance between the solvers. While Solver 4, composed of the MOC-FVM hybrid and weighted friction models, showed the highest prediction performance, Solver 1, composed of the Stoner-MOC and tuned friction models, showed the lowest prediction performance.

Comparing the prediction performance of each solver through EGR as shown in Figure 4-14, it was verified that the EGR of the solvers based on tuned friction models were relatively high at 5.82 % and 6.07 %, whereas the EGR of the weighted friction models were relatively low at 1.27 % and 1.35 %. However, no significant differences in predictability were observed according to the changes in the flow models.

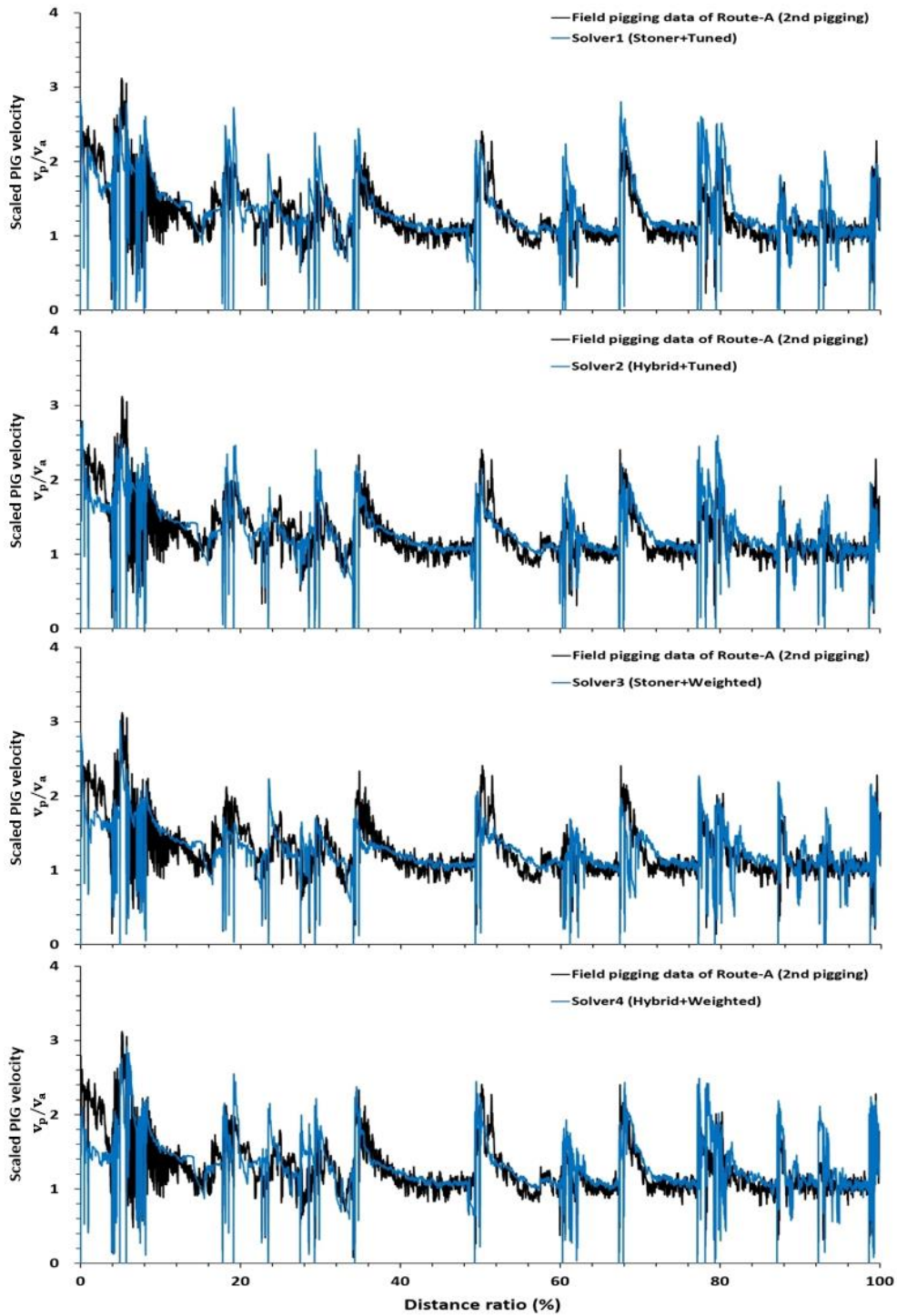


Figure 4-13. Predicted PIG velocities obtained from four solvers for second pigging.

Table 4-4. Prediction performance of solvers through error evaluation

Error model	Solver 1	Solver 2	Solver 3	Solver 4	Criteria
MAE [m/s]	0.488	0.454	0.477	0.449	< 1 m/s
RMSE	0.7337	0.6540	0.6895	0.7385	-
CRM	-0.077	-0.0411	-0.0111	-0.023	CRM>0 underestimate CRM<0 overestimate

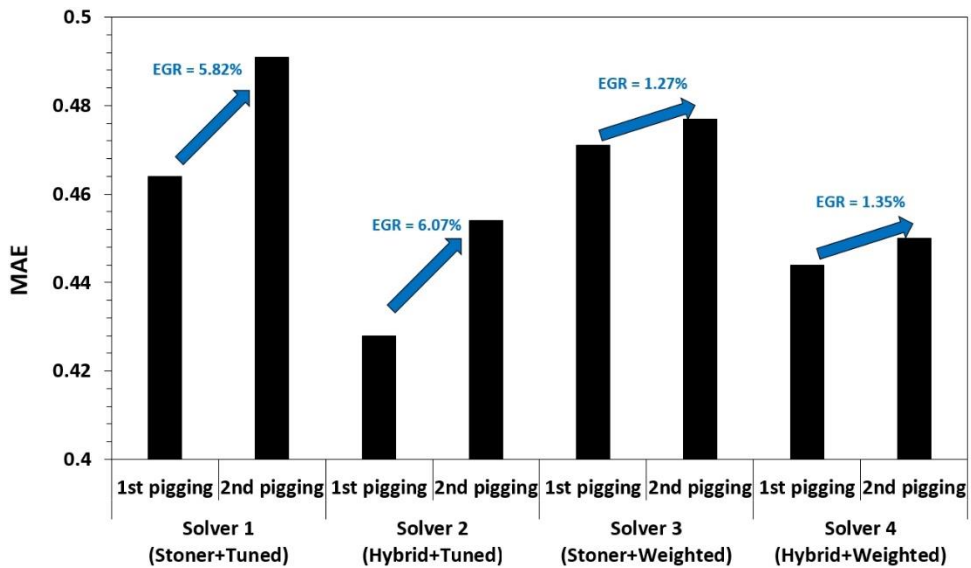


Figure 4-14. Comparison of prediction performance of solvers.

4.4.3 Difference between flow models

First, considering the branching equations of the governing equation, such as in the case of Stoner's equation, the inertial (convective) term was neglected assuming that the flow velocity in the pipe is low. Additionally, by applying the isothermal assumption, which is often employed in conventional pipe flow analysis, the governing equation can be considerably simplified. However, as the FVM solver uses the full Euler equation, wherein the aforementioned assumptions are not applied to the governing equation, differences are expected in our analysis results.

Specifically, in the process of low-pressure/low-flow-rate pigging, the PIG temporarily stops or decelerates in the section where the frictional force increases locally. Subsequently, a pressure pocket built by compressed gas was observed at the rear end of the PIG, and the PIG was rapidly catapulted when the differential pressure exceeded the frictional force. In this series of processes, the compression and expansion of the gas occur around the PIG, which deviates from the situation assumed in the Stoner's equation.

Regarding the numerical difference, a relatively dense grid size is required to obtain high-resolution solution variables near the PIG, whereas a coarse grid is sufficient for the area with quiescent flow. In the case of the Stoner-based solver, it was difficult to maintain sufficient number of grids around the PIG while maintaining computational efficiency because the MOC is fundamentally a type of finite difference method; therefore, it was necessary to construct a uniform and constant grid size.

In addition, calculations were performed with second-order spatial accuracy in the FVM calculation area within the hybrid solver, which is an added advantage near the PIG, where the flow change is large although it was difficult to extend the spatial accuracy in MOC. Figure 4-15 shows the differences between the Stoner-MOC and MOC-FVM hybrid models.

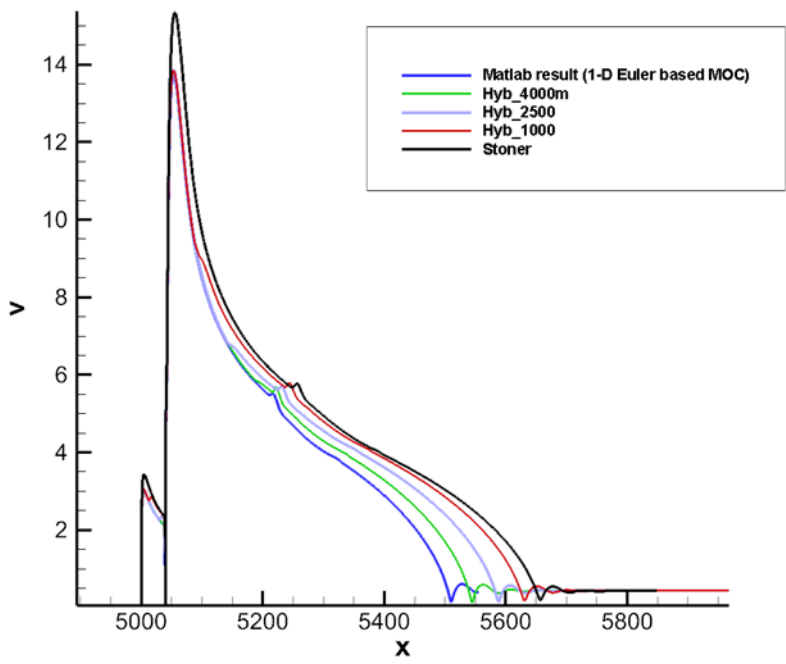


Figure 4-15. Difference between the Stoner-MOC and MOC-FVM hybrid models.

4.4.4 Difference between friction models

The tuned and the weighted friction models have opposite advantages and disadvantages as shown in Figure 4-14. The tuned friction model performed better in the simulation of the first pigging and the weighted friction model performed better in prediction the second pigging. This trend was also observed in our previous study [26] and verified in this study.

The tuned friction model exhibited better simulation accuracy because the friction-constant values could be entered into the dynamic friction table, and these values could be individually tuned.

For example, Figure 4-16 (a) shows the simulation results of the tuned friction model in a specific section, and it can be observed that the pigging velocity is simulated with better accuracy by tuning the dynamic friction table for all friction variations.

However, the weighted friction model exhibited lower accuracy because the variable groups that reflected the characteristics of bends and wall thickness changes adjusted the weighted parameters. For example, Figure 4-16 (b) shows the simulation result of the weighted friction model in a specific section, and it can be observed that the accuracy is relatively low in the section with a type C bend. If the weight parameter corresponding to the type C bend is adjusted to reduce this error, the error in the other sections of the bend eventually increases.

In the prediction performance, the tuning of the tuned friction model was precise based on the first pigging data; however, a large error occurred when predicting the second pigging data. This implies that the friction constant values in the tuned friction model do not properly reflect the friction change owing to the change in operating conditions. However, the linear friction equation and weighted parameters, considering the characteristics of the bends and wall thickness change, reflect the friction change according to the change in operating conditions relatively well. As the friction calculated in each model was different, the calculated PIG velocities were also slightly different.

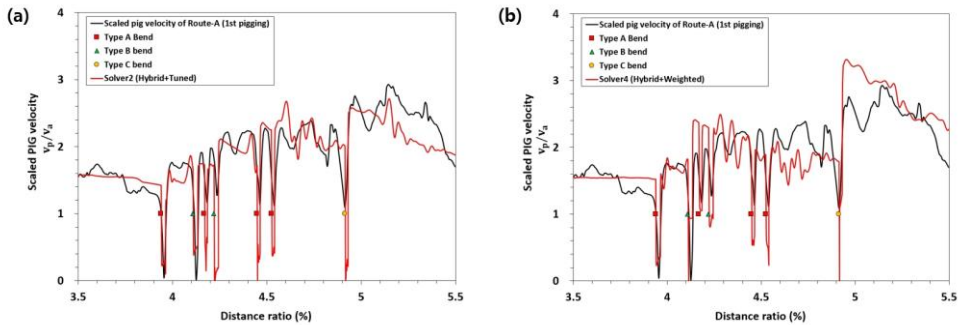


Figure 4-16. PIG velocity differences in the friction models: (a) Tuned friction model; (b) Weighted friction model.

4.5. Summary

This study presented four pigging solvers that were developed by employing different combinations of flow and friction models. The simulation and prediction performances of each solver were evaluated through statistical error evaluation, and it was verified that the MOC-FVM hybrid model showed higher simulation performance than that of the Stoner-MOC model among the flow models.

The Stoner-MOC solver exhibited low simulation accuracy; however, it computed four times faster than the MOC-FVM hybrid solver. Furthermore, among the friction models, the tuned friction model showed a higher simulation performance, whereas the weighted friction model showed a higher prediction performance. Therefore, Solver 2, which had employed a hybrid-tuned model combination, exhibited the highest simulation performance, whereas Solver 4, which had employed a hybrid-weighted model combination, exhibited the highest prediction performance. These results indicate that the flow and friction models can be strategically combined to build a solver depending on the usage requirements as the difference in simulation and prediction performance between solvers has been verified.

4.6. Acknowledgement

This chapter is partially adapted from Speed excursion predictions of pipeline inspection gauge in natural-gas pipeline using pigging solvers based on flow and friction model combinations, prepared to submit in Mechanical Systems and Signal Processing with authors S. Kim, S. Jang, S. Lee, K. Yoo, B. Koo, D. Kim, H. Yoo, C. Kim, Y. Seo. Flow model and solver development were mainly contributed by S. Jang, S. Lee and C. Kim. Conceptualization, friction model, simulation, and validation were mainly contributed by S. Kim, and Y. Seo. This work was supported by Development of Next Generation Pipeline Robot Technology for the Long-Distance Inspection of the Low Pressure/the Low Flow of Gas Pipelines (RD 2019-0251) research project from Korea Gas Corporation (KOGAS)

Chapter 5. Industrial application for CO₂ and H₂ pipeline pigging

5.1. Introduction

Offshore CCS (Carbon Capture and Storage) is a technology that captures CO₂ generated from large-scale thermal power plants, transports them to depleted oil and gas fields, and stores them. Norway and the United Kingdom are conducting a lot of R&D for commercialization and demonstration of offshore CCS [60]. As interest in carbon neutrality increases worldwide, the importance of CCS technology to capture, transport, and store CO₂ contained in flue gas is growing. Recently, in South Korea, an offshore CCS project is underway to re-inject CO₂ in the depleted reservoir of Donghae gas field [61].

In order to safely and efficiently transport CO₂ through offshore pipelines, it is necessary to maintain a dense phase and to operate at high pressures ranging from about 80 bar up to 200 bar [60]. However, due to the aging of pipelines that are more than 20 years old, operation at high pressure is burdensome, and the pipeline integrity should be checked by intelligent pigging before CO₂ transport.

Growing global demand for hydrogen is increasing challenges across the supply chain, from production to consumption. One of the biggest challenges is transporting the hydrogen produced. The most efficient way to solve this is to transport natural gas and hydrogen in the existing pipeline infrastructure [62]. However, the method of transporting a mixture of hydrogen and natural gas still has problems such as leakage and brittleness. Since standards such as the necessary conditions for mixing the two gases have not been established, small hydrogen molecules leaking into pipes or equipment can lead to big problems. Also, when the pressure in the pipeline increases, small amounts of hydrogen can cause brittleness in metal parts. Therefore, the need for monitoring and maintenance activities also increases [63].

Despite growing demand for CO₂ and H₂ pipelines, most previous studies have been limited range to natural gas pipeline pigging. Integrity assessment of CO₂ and

H₂ pipeline with a 'smart PIG' is also viable, but very few inspections runs with smart PIG are reported. Inspection pigging of CO₂ and H₂ pipelines is not routinely done and regarded as more difficult than natural gas pipeline pigging. Objective of this part is firstly to propose a methodology of speed excursion analysis for the CO₂ and H₂ pipeline pigging using Kim's solver, and secondly to identify the PIG behavior properties in the CO₂ and H₂ pipeline, thirdly to compare the risk of operation and speed excursion according to the fluid mixture.

5.2. Methodology

There are limitations in simulating CO₂ and H₂ pipeline pigging using Kim's proposed solver. Simulations using Kim's solver are carried out using ideal gas EOS, therefore, the calculation result of the fluid mixture may be inaccurate. To compensate for this limitation, pre-simulation was performed with the Multiflash and OLGA to obtain accurate physical properties calculated through real gas EOS. Figure 5-1 shows a two-stage simulation methodology for modeling speed excursion using the Multiflash/OLGA and Kim's solver

The first simulation is performed using the Multiflash/OLGA for phase behavior analysis to recognize the speed excursion zone (Vapor phase), and for flow simulation to find the physical properties calculated through the real-gas EOS. The obtained operation pressure range and fluid density are used in the numerical input of Kim's solver. The second simulation is performed using Kim's solver which is based Stoner-MOC for flow model part, and Tuned friction model for friction model part. Using the obtained numerical inputs in the first simulation, speed excursion analysis was conducted to evaluate the risk of operation under speed excursion zone. Finally, optimized operating conditions, and PIG behavior according to fluid mixture can be obtained as output through the speed excursion analysis.

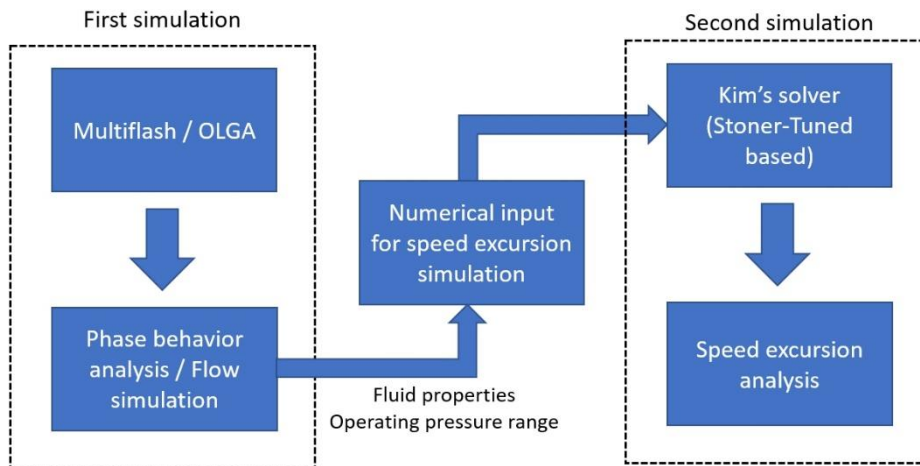


Figure 5-1. A two-stage simulation methodology for modeling speed excursion considering fluid composition

5.3. Phase behavior analysis for speed excursion zone

A Phase diagram due to H₂ blending into natural gas pipeline was obtained in Figure 5.2 using the Multiflash. The critical point of CH₄ 100% is 45.7 bar at -82.8°C, and the vapor phase can be identified based on this point. Speed excursion is a phenomenon that occurs mainly and severely in the vapor phase, and the vapor phase can be called the speed excursion zone. In the case of CH₄ 100%, it can be confirmed from the phase diagram, that speed excursion can be avoided when operating at 45.7 bar or higher at room temperature.

However, as H₂ is mixed, the critical pressure gradually increases and the temperature decreases as shown in Table 5-1. Therefore, because the vapor phase is widened due to hydrogen mixing, the speed excursion zone is widened as shown in the Figure 5-2. For CH₄ 80% + H₂ 20%, minimum required operating pressure is 68.3 bar. The reason why the speed excursion zone is wide due to this hydrogen blending is that the density of hydrogen ($\rho_{H_2} = 0.0899 \text{ kg/m}^3$) is much lighter than that of methane ($\rho_{CH_4} = 0.657 \text{ kg/m}^3$).

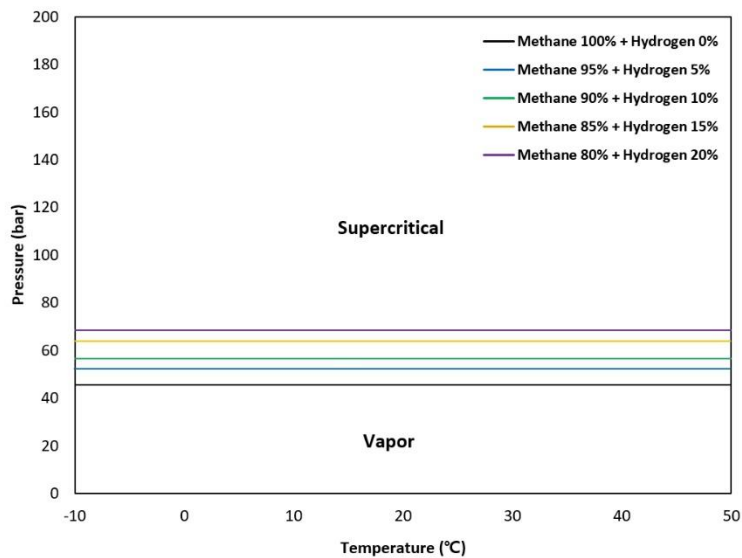


Figure 5-2. Phase diagram for CH₄ + H₂ mixture

Table 5-1. Critical point according to fluid mixture

Fluid mixture	Critical point	
	Pressure (bar)	Temperature (°C)
CH ₄ 100%	45.7	-82.8
CH ₄ 95% + H ₂ 5%	52.4	-84.4
CH ₄ 90% + H ₂ 10%	56.8	-86.3
CH ₄ 85% + H ₂ 15%	64.9	-88.3
CH ₄ 80% + H ₂ 20%	68.3	-90.3
CO ₂ 99% + N ₂ 1%	75.6	30.5

A Phase diagram for CO₂ 99% and N₂ 1% obtained in Figure 5.3 using the Multiflash. The critical point of this mixture is 75.6 bar at 30.5°C, and the vapor phase can be identified based on this point. Speed excursion is a phenomenon that occurs mainly and severely in the vapor phase, and the vapor phase can be called the speed excursion zone. In this case, it can be confirmed from the phase diagram, that speed excursion can be avoided when operating at 75.6 bar or higher at over 30.5°C. However, below the temperature of 30.5°C, the minimum required operating pressure depends on the temperature. Since CO₂ has a higher density ($\rho_{CH_4} = 1.977 \text{ kg/m}^3$) than CH₄, it is expected to be more stable than natural gas pipeline pigging.

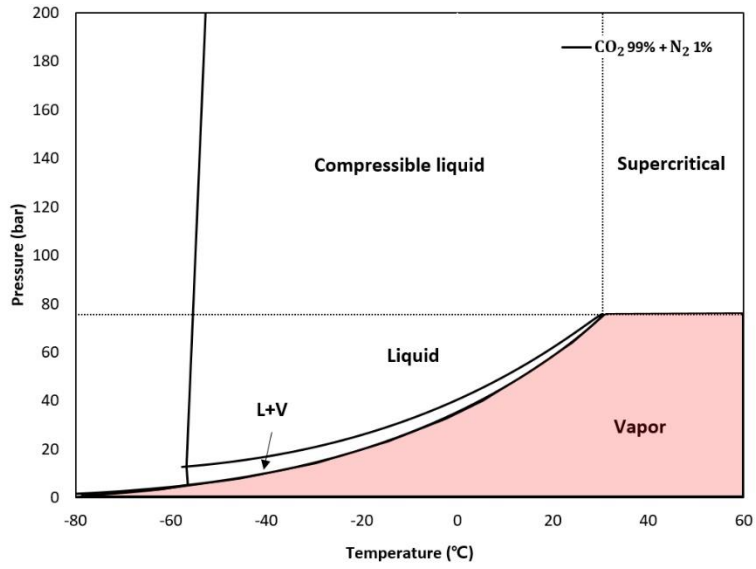


Figure 5-3. Phase diagram for CO_2 + N_2 mixture

5.4. Simulation

5.4.1 Simulation case

This section includes simulation inputs and cases for CO₂, H₂, CH₄ pipeline pigging simulation using Kim's solver. All simulation inputs are identical to those shown in Table 5.2, except for fluid properties. Table 5-3 shows the simulation case for this section. Since hydrogen is lighter than methane, speed excursion is expected even at pressures higher than the critical pressure, so more simulations were performed for three cases (C1 to C3) of 90, 110, and 130 bar.

Conversely, CO₂ is heavier than methane, the speed excursion is expected to be small at a pressure lower than the critical pressure, so more simulations were performed for three cases (C4 to C6) of 50, 40, 30 bar. C0 is the case of CH₄ 100%.

Table 5-2. Numerical parameters for CO₂, H₂, CH₄ pipeline pigging simulation using Kim's solver

Parameter	Value	Unit
L_{pipe}	500	m
k	0.005	mm
T	30	°C
F_s	0.533	bar
F_d	0.365	bar

Table 5-3. Simulation case CO₂ and H₂ pipeline pigging simulation

Case No.	Fluid mixture	Operating pressure (bar)
C0	CH ₄ 100%	-
C1	CH ₄ 80% + H ₂ 20%	90
C2	CH ₄ 80% + H ₂ 20%	110
C3	CH ₄ 80% + H ₂ 20%	130
C4	CO ₂ 99% + N ₂ 1%	50
C5	CO ₂ 99% + N ₂ 1%	40
C6	CO ₂ 99% + N ₂ 1%	30

5.4.2 Case study – H₂ pipeline pigging

This section includes case study results for H₂ pipeline pigging. The simulation results for C1~C3 can be seen in Figure 5-4. The flow velocity is high due to its low density. Average PIG velocity exceeds 5 m/s under 80 bar conditions. It can be confirmed that the pressure of 110 bar of C2 is the minimum allowable pressure to avoid speed excursion at 5 m/s or less. In Figure 5-4, despite the high operating pressure, speed excursions similar to that of natural gas pipeline pigging in the medium operating pressure occurred. Therefore, as in Figure 5-6, The pressure range of 68.3 to 110 bar is "S.E but safe" zone. In the range, Speed excursion is not severe due to the high operating pressure, but flow velocity is high due to its low density.

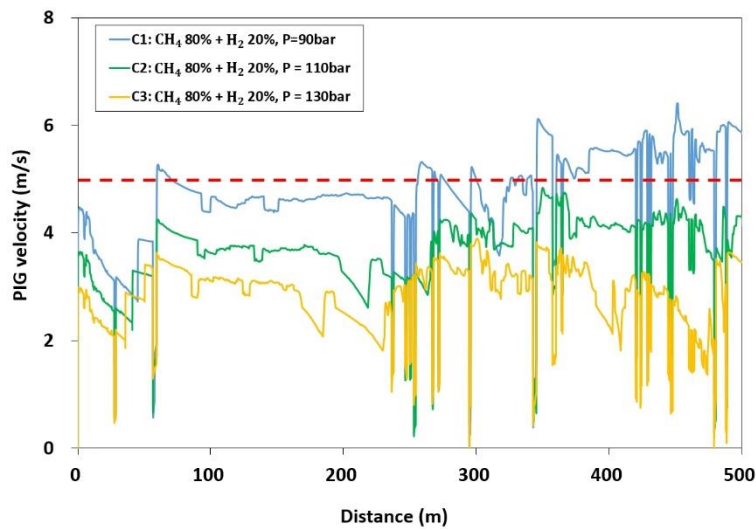


Figure 5-4. Simulation results for H₂ pipeline pigging according to operating pressure

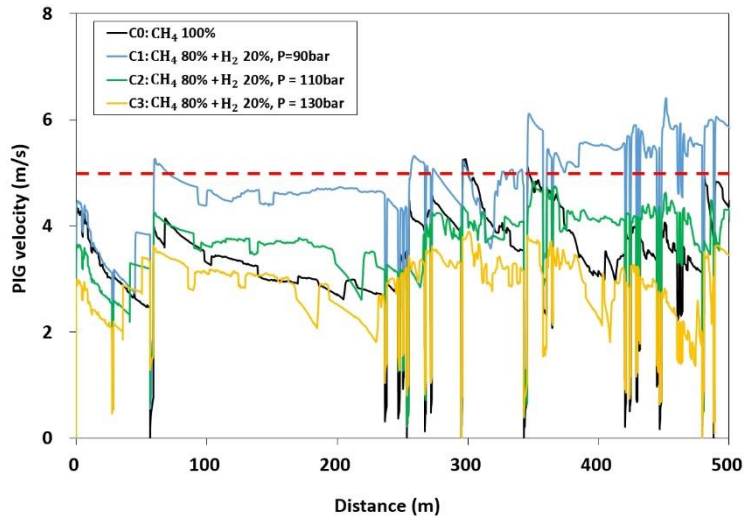


Figure 5-5. Comparison of H₂ and Natural gas pipeline pigging

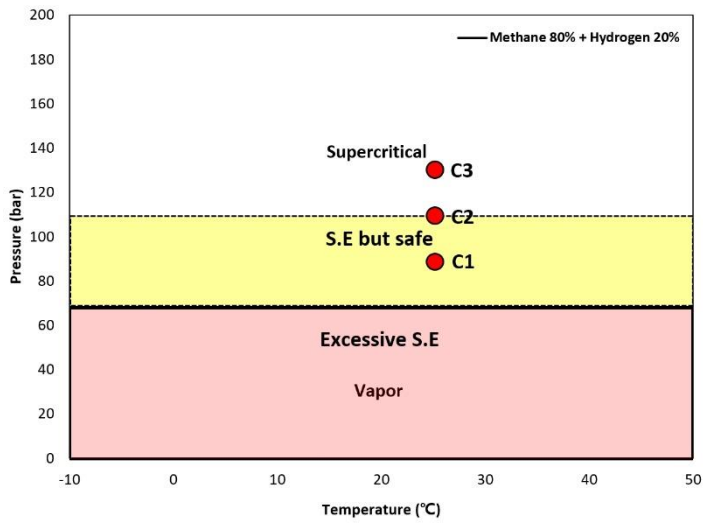


Figure 5-6. Phase diagram of CH₄-H₂ including simulation results

5.4.3 Case study – CO₂ pipeline pigging

This section includes case study results for CO₂ pipeline pigging. The simulation results for C4~C6 can be seen in Figure 5-7. Contrary to the hydrogen simulation result, the flow velocity is low due to its high density. Critical pressure is 75.6 bar, but excessive speed excursion starts to occur from below 40 bar. Thus, the pressure range of 75.6 bar to 40 bar is “S.E but safe” zone as shown in Figure 5-9. This result means that pigging operation in the S.E but safe zone is possible when high-pressure pigging is difficult for aging pipeline.

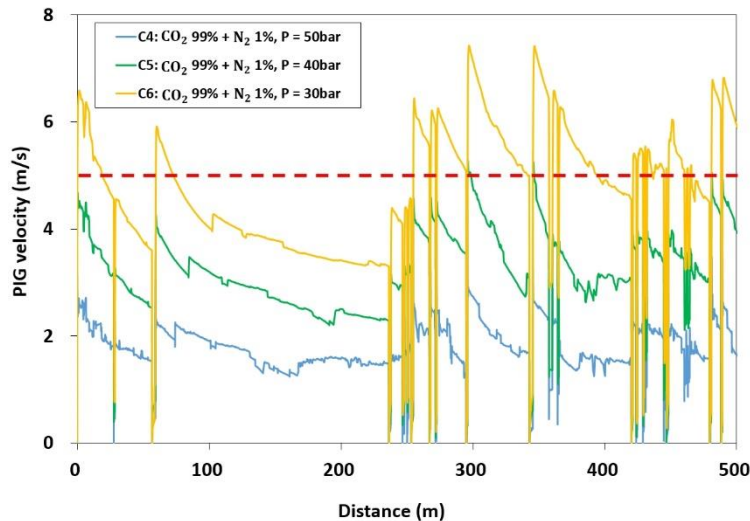


Figure 5-7. Simulation results for CO₂ pipeline pigging according to operating pressure

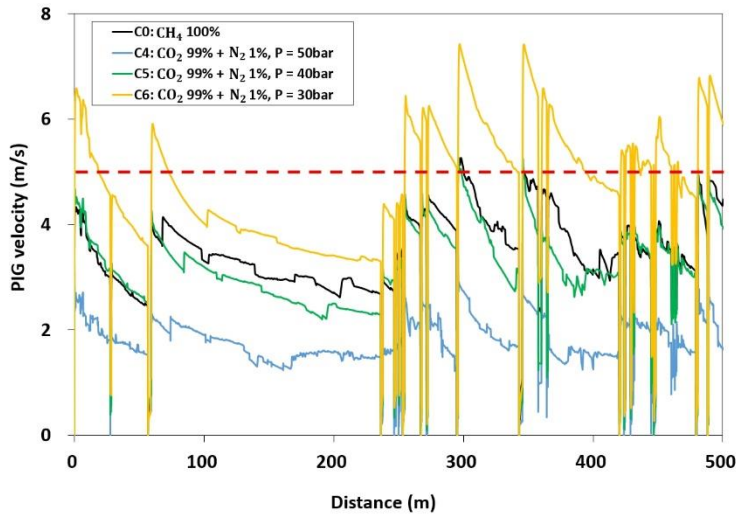


Figure 5-8. Comparison of CO₂ and Natural gas pipeline pigging

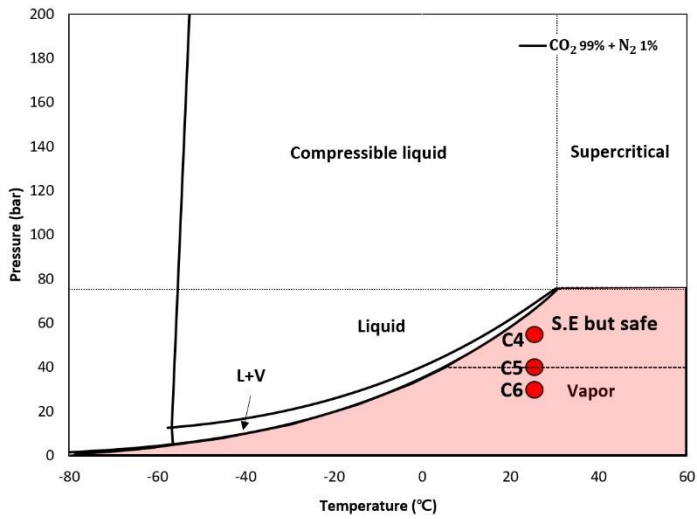


Figure 5-9. Phase diagram of CO₂-N₂ including simulation results

5.5. Summary

This study presented methodology of speed excursion analysis for the CO₂ and H₂ pipeline pigging using Kim's solver. The methodology includes a two-stage simulation for modeling speed excursion considering fluid composition using Multiflash, OLGA, Kim's solver. The first simulation is performed using Multiflash/OLGA for phase behavior analysis to recognize the speed excursion zone (Vapor phase), and for flow simulation to find the physical properties calculated through the real-gas EOS. The obtained operation pressure range and fluid density are used in the numerical input of Kim's solver. The second simulation is performed using Kim's solver which is based Stoner-MOC for flow model part, and Tuned friction model for friction model part. Using the obtained numerical inputs in the first simulation, speed excursion analysis was conducted to evaluate the risk of operation under speed excursion zone. Finally, optimized operating conditions, and PIG behavior according to fluid mixture can be obtained as output through the speed excursion analysis.

With the proposed methodology, speed excursion analysis was performed for H₂ and CO₂ pipeline pigging. PIG behavior properties in the CO₂ and H₂ pipeline were identified. Summarizing the case study results, increased speed excursion zone due to H₂ blending and low density in the CH₄-H₂ pipeline, and decreased speed excursion zone due to high density in the CO₂-N₂ pipeline. Also, in terms of speed excursion, H₂ pipeline pigging was the most difficult and CO₂ pipeline pigging was the easier than the natural gas pipeline pigging.

Chapter 6. Concluding remarks

6.1. Conclusions

This study presented various models, solvers, and methodologies that can predict unstable behavior of PIG such as speed excursion through modeling, simulation and experiment.

Firstly, two novel friction models of pipeline inspection gauges were proposed to simulate and predict speed excursions occurring in the total distance ratio of a pipeline generated by numerous bends and changes in wall thickness. These two friction models are tuning models based on field data to simulate speed excursions due to frictional variation, and can be strategically selected according to the purpose of the simulation. These results mean that the speed excursion at the total distance ratio can be simulated and predicted with high accuracy using the proposed friction models. Therefore, these two novel friction models would provide insights for the operators to simulate and predict the dynamics of the PIGs in their pipeline networks.

Secondly, speed excursion due to changes in wall thickness were experimented to investigate the mechanism of speed excursion and the relationship between speed excursion and main variables as flowrate, wall thickens change, and linepack length.

Based on the differential pressure measurement results, the speed excursion process was divided into four phases: build-up phase, pre-speed excursion phase, speed excursion phase, and recovery phase. The PIG behavior was analyzed based on the results of these five phases. The flow velocity has a linear relationship with the speed excursion, but the excursion ratio has an exponential curve that rapidly increases at low flow velocity. These results indicate that low-flow pigging produces relatively low-speed excursions but can be risky because of the rapid increase in the excursion ratio. The build-up and recovery times also showed an exponential curve that increased rapidly at low flow velocities. These results indicate that pigging behavior is significantly unstable owing to the long buildup and recovery times during low-flow pigging. When the wall thickness change ratio increased from 1.94% to 3.94%,

the increase in friction caused the speed excursion to increase from 46% to 110%, showing a linear relationship. The rate of increase was higher as the flow rate decreased. In the excursion ratio result, an exponential curve was obtained even when the friction increased due to the wall thickness change. The excursion ratio dramatically increased as the flow rate decreased. The build-up time and recovery time results showed an exponential curve that rapidly increased at low flow rates due to increased friction. These results indicate that the PIG behavior is more unstable due to increased friction, especially at low flow rates. When the linepack length changed from 4.5 m to 9 m, higher-speed excursions occurred as the linepack length increased, even under the same friction conditions. These results are important as they indicate that the linepack length is the main factor in the speed excursion. Finally, the equation of friction increase ratio according to the wall thickness change ratio was proposed from the experiment and was validated by Kim's solver within 8.5% error.

Thirdly, four pigging solvers that were developed by employing different combinations of flow and friction models were proposed. The simulation and prediction performances of each solver were evaluated through statistical error evaluation, and it was verified that the MOC-FVM hybrid model showed higher simulation performance than that of the Stoner-MOC model among the flow models. The Stoner-MOC solver exhibited low simulation accuracy; however, it computed four times faster than the MOC-FVM hybrid solver. Furthermore, among the friction models, the tuned friction model showed a higher simulation performance, whereas the weighted friction model showed a higher prediction performance. Therefore, Solver 2, which had employed a hybrid-tuned model combination, exhibited the highest simulation performance, whereas Solver 4, which had employed a hybrid-weighted model combination, exhibited the highest prediction performance. These results indicate that the flow and friction models can be strategically combined to build a solver depending on the usage requirements as the difference in simulation and prediction performance between solvers has been verified.

6.2. Further study

This dissertation has given several insights on speed excursion of PIG. However, it also left some challenges.

Firstly, since the weighted friction model and the tuned friction model show opposite advantages and disadvantages, hybrid friction model can be proposed to adopt the advantages from both friction models by using integrated algorithm of both friction models at the same time. The core concept is to use the weighted friction model as the main model to simulate all friction variation, and then configure the algorithm to separately reinterpret some sections with large errors as a tuned friction model.

Secondly, since the speed excursion must be controlled, it is necessary to apply the bypass PIG model to the proposed model, solver, and methodology. Therefore, in the end, speed excursion occurs, and speed simulation should be possible to be aware of that how much the speed excursion decreases according to the bypass performance.

Thirdly, Kim's solver adopted the ideal gas equation because it was assumed that the error due to the application of the ideal gas was small. However, if real gas EOS is applied to Kim's solver, the error can be further reduced.

Bibliography

1. Azpiroz, J.E., Hendrix, M.H.W., Breugem, W.P., et al., 2015. CFD modelling of bypass pigs with a deflector disk. In: 17th International Conference on Multiphase Production Technology. BHR Group, pp. 141–155.
2. A.E. McDonald, O. Baker, A method of calculating multiphase flow in pipelines using rubber spheres to control liquid holdup, *Drilling and production practice*, 1964, pages 56-68
3. A. Singh, R.A.W.M. Henkes, CFD Modeling of the Flow Around a By-pass Pig, 8th North American Conference on Multiphase Technology, 2012
4. Botros, K.K., Golshan, H., 2010. Field validation of a dynamic model for an MFL ILI tool in gas pipelines. In: 2010 8th International Pipeline Conference. American Society of Mechanical Engineers, pp. 325–336.
5. Chen, J., Luo, X., Zhang, H., He, L., Chen, J., Shi, K., 2018 Experimental study on movement characteristics of bypass pig. *J. Natural gas Sci. Eng.*, 59, 212-223.
6. Chen, J., He, L., Luo, X., Lu, L., et al 2020. Bypass pigging technology on amelioration of pigging-induced liquid flow: An experimental and modelling study. *Ocean Eng.* 198, 106974
7. Chen, J., He, L., Luo, X., Zhang, H., et al 2020. Characterization of bypass pig velocity in gas pipeline: An experimental and analytical study
8. Davoudi, M., Heidari, Y., 2014. Field experience and evaluation of the south pars sea line pigging based on dynamic simulations. *J. Natural gas Sci. Eng.* 18, 210-218.
9. Den, Heijer A., 2016. Frictional Behavior of Pigs in Motion. Delft University of Technology.
10. Esmaeilzadeh, F., Mowla, D., Asemani, M., 2009. Mathematical modeling and simulation of pigging operation in gas and liquid pipelines. *J. Petrol. Sci. Eng.* 69 (1), 100–106.
11. F. Esmaeilzadeh, D., Mowla, M., Asemani, et al., Modeling of Pig Operations in Natural Gas and Liquid Pipeline, SPE Annual Technical Conference, 2006, 102049
12. Gao, X., Huang, Q., Zhang, X., et al. 2021. Experimental study on the wax removal physics of foam PIG in crude oil pipeline pigging. *J. Petrol. Sci. Eng.* 205, 108881.
13. Groote, G.A., Van De Camp, P.B.J., Veenstra, P., et al., 2015. By-pass pigging without or with speed control for gas-condensate pipelines. In: Abu Dhabi

- International Petroleum Exhibition and Conference. Society of Petroleum Engineers, pp. 1–13.
14. He, H., Liang, Z., 2019. Speed simulation of pig restarting from stoppage in gas pipeline. pp. 10.
 15. He, H., Liang, Z., 2019. Simulation of pigging with a brake unit in hilly gas pipeline. *J. Applied Fluid Mechanics*, vol. 12, No. 5, pp. 1497-1509
 16. Hendrix, M.H.W., Den Heijer, A., Breugem, W.P., et al., 2016. Frictional forces during pigging of multiphase pipelines. In: 10th North American Conference on Multiphase Technology. BHR Group, pp. 103–114.
 17. Hendrix, M.H.W., Ijsseldijk, H.P., Breugem, W.-P., Henkes, R.A.W.M., 2018. Experiments and modeling of by-pass pigging under low-pressure conditions. *J. Proc. Cont.*, 71, 1-13.
 18. Hendrix, M.H.W., Liang, X., Breugem, W.P., et al., 2017. Characterization of the pressure loss coefficient using a building block approach with application to by-pass pigs. *J. Petrol. Sci. Eng.* 150, 13–21.
 19. Hendrix, M.H.W., Ijsseldijk, H.P., Breugem, W.-P., et al. 2018. Experiments and modeling of by-pass pigging under low-pressure conditions. *J. Proc. Cont.*, 71, 1-13.
 20. Hosseinalipour, S.M., Khalili, A.Z., Salimi, A., 2007. Numerical simulation of pig motion through gas pipelines. In: 16th Australian Fluid Mechanics Conference. Gold Coast, Queensland, Australia, pp. 971–975.
 21. Ijsseldijk, H.P. 2016. By-Pass Pigging – Experiments and Simulations (Master’s thesis), Delft University of Technology.
 22. Jamshidi, B., Sarkari M., 2016. Simulation of pigging dynamics in gas-liquid two-phase flow pipelines. *J. Natural gas Sci. Eng.*, 32, 407-414.
 23. J. Cordell, H. VanZant, Pipeline Pigging Handbook, 2003
 24. K. Kohda, Y. Suzukawa, H. Furukawa, Analysis of transient gas-liquid two-phase flow in pipelines, *J. Energy Resour. Technol.* 1987, 110(2), 93-101
 25. Kim, S., Seo, Y., 2020. Simulation and parametric study of speed excursion of pig in low-pressure gas pipeline. *Proc. of the Thirtieth Int. Ocean and Polar Eng. Conference.*
 26. Kim S., Yoo K., Koo B., et al. 2022. Speed excursion simulation of PIG using improved friction models. *J. Natural gas Sci. Eng.* 97, 104371.
 27. L.F.A. Azevedo, A.M.B. Braga, A.O. Nieckeke, et al., Simple Hydrodynamic Models for the Prediction of Pig Motions in Pipelines, Offshore Technology Conference, 1996, 8232

28. Lesani, M., Rafeeyan, M., et al., 2012. Dynamic analysis of small pig through two and three-dimensional liquid pipeline. *J. Applied Fluid Mechanics*, vol. 5, No. 2, pp. 75-83
29. Li, C. B., Pavelescu, D., et al., 1982. The friction-speed relation and its influence on the critical velocity of stick-slip motion. *Wear*, 82, 277-289.
30. Li, X., He, L., Luo, X., et al. 2021. Transient pigging dynamics in gas pipelines: Models, experiments, and simulations. *Ocean Eng.* 232, 109126
31. Liang, Z., He, H., et al., 2017. Speed simulation of bypass hole PIG with a brake unit in liquid pipe. *J. Natural gas Sci.* 42, 40-47
32. Lima, G. F., Freitas, V.C.G., et al., 2017. Pig's speed estimated with pressure transducers and hall effect sensor: an industrial application of sensors to validate a testing laboratory. *Sensors* 2017, 17, 2119
33. Naeini, H.S., Soorgee, M.H. 2021. Experimental investigation on sphere PIG movement in multiple thickness pipe. *J. Natural gas Sci. Eng.* 95, 104152.
34. Nguyen, T.T., Yoo, H.R., Rho, Y.W., et al., 2001. Speed control of pig using bypass flow in natural gas pipeline. *Industrial Electronics In: Proceedings. ISIE 2001. IEEE International Symposium on. IEEE.* 2001. pp. 863–868 (2).
35. Nguyen, T.T., Kim, S.B., Yoo, H.R., et al., 2001. Modeling and simulation for pig with bypass flow control in natural gas pipeline. *KSME Int. J.* 15 (9), 1302–1310
36. Nieckele, A.O., Braga, A.M.B., Azevedo, L.F.A., 2001. Transient pig motion through gas and liquid pipelines. *J. Energy Resour. Technol.* 123 (4), 260–269.
37. M.H.W. Hendrix, C.M. Graafland, R.A.J. van Ostayen, Frictional forces for disc-type pigging of pipelines, *J. Petrol. Sci. Eng.*, 2018, 905-918
38. M.W. Scoggins Jr., A Numerical Simulation Model for Transient Two-phase Flow in a pipeline, Dotor's thesis, University of Tulsa, 1977
39. Mirshamsi, M., Rafeeyan, M., 2015. Dynamic analysis and simulation of long pig in gas pipeline. *J. Natural gas Sci. Eng.* 23, 294-303
40. Moreels, E., Neve, S.D., et al., 2003. Simulating nitrate leaching in bare fallow soils: a model comparison. *Nutrient Cycling in Agroecosystems* 67, 137-144.
41. Money, N., Cockfield, D., Mayo, S., et al. 2012. Dynamic speed control in high velocity pipelines. *Pipeline Gas J.* 239 (8), 30-38.
42. O'donoghue, A.F., 1996. On the Steady State Motion of Conventional Pipeline Pigs Using Incompressible drive media. Cranfield University.
43. Pinto, A., Voss, w., et al., 2017. Operational bypass pigging in multiphase lines

- a flow assurance study comparison to real operation and model validation. SPE Abu Dhabi Int. Petrol. Exhibition and Conference 2017.
44. S. Barua, An Experimental Verification and Modification of the McDonald-Baker Pigging Model for Horizontal Flow, Doctor's thesis, University of Tulsa, 1982
 45. Tiratsoo, J.N.H., 2003. Pipeline Pigging & Integrity Technology, third edition
 46. White, F.M., 1999, Fluid mechanics, McGraw-Hill Pub.
 47. X. Zhu, D. Wang, H. Yeung, et al., Comparison of linear and nonlinear simulations of bidirectional pig contact forces in gas pipelines, J. Natural gas Sci. Eng., 2015. 151-157
 48. Xu, X.X., Gong, J., 2005. Pigging simulation for horizontal gas-condensate pipelines with low-liquid loading. J. Petrol. Sci. Eng., 48, 272-280.
 49. Zhang, L., Zhou, J., et al., 2020. Modeling and simulation of pigging for a gas pipeline using a bypass pig. Mathematical Problems in Engineering, pp. 12.
 50. Zhu, X., Zhang, S., Li, X., et al. 2015. Numerical simulation of contact force on bi-directional PIG in gas pipeline: At the early stage of pigging. J. Natural gas Sci. Eng. 23, 127-138.
 51. Zhu, X., Li, X., Zhao, C., et al. 2016. Dynamic simulation and experimental research on the motion of odometer passing over the weld. J. Natural gas Sci. Eng. 30, 205-212.
 52. Zhu, X., Zhang, S., Tan, G., Wang, D., Wang, W. 2014. Experimental study on dynamics of rotatable bypass-valve in speed control pig in gas pipeline. Measurement. 47, 686-692.
 53. Weiss, J. M., Smith, W. A. 1995. Preconditioning applied to variable and constant density flows. AIAA journal, 33(11), 2050-2057.
 54. Venkateswaran, S., Merkle, W. A. 1995. Dual Time Stepping and Preconditioning for unsteady computations. AIAA journal, 95-0078.
 55. Kim, H., Kim, H., Kim, C. 2018. Computations of homogeneous multiphase real fluid flows at all speeds. AIAA journal, 2623-2634.
 56. Koo, B. 2022. Comparison of finite-volume method and method of characteristics for simulating transient flow in natural-gas pipeline. Journal of Natural Gas Science and Engineering 98, 104374.
 57. Kim, S., et al. 2003. Cures for the shock instability: Development of a shock-stable Roe scheme. Journal of Computational Physics, 342-374.
 58. Mavriplis, D. J., Zhi, Y. 2006. Construction of the discrete geometric

- conservation law for high-order time-accurate simulations on dynamic meshes. *Journal of Computational Physics*, 557-573.
59. Donea, J, et al. 2004. Arbitrary Lagrangian–Eulerian Methods. *Encyclopedia of computational mechanics*.
 60. Antonie, O, Joakim R., 2008. State-of-the-Art Overview of CO₂ Pipeline Transport with Relevance to Offshore Pipelines.
 61. Yong-Chan, P., et al. 2014. Estimation of CO₂ Storage Capacity in a Depleted Gas Field on the Korean Continental Shelf. 14th International Conference on Greenhouse Gas Control Technologies.
 62. Joan, O., et al. 2018. Natural gas as a bridge to hydrogen transportation fuel: Insights from the literature. *Energy Policy*, P 317-329
 63. Tod B., 2020. In-line Inspection Tool Design and Assessment of Hydrogen Pipeline. PPSA Seminar.
 64. R. Davidson, 1995. An introduction to pipeline pigging. Gulf Professional Publishing.
 65. H. Goedecke, 2003. Ultrasonic or MFL Inspection: Which Technology Is Better for You?. In: *Pipeline and Gas Journal* 230, pp. 34–41.
 66. C. M. Graafland, 2017. Frictional behavior of pigs. MSc thesis. Delft University of Technology, 2017.
 67. C. M. Graafland M. H.W. Hendrix and R. van Ostayen, 2018. Frictional forces during pipeline pigging.” *Journal of Petroleum Science and Engineering* 171, pp. 905–918.
 68. K. Minami and O. Shoham, 1995. Pigging dynamics in two-phase flow pipelines: Experiment and modeling. *SPE Production and Facilities* 10.4, pp. 225–231.
 69. M. Mirshamsi and M. Rafeeyan, 2012. Speed control of pipeline pig using the QFT method. In: *Oil and Gas Science Technology* 67.4, pp. 693–701.
 70. J. Quarini and S. Shire, 2007. A review of fluid-driven pipeline pigs and their applications. *Journal of Process Mechanical Engineering* 221.1, pp. 1–10.
 71. C. Ramella et al., 2015. A novel smart caliper foam pig for low-cost pipeline inspection - Part B: Field test and data processing. English. *Journal of Petroleum Science and Engineering* 133, pp. 771–775.
 72. Z. Rui, G. Han, H. Zhang, S. Wang, H. Pu, and K, 2017. Ling. A new model to evaluate two leak points in a gas pipeline. *Journal of Natural Gas Science and Engineering* 46.36, pp. 491–497.
 73. S. T. Tolmasquim and A. O. Nieckele, 2008. Design and control of pig

- operations through pipelines. *Journal of Petroleum Science and Engineering* 62.3-4, pp. 102–110.
74. H. Zhang, C. Sanchez, S. Liu, S. Zhang, and H. Liang, 2017. Wear of a polyurethane rubber used in dry gas pipeline as inspection gauges. *Journal of Natural Gas Science and Engineering* 41, pp. 40–48.
 75. X. Zhu, W. Wang, S. Zhang, and S. Liu, 2017. Experimental Research on the Frictional Resistance of Fluid-Driven Pipeline Robot with Small Size in Gas Pipeline. *Tribology Letters* 65.2.
 76. R. Davidson, 1995. *An introduction to pipeline pigging*. Gulf Professional Publishing.
 77. J. Cordell, H. Vanzant, 2003. *The pipeline pigging handbook*. ISBN: 0-9717945-3-7. Clarion Technical Publishers & Scientific Surveys Ltd., 3rd edition.
 78. B.N.J. Persson, 1998. *Sliding Friction*. ISBN: 3-540-63296-4. Springer.
 79. M. Saeidbakhsh, M. Rafeeyan, S. Ziaei-Rad, 2009. Dynamic analysis of small pigs in space pipelines. *Oil and Gas Science and Technology*, 64(2):155–164.
 80. Boghi, A., Brown, L., Sawko, R., Thompson, C.P., 2018. A non-inertial two-phase model of wax transport in a pipeline during pigging operations. *J. Petrol. Sci. Eng.* 165, 664–672
 81. Liu, Shangjunnan, Liu, Shuhai, Xiao, H., 2020. Optimization of structural parameters of jet end in the underwater intelligent pigging robot. *Ocean Eng.* 216
 82. Patricio, R.A.C., Baptista, R.M., Rachid, B. de F., Bodstein, G.C.R., 2020. Numerical simulation of pig motion in gas and liquid pipelines using the Flux-Corrected Transport method. *J. Petrol. Sci. Eng.* 189, 106970
 83. Bendiksen, K.H., Maines, D., Moe, R., Nuland, S., 1991. The dynamic two-fluid model olga: theory and application. *SPE Prod. Eng.* 6 (2), 171–180
 84. Cao, Y. G., C. Liu, H. J. Tian, S. H. Zhang, and Y. T. Sun. 2020. Prediction of the driving force for a cup pig based on the distribution of contact stress. *J. Nat. Gas Sci. Eng.* 81: 103415.
 85. Cao, Y. G., Y. Zhen, Y. J. Shi, S. H. Zhang, Y. T. Sun, and W. J. Nie, 2018. Stress distribution of the power section cup of pipeline inspection gauges by finite element method.” *J. Pipeline Syst. Eng. Pract.* 9 (2): 04017039.
 86. Liu, C., Y. G. Wei, Y. G. Cao, S. H. Zhang, and Y. T. Sun, 2020. Traveling ability of pipeline inspection gauge (PIG) in elbow under different friction coefficients by 3D FEM. *J. Nat. Gas Sci. Eng.* 75: 103134.
 87. Zhang, H., S. M. Zhang, S. H. Liu, and Y. Wang, 2017. Collisional vibration of

- PIGs (pipeline inspection gauges) passing through girth welds in pipelines. *J. Nat. Gas. Sci. Eng.* 37: 15–28.
88. Zhang, H., S. M. Zhang, S. H. Liu, Y. Wang, and L. Lin, 2015. Measurement and analysis of friction and dynamic characteristics of PIG's sealing disc passing through girth weld in oil and gas pipeline. *Measurement* 64: 112–122
 89. Zhang, H., S. M. Zhang, S. H. Liu, X. X. Zhu, and B. Tang, 2015. Chatter vibration phenomenon of pipeline inspection gauges (PIGs) in natural gas pipeline. *J. Nat. Gas Sci. Eng.* 27 (Nov): 1129–1140
 90. Zhu, X. X., W. Wang, S. M. Zhang, and C. Wang. 2017. The pig gravity impact on its frictional force in oil and gas pipeline. In *Proc., 27th Int. Ocean and Polar Eng. Conf.*, 140–144. San Francisco: International Society of Offshore and Polar Engineers.

Abstract in Korean

천연가스 배관망에서 배관 검사 로봇은 속도 이탈(Speed excursion)로 인해 거동이 매우 불안정하여, 데이터 손실 및 및 구조적 충격 위험성이 크게 증가한다. 특히, 저압/저유량의 운영조건에서 로봇의 속도이탈이 심해지며, 이러한 운영조건의 배관을 배관 검사가 불가능한 Unpiggable 배관으로 구분한다. Unpiggable 배관은 전세계에 약 40%, 국내 가스 배관망의 경우 약 35%를 차지하므로 속도이탈로 인해 상당수의 배관의 건전성을 관리하지 못하고 있는 실정이다.

본 연구는 천연가스 배관망에서 배관 검사 로봇의 동적 거동에 관한 모델링, 시뮬레이션, 실험 연구를 통하여 속도 이탈 현상과 같은 불안정 거동에 대해 예측 할 수 있는 다양한 모델, Solver, 방법론을 제시한다.

첫째로, 마찰 변화로 인한 속도 이탈 현상을 모사하기 위한 두 가지 마찰력 모델을 제안한다. 첫 번째 마찰 모델은 Tuned friction model로 지수형 마찰 모델 (Exponential friction model)과 결합된 동마찰 테이블을 채택하여 마찰 변화를 반영할 수 있고, 두 번째 마찰 모델은 Weighted friction model로 곡관과 단차로 인한 마찰 변화에 대해 선형 방정식을 구성하고 가중치(weight parameter)로 각 요인의 영향을 결정하는 방식을 채택하였다. 이 두 가지 마찰 모델은 마찰 변화로 인한 속도 이탈을 시뮬레이션하기 위해 현장 데이터를 기반으로 한 튜닝 모델 (Tuning models based on field data)이다. 수치 모사를 위해 과도 기체 유동방정식은 특성법(MOC)으로 풀고, Runge-Kuta 방법을 사용하여 PIG의 운동방정식을 풀었다. 제안된 마찰 모델을 적용한 시뮬레이션 결과는 한국가스공사(KOGAS)가 운영하는 3개 노선의 현장 Piggig 데이터와 비교하였으며, 전반적으로 모사 결과가 현장 Piggig 데이터와 잘 일치하였다. 첫 번째 모델인 Tuned friction model은 높은 정확도로 평균 Piggig 속도와 속도 이탈을 모사 할수 있었고, 두 번째 모델인

Weight friction model은 첫 번째 마찰 모델보다 낮은 정확도를 보였지만 다양한 작동 조건에서 평균 Pigging 속도와 속도 이탈을 예측할 수 있었다.

둘째로, 속도 이탈의 발생 메커니즘과 주요 변수와의 관계를 규명하기 위해 실험실 규모의 배관 로봇 주행 실험 장치를 구축하여 최초로 속도 이탈 실험을 수행하였다. 차압 결과에 기초하여 속도 이탈의 메커니즘은 5단계(Stable behavior, build-up phase, pre-speed excursion phase, speed excursion phase, recovery phase)로 규명하고, 주요 변수와 속도 이탈의 관계를 분석한 결과 유속은 속도 이탈과 선형 관계를 갖지만, 이탈 비율은 저 유속에서 급격히 증가하는 Exponential fit 관계임을 알 수 있었다. 이러한 결과는 저유량 Pigging이 상대적으로 저속의 속도 이탈을 유발하지만, 이탈 비율의 급격한 증가로 인해 매우 위험한 작업이 될 수 있음을 의미한다. Build-up 시간과 Recovery 시간 모두 낮은 유속에서 급격히 증가하는 Exponential fit 관계를 보여줬다. 이는 저유량에서 긴 빌드 업 시간과 회복 시간으로 인해 배관 로봇 거동이 Stick-slip 운동을 보인 매우 불안정한 거동을 할 수 있음을 나타낸다. 또한 Linepack 길이가 변경되면 동일한 마찰 조건에서도 Linepack 길이가 증가함에 따라 더 높은 속도 이탈이 발생하였다. 이 결과는 Linepack 길이가 Pigging 거동의 주요 요인임을 보여주며, 장거리 파이프라인 Pigging시 속도 이탈 및 거동에 영향을 미치는 중요한 변수로도 고려 되어야함을 의미한다.

셋째로, 제안된 2개의 마찰 모델과 2개의 유체 모델, Stoner-MOC, MOC-FVM Hybrid를 결합하여 총 4개의 배관 로봇 거동 Solver를 제안하고, 각 Solver의 결과를 한국가스공사의 현장 데이터와 비교하여 속도 이탈에 대한 모사, 예측 성능을 평가하였다. 전반적으로 모든 Solver의 모사 결과가 현장 Pigging 데이터와 잘 일치하였지만, Solver

간의 성능 차이가 오차 평가를 통해 명확하게 식별되었다. 유동 모델의 경우 MOC-FVM Hybrid가 모사, 예측 성능 모두 Stoner-MOC보다 높은 정확도를 보였다. 마찰 모델의 경우, Tuned friction model이 모사 성능에서 더 높은 정확도를 보였지만, Weighted friction model이 예측에서 더 높은 성능을 보였다. 따라서 4개의 Solver 중 Hybrid-Tuned 기반 Solver가 가장 높은 모사 성능을 보였고, Hybrid-Weighted 기반 Solver가 예측에서 최고의 성능을 보였다. 이러한 결과는 제안된 유동 및 마찰 모델에 따른 Solver 간의 모사, 예측 성능의 차이가 확인되었으므로 유동 모델과 마찰 모델을 전략적으로 채택하여 사용 목적에 따라 Solver를 구축할 수 있음을 의미한다.

Keyword : 배관 검사 로봇, 가스 배관, 속도 이탈, 동적 모델, 유동 모델, 마찰 모델, 수치 시뮬레이션

Student Number : 2018-32032

Acknowledgement in Korean

이 글을 통해 박사과정 동안 많은 도움을 주신 분들께 감사의 인사를 드리고자 합니다. 먼저, 박사과정 동안 아낌없는 지도와 조언을 통해 올바른 연구자의 길로 인도해주신 서유택 교수님께 감사드립니다. 교수님 덕분에 좋은 연구를 할 수 있었고, 연구에 흥미를 잃지 않을 수 있었습니다. 대학원 과정동안 배운 것들을 머리와 마음에 새기고 주체적인 연구자로서 열심히 나아가도록 하겠습니다. 바쁘신 와중에도 부족한 연구와 앞으로 나아갈 방향에 대한 아낌없는 조언해주신 임영섭 교수님, 김도균 교수님, 남보우 교수님, 안윤희 교수님께도 감사드립니다.

힘든 대학원 생활 속에서도 항상 즐겁게 연구실 생활을 할 수 있게 도와준 에너지시스템 연구실 학생들 및 연구원 분들에게도 감사합니다. 연구실 생활 전반에 대한 다양한 고민을 함께 나누고 조언해 주셨던 김자경 박사님, 김현호 박사님, 손영훈 박사님, 박기흠 박사님께 감사드립니다. 또한, 박사과정동안 많은 도움을 받았지만, 선배로서 많은 도움이 되지 못한 것 같아 항상 미안한 마음이 드는 나영이, 종연이, 진관이, 건우, 준엽이에게도 감사의 말을 전하고 싶습니다.

마지막으로 자주 찾아 뵈지도 못하고 살갑지도 못한 저를 믿어주시고 묵묵히 응원해주시는 부모님께 감사드립니다. 가족분들의 사랑 덕분에 박사 학위 논문을 무사히 마무리 지을 수 있었습니다. 이 논문이 나오기까지 아낌없는 도움을 주시고 지면의 한계로 여기에 미처 적지 못한 많은 분들께 다시 한번 감사의 마음을 전합니다. 저도 여러분께

힘이 될 수 있는 존재가 될 수 있도록 노력하겠습니다.

이제 졸업을 하고 사회에 한발 짝 더 나아가려고 합니다. 흘러가는 물처럼 살지 아니하고 하나님께서 저에게 주신 소명, 용기, 지혜로 세상의 빛과 소금이 되는 삶을 살고자 하기에 영원히 살 것처럼 배우고 익히며, 가장 소중하고 의미 있는 오늘을 살겠습니다.

감사합니다.

2022년 08월

김승만 올림